NASA TECHNICAL NOTE

NASA TN D-4964

NASA TN D-4964

DEVELOPMENT OF IMPROVED THROAT INSERTS FOR ABLATIVE ROCKET ENGINES

by Jerry M. Winter and Donald A. Peterson

Lewis Research Center
Cleveland, Ohio

NATIONAL AERONAUTICS AND SPACE ADMINISTRATION • WASHINGTON, D. C. • JULY 1969

NASA TN D-4964

DEVELOPMENT OF IMPROVED THROAT INSERTS FOR ABLATIVE ROCKET ENGINES

By Jerry M. Winter and Donald A. Peterson

Lewis Research Center
Cleveland, Ohio

NATIONAL AERONAUTICS AND SPACE ADMINISTRATION

For sale by the Clearinghouse for Federal Scientific and Technical Information
Springfield, Virginia 22151 – CFSTI price $3.00

ABSTRACT

Seventy-five throat inserts and nine complete nozzle designs were evaluated in a storable propellant (nitrogen tetroxide and a 50-percent blend of unsymmetrical dimethyl hydrazine with hydrazine) rocket engine. An insert of iridium-rhenium on a tungsten substrate ran successfully until gas diffusion through the porous iridium caused substrate oxidation. Composites of hypereutectic carbides; anion deficient zirconium oxide; mixed oxides of hafnium, titanium, and zirconium; wire reinforced zirconium oxide; and a refractory macrolaminate were all run through a varied and extended duty cycle. Rocket-engine testing, in the combustion environment of interest, for the intended duty cycle, was the most efficient method of advanced material evaluation. A motion-picture film supplement is available on request.

Motion-picture film supplement C-261 is available on loan. Requests will be filled in the order received. You will be notified of the approximate date scheduled.

The film (16 mm, 30 min, color, sound) shows the design and test firings of five refractory coated inserts, seven composite material inserts, and five nozzle designs. The wide spectrum of possible failure mechanisms associated with the earth-storable propellant systems is illustrated.

Film supplement C-261 is available on request to:

Chief, Technical Information Division (5-5)
National Aeronautics and Space Administration
Lewis Research Center
21000 Brookpark Road
Cleveland, Ohio 44135

CUT

Date _____

Please send, on loan, copy of film supplement C-261 to
TN D-

_____
Name of Organization

_____
Street Number

_____
City and State Zip Code

Attention: Mr. _____
Title _____

Place
stamp
here

Chief, Technical Information Division (5-5)
National Aeronautics and Space Administration
Lewis Research Center
21000 Brookpark Road
Cleveland, Ohio 44135

DEVELOPMENT OF IMPROVED THROAT INSERTS FOR ABLATIVE ROCKET ENGINES

by Jerry M. Winter and Donald A. Peterson

Lewis Research Center

SUMMARY

Seventy-five throat inserts and nine complete nozzle designs were evaluated in a rocket engine using storable propellants (nitrogen tetroxide and a 50-percent blend of unsymmetrical dimethylhydrazine with hydrazine). The purpose was to develop materials and design concepts capable of surviving an extended duty cycle consisting of an initial 300-second firing followed by five 20-second firings and ending in another 300-second firing. The nominal engine operating condition included an oxidant to fuel mixture ratio of 2.0, a chamber pressure of 100 psia (689 N/m^2 abs) with an initial throat diameter of 1.2 inches (3.05 cm).

Refractory coating systems, refractory composite materials, and complete designs were studied. Coatings did not prevent erosion over the required duty cycle although a semi-impervious coating of iridium-rhenium on a tungsten substrate was encouraging. Of the refractory composites tested, those containing zirconium oxide or hafnium oxide, modified by reinforcement or stabilized with additives, were most successful. The only material tested that completed the 700-second total duty cycle with neither erosion in excess of 5 percent area change nor cracking was a hafnium oxide - molybdenum macrolaminate composite.

It was concluded that rocket-engine testing is necessary in order to establish the general suitability of a material-design system in a specific environment.

Promising concepts for further development and scale-up studies include the hafnium oxide - molybdenum macrolaminate; mixed oxides of hafnium, zirconium, and titanium; hypereutectic compounds; tungsten-rhenium wire reinforced zirconia; segmented designs utilizing zirconium oxide or beryllium oxide; and the use of iridium coatings on suitable substrates.

INTRODUCTION

Ablative thrust chambers are presently used in many important applications, including small reaction control engines and main propulsion systems. The advantages of ablative thrust chambers include simplicity and reliability as well as throttling capabilities. Throst erosion is a problem, however, particularly for long duration missions. Refractory throat inserts are employed to extend the useful life of ablative thrust chambers presently in service. Greater utilization of throat inserts is anticipated for future propulsion systems if suitable material-design combinations are available for the required duty cycles.

As a necessary precondition of insert material development, a significant portion of available manpower and funds are being expended in generally upgrading materials. Except in the broad sense of improving melting temperature, oxidation resistance, thermal shock, and erosion characteristics, most refractory materials research and development has not been concerned with the specific environment to which these materials will be subjected.

There are two primary areas that must be characterized if efficient, reliable, and economical systems are to be designed. The first area of interest is environmental definition. The possible variations of internal surface temperature and boundary-layer chemistry, within the framework of a particular propellant combination, are primarily a function of injector design. Run duration and cyclic operation also contribute to the complexity of the problem. The other prime area is material compatibility. Complex interrelations between material design concepts, internal environment, limitations of weight, size, and external temperature, and maintenance of structural integrity, raise the more obvious material problems which must be resolved if maximum reliability is to be ensured.

In essence then, the objective of any study on throat inserts should be concerned with first defining the actual combustion environment associated with a specific mission requirement and then developing a suitable material-design combination which is applicable for that particular environment and duty cycle.

As a first step in that direction, NASA-Lewis has recently published two reports. Reference 1 discussed some specific failure mechanism of small (1.2-in. (3.05-cm) diam) throat inserts in the Earth storable-propellant combustion environment as a preliminary approach to advanced material design. In reference 2, the failure modes of 7.8-inch (19.8-cm) diameter throat inserts were determined and the scaling effects between the 1.2- and 7.8-inch (3.05- and 19.8-cm) throats in a storable-propellant rocket engine were compared. The purpose of the investigation reported herein was to continue the program initiated in reference 1 but with the primary concern on developing advanced or unique material and design concepts.

Materials used for nozzle throats fail for a number of reasons. Among the most

important failure mechanisms are oxidation or chemical reaction, thermal stress cracking, erosion due to melting, and physical removal due to local shear forces. A materials-design combination is required that will successfully resist all these failure mechanisms during a given operational cycle. From the standpoint of time and cost, it is most desirable to perform the subscale testing in a simple design configuration. To that aim, two main classes of insert material-systems were investigated: (1) refractory coating systems and (2) composite materials systems. All the insert materials of these two classes were essentially identical in design and were bonded into an ablative chamber. A detailed thermal-stress analysis was not attempted for the throat inserts. Prior to the start of the program, a search was made for analytical techniques or computer programs that would aid design. All the analytical approaches were found to be seriously lacking in two main areas. The first area concerns methods of describing the actual test environment. The second area concerns the material physical properties. Very little information exists as to material property data at high temperature. This is particularly true for composite materials of new or unique composition. Most of the materials studied in this program were of unique composition, and it was felt that an actual rocket firing was the most direct method to adequately evaluate these materials.

Nine complete nozzle designs were also evaluated together with the throat inserts. Seven of the nozzle designs were accomplished under a separate program reported in reference 3. A complete temperature profile, detailed stress analyses, and small-scale thermal shock tests were performed on each of the nozzle designs. One of the objectives was to determine whether detailed analytical techniques could be used to select the materials and make the designs necessary to give satisfactory performance in a specific rocket-engine environment without prior engine testing. Another objective was to compare the firing results of similar materials tested in the insert configuration to the firing results of nozzle designs developed primarily with analytical techniques.

The choice of a particular material-design system for each of the three sections of the report is discussed in relation to past experience and inherent material properties with respect to anticipated results. The materials are evaluated and discussed in terms of their ability to survive a duty cycle consisting of an initial 300-second continuous firing, followed by five 20-second firings, and terminating in another 300-second continuous firing. This duty cycle was chosen so that both erosion and thermal stress cracking could be evaluated during repeated firings. The engine had an initial throat diameter of 1.20 inches (3.05 cm). The nominal firing conditions included a constant chamber pressure of 100 psia (689 N/m^2) and an oxidant-to-fuel ratio of 2.0 (a few tests were made at an oxidant-to-fuel mixture ratio of 1.6). The theoretical combustion temperature was 5630° R (3130° K), which resulted in a throat surface temperature of approximately 4400° R (2445° K). The combustion gas species theoretically contained 39-mole-percent water vapor and was highly oxidizing.

Eighty-four throat inserts and nozzle designs were tested. The tests were run in a manner to provide maximum information on the survival characteristics of each material evaluated. For example, when severe cracking occurred or when the erosion rate increased drastically, the test was terminated immediately, and the test specimen was sectioned to identify the mode of degradation. Throat erosion and insert cracking were used as the prime criteria for evaluating and rating the throat inserts. Cracking is defined as any fissure originating on either the inside surface, outside surface, or within the material structure. Cracking was considered most serious when it extended completely through the insert structure or when cracking was likely to lead to a catastrophic loss of material. Cracks extending through coatings were considered serious, but surface checking or crazing was not considered serious in refractory composite inserts unless it led to throat erosion. The importance of eliminating cracking is due to the unpredictability of the number, location, and propagation characteristics of cracks, which, in turn, can lead to catastrophic failure and subsequent loss of the mission. In most cases, the engine was examined after each cycle and the test was terminated if either severe erosion or cracking was noted. When a rapid increase in the throat diameter occurred during a firing, the test was ended manually.

Following the brief discussion of individual material results, a summary is included for each of the three areas: refractory coated inserts, refractory composite inserts, and nozzle designs. These summary sections are intended to assess the degree of success achieved in the program. Failure modes are discussed in terms of possible corrective measures and recommendations for future efforts are made. A film supplement is included to graphically illustrate material behavior in the rocket engine environment.

APPARATUS

Figure 1 is a photograph of the test facility with an engine installed. Figure 2 is the flow-system schematic. Also shown is the camera arrangement for photographing the rocket throat during firing. A typical engine assembly including injector and nozzle is given in figure 3(a). Figure 3(b) gives the pertinent engine dimensions. (The nozzle used for the throat inserts is shown.) The transition ring was not used for insert assemblies that matched the chamber diameter. The injectors used for the test program were 10-element oxidant-on-fuel triplets. The standard injector design is shown in figure 4. Three identical injectors were used but injector 1 was modified and then used for 28 insert firings. The included impingement angle was changed from 30° to 60° and the oxidant hole size was changed from 0.0292-inch (0.0742-cm) diameter to 0.033-inch (0.0839-cm) diameter. The modification was necessary to extend injector lifetime until spare injectors

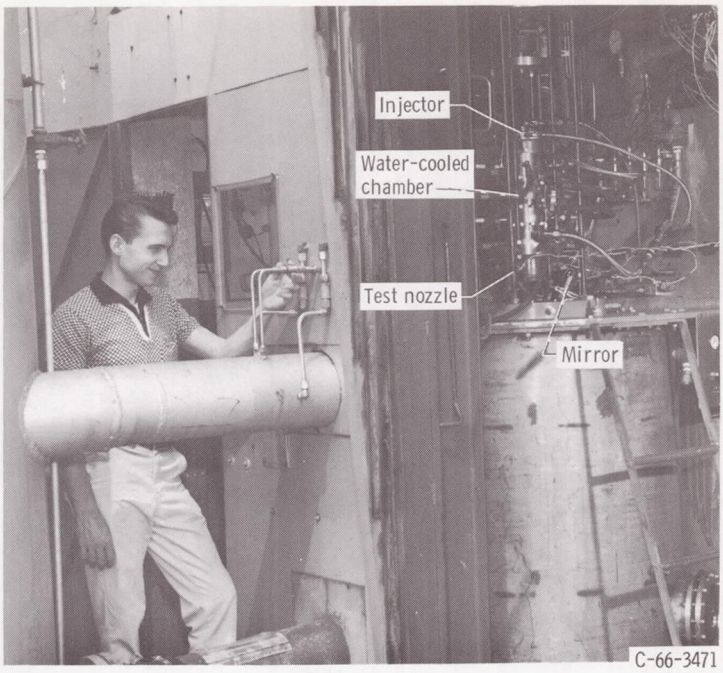

Figure 1. - Test facility.

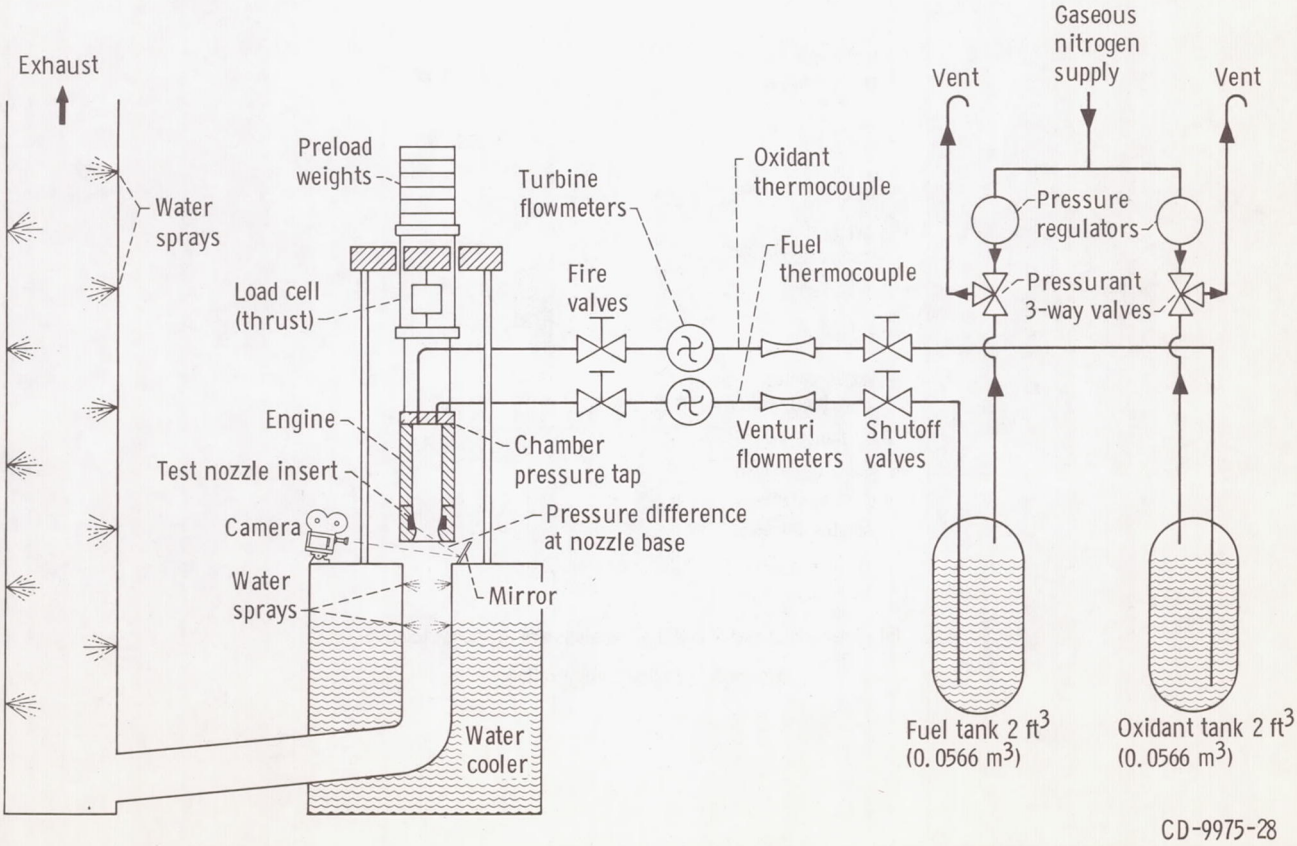

Figure 2. - Test installation.

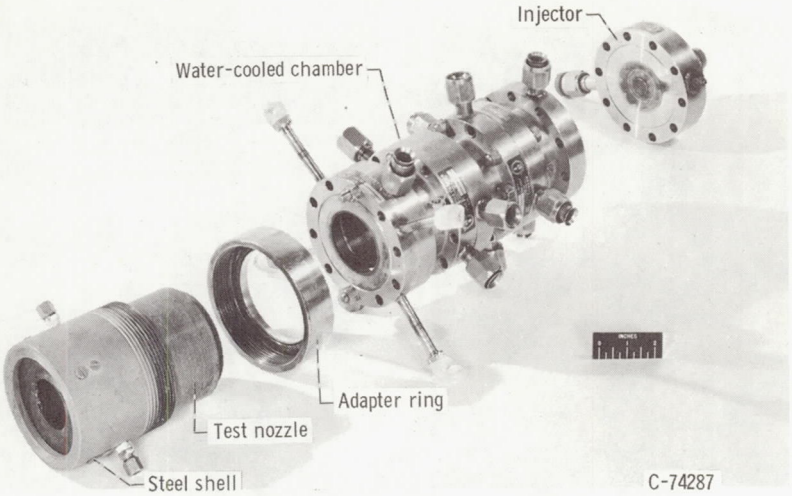

(a) Disassembled.

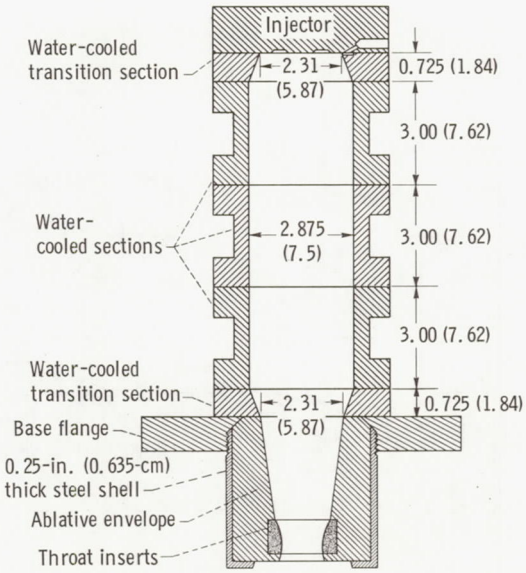

(b) Dimensional sketch. (All dimensions are in inches (cm)).

Figure 3. - Engine configuration.

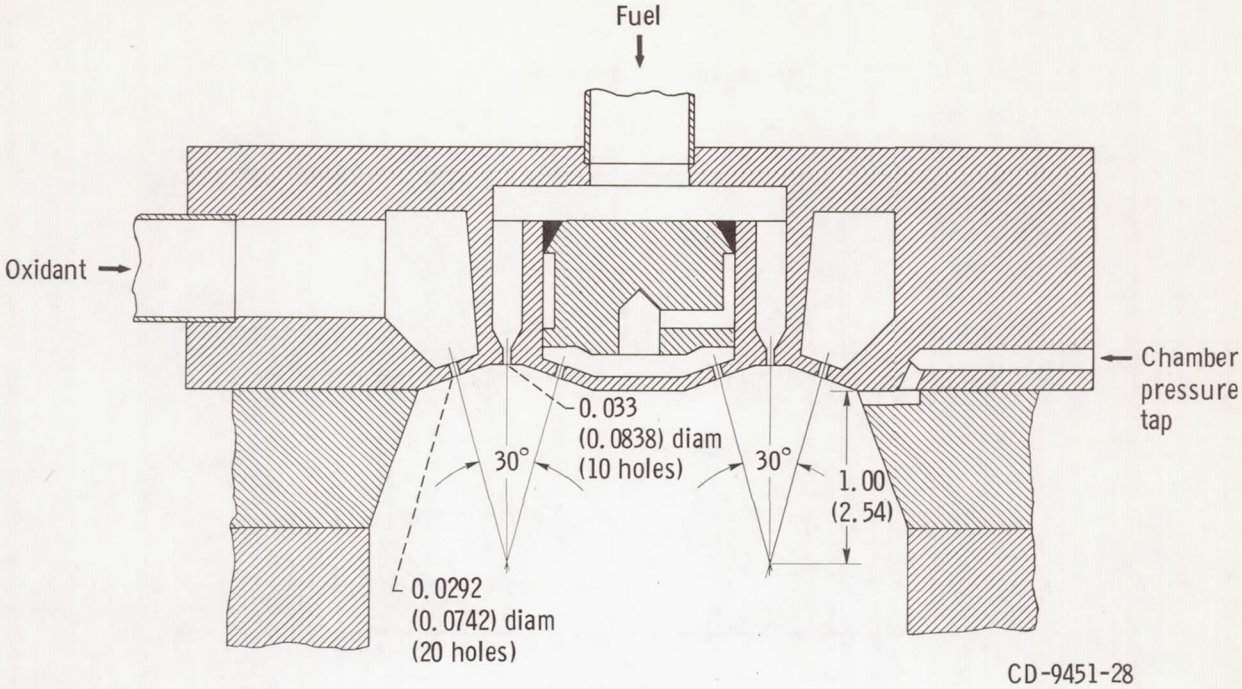

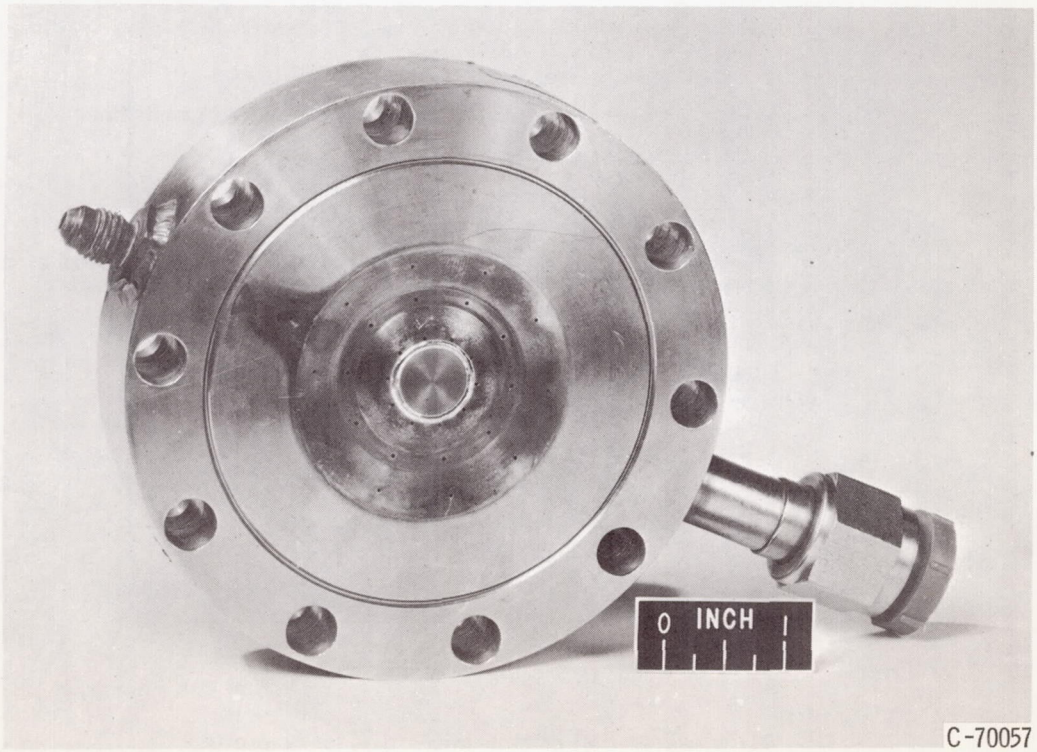

Figure 4. - Injector configuration. (All dimensions are in inches (cm).)

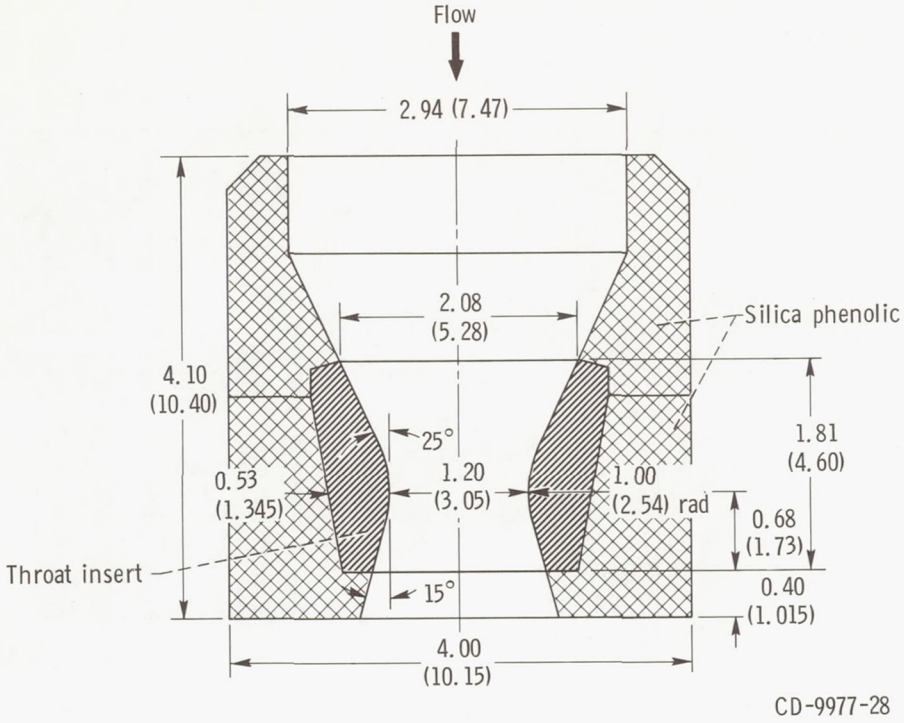

(a) Configuration A; standard. Used for 24 inserts.

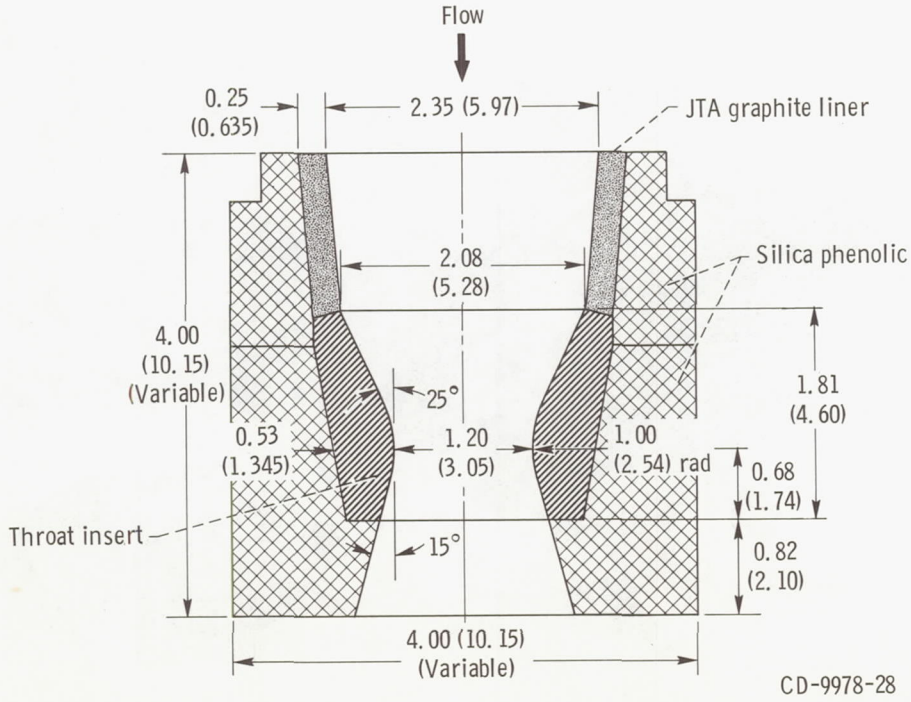

(b) Configuration B; graphite liner. Used for 49 inserts.

Figure 5. - Throat insert configurations. (All linear dimensions are in inches (cm).)

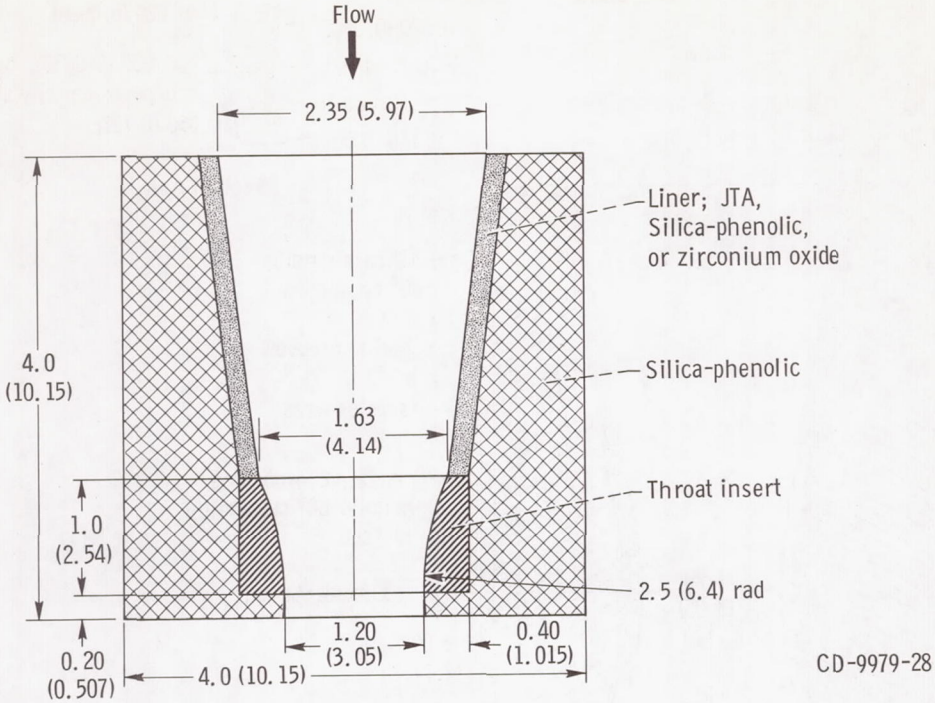

(c) Configuration C. Used for 3 inserts.

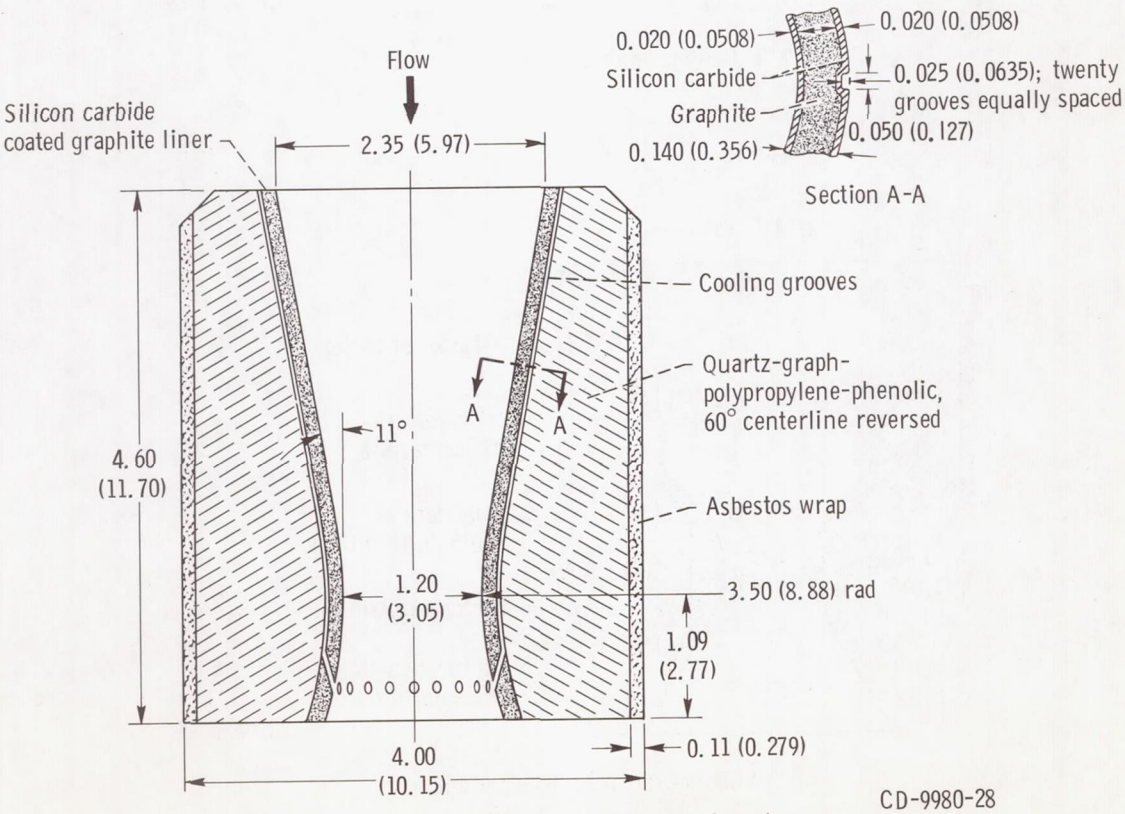

(d) Configuration D. Used for one insert.

Figure 5. - Continued.

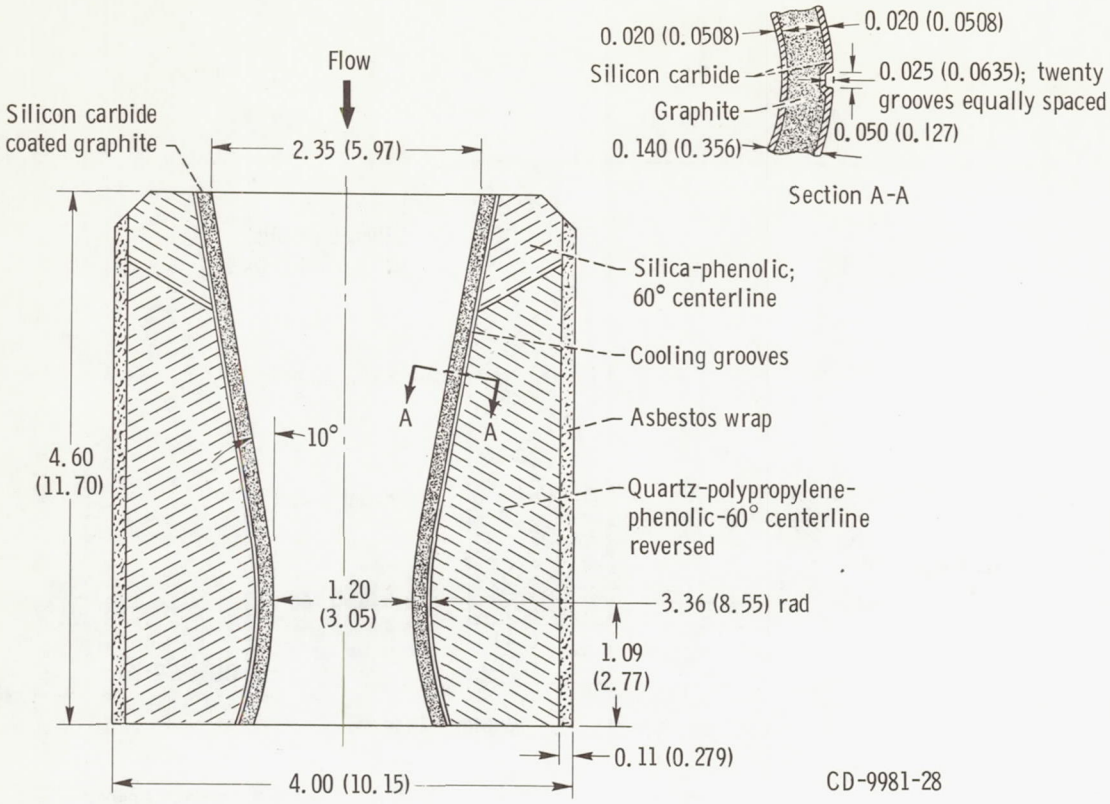

(e) Configuration E. Used for two inserts.

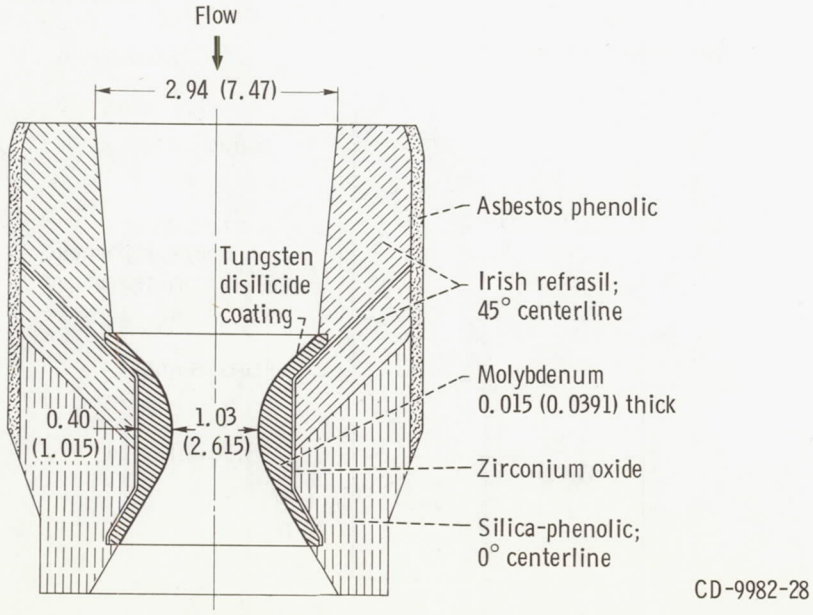

(f) Configuration F. Used for one insert.

Figure 5. - Continued.

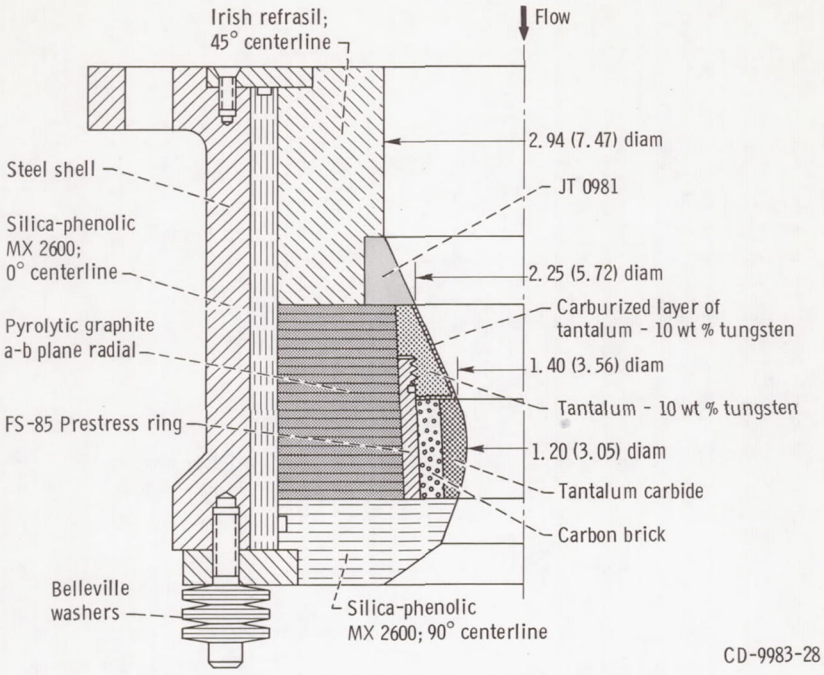

(g) Configuration G; prestressed design. Used for one insert.

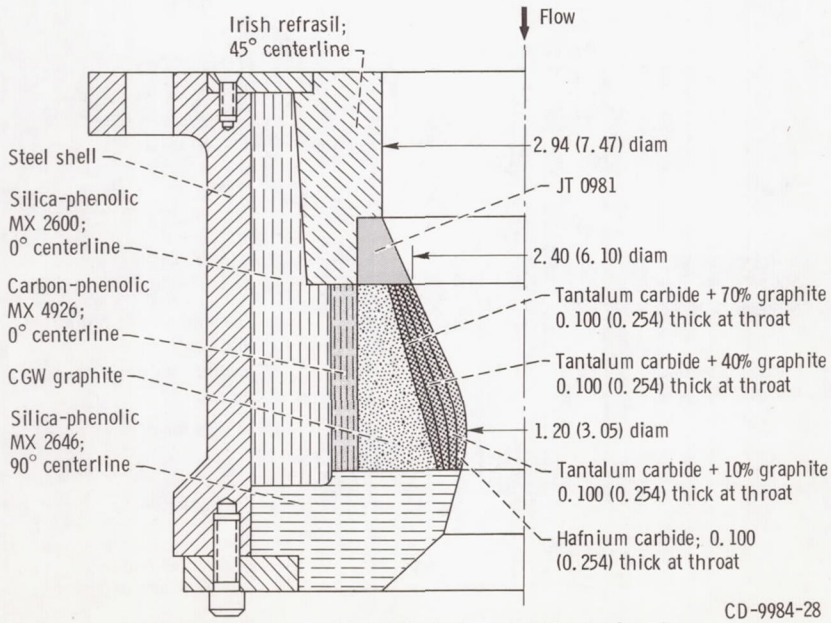

(h) Configuration H; graded carbide design. Used for one insert.

Figure 5. - Continued.

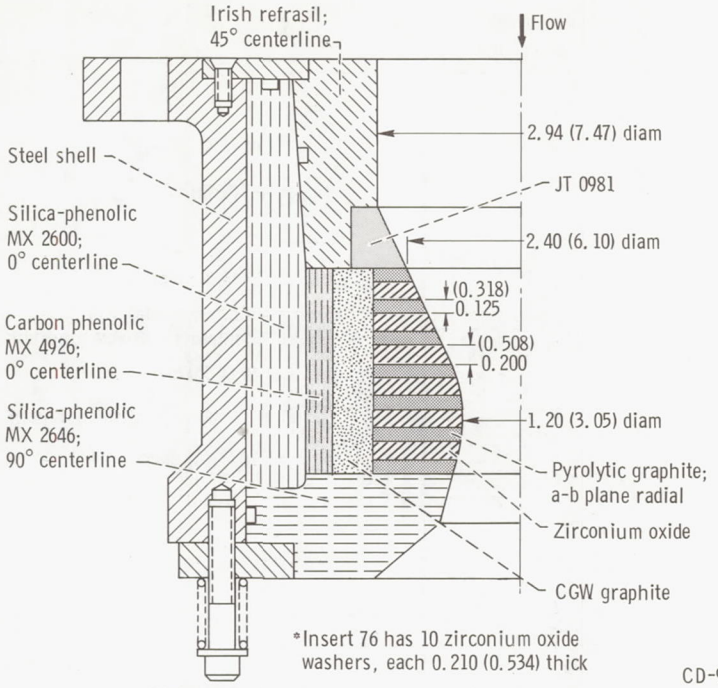

(i) Configuration I; laminate design. Used for two inserts.

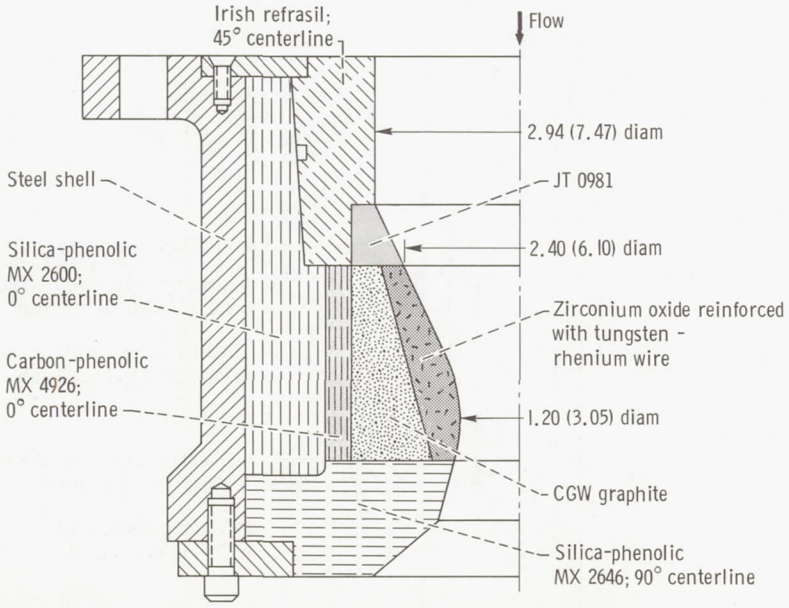

(j) Configuration J; reinforced oxide. Used for two inserts.

CD-9986-28

Figure 5. - Concluded.

could be procured.

Table I lists the measured variables along with an estimate of the precision of each measurement. The schematic diagram of figure 2 also shows where the variables were measured. The run time was measured with a clock timer arranged to start and stop simultaneously with the opening and closing of the fire valves. Measured variables were recorded on magnetic tape by a high-speed digital recording system.

The various nozzle-insert configurations used for testing are shown in figure 5. The inserts of figures 5(a) and (b) were identical, except for the use of a JTA liner upstream of the throat insert.

The chamber liners shown in figures 5(b) and (c) were used to prevent ablative erosion upstream of the insert during extended duration firings. Liners also prevented molten silica ablation products from flowing over the insert surface and reacting with the insert material. Configuration C was used because of material size limitations in manufacturing the insert. Configurations D to J (figs. 5(d) to (j)) were the result of both previous experience and a complete theoretical design analysis (ref. 3).

The ablative material used for the envelope was 70-percent silica reinforcement with 30-percent phenolic binder in the majority of cases. Each insert tested is listed in table II. The test results are reported by classes, including 18 refractory coating systems, 57 refractory composites (graphites, carbides, oxides) and 9 nozzle designs. Seven nozzle designs were derived from a separate program (ref. 3), which included thermal and stress analyses, laboratory thermal shock tests, and envelope design, including insert, intermediate layers, ablative materials, and pressure vessel.

PROCEDURE

Just before each firing, the propellant tanks were pressurized with nitrogen gas. The fire valves were opened to start the test utilizing a slight oxidant lead. Automatic closed-loop controllers were used to maintain constant chamber pressure and oxidant-to-fuel mixture ratio during each test. The duration of each run was determined by an automatic timer, excess throat erosion, gas leakage, or other emergencies.

The combustion performance of the system was measured periodically with fixed-diameter, heat-sink nozzles and 7-second test firings. The method used for characteristic velocity efficiency calculations is given in table III. The calculations of table III were made by digital computer for each of the test firings.

A visual inspection of the throat insert was made after each test firing. Before and after each firing series, the throat profile was traced from an optical comparator which enlarged the actual diameter 10 times. The tracing was measured with a planimeter, and the measured area was converted to an effective diameter from which the effective throat radius change was obtained. The effective throat radius change was also calculated during each firing by the equation listed in table III. The initial throat radius of

the equation was the initial optical comparator measurement. The C_k^* used in the equation was a constant value determined from heat-sink calibration firings.

Most of the nozzles were bisected and photographed following the final test firing. Metallographic analyses were made of the fired nozzles when necessary to assist in assist in analyzing the test results.

RESULTS AND DISCUSSION

COMBUSTION PERFORMANCE

The combustion performance of each injector was obtained during 7-second firings using a fixed-diameter, heat-sink nozzle with a water-cooled combustion chamber. The characteristic velocity efficiency ηC^* was calculated both from chamber pressure and thrust measurements (see table III). The C^* efficiency calculated from thrust is listed in table IV for each injector. The standard deviation of these C^* efficiency values was ±1.5 percent. The C^* efficiency values calculated from chamber pressure agreed with the listed values within 1 percent when a thrust coefficient efficiency ηC_F of 95.5 percent was used. The value for ηC_F was less than the conventional 98.3 percent value used for larger contoured nozzles with the same radius of curvature to radius of throat ratio (0.5). The 95.5-percent value is considered to be realistic for the small 1.2-inch (3.05-cm) throat-diameter nozzle because of an increased effect of boundary-layer displacement thickness and momentum deficiency. It is believed that the test results were not appreciably affected by the injector modification or the reported variation in C^* efficiency.

TEST RESULTS

The firing time to produce a ±5-percent area change (0.014-in. (0.0356-cm) effective throat radius change) and the time when cracking was first detected are summarized in table V as indicators of the capabilities or shortcomings of the various inserts and nozzles. Note that cracking may have actually occurred sooner than the earliest time of detection. Final relative ratings are arrived at on the basis of a total evaluation of the throat insert behavior, with erosion rate, oxidation, cracking, likelihood of catastrophic loss of material, charring of the ablative envelope, gas leaks, reaction with upstream material, undercutting at the leading or trailing edge, etc., taken into consideration. The total system, including the upstream ablative, was considered when determining the ratings. The primary failure mode in table V summarizes the most important characteristics noted during test and is, therefore, a measure of success on which the rating is

based. The duty cycle was an initial firing of 300 seconds, five 20-second firings with cool-down to ambient temperature between each firing, and a final 300-second firing. The duty cycle was chosen to represent a severe test for all the materials and to learn as much as possible from the initial firing. Details on the type and severity of structural degradation as well as the causes of surface erosion are discussed separately for individual inserts in the text. After initial failure was observed, some inserts were tested further to assess the magnitude and propagation characteristics of failure.

A detailed description of each insert and nozzle together with the complete firing data are included in table VI. Also included in table VI is a post-test photograph of the sectioned nozzle to aid in assessing the results.

The throat erosion values listed in the table VI were calculated from the optical comparator measurements. Agreement between measured and calculated values was generally good except where gas leakage resulted in erroneous calculated values of erosion. Accurate optical projection of the throat plane is difficult when the nozzle surface is rough. Protruding material above and below the throat plane obstruct the light and cause the projected area to be less than the actual area.

REFRACTORY COATING SYSTEMS

Ideally, a coated refractory material system should have the following properties: The coating should be impervious to the combustion gases, be thermally stable, be oxidation resistant, and not melt at the operating temperature. To withstand the applied stress, the coating-substrate combination should be structurally sound. Because the main purpose of the substrate material is to provide a structural support for the coating, the substrate should have a high strength-to-weight ratio. Many materials will meet one or more of these requirements, but few materials will meet them all. One of the more difficult problems to overcome has been coating-substrate compatibility. Adequate coating adhesion to the substrate is necessary, and methods to relieve the residual stresses incurred by some of the more common coating techniques must be found. The compound curvature of a typical nozzle geometry complicates the thermal-stress problem. And differential thermal expansion of coating and substrate are difficult to calculate because the actual temperature of each must be known throughout the firing cycle. The coated inserts tested were intended to be structurally sound and, in addition, to provide oxidation resistance in the storable-propellant combustion environment.

Refractory Metal Substrates

Aluminum oxide - chromium oxide on TZM. - Plasma arc spraying followed by gas-pressure bonding was the technique used for the fabrication of both inserts 1 and 2. An intermediate layer of aluminum oxide (Al_2O_3) and chromium (Cr) was used to increase the adhesion of the coating to the TZM (molybdenum base alloy containing zirconium and titanium) and provide an intermediate match for the thermal expansion. A detailed description of the materials and processes involved is included in reference 4.

Plasma spray coatings have traditionally been relatively weak and porous. Gas-pressure bonding was utilized to increase the coating density. The higher density should provide a stronger material and one more impervious to the combustion gas products. Increased coating adhesion was also anticipated because of the greater depth of coating diffusion into the substrate during bonding.

Inserts 1 and 2 were tested for approximately 50 seconds when a rapid increase in the throat area of each insert was noted. This rapid increase in the throat area shown

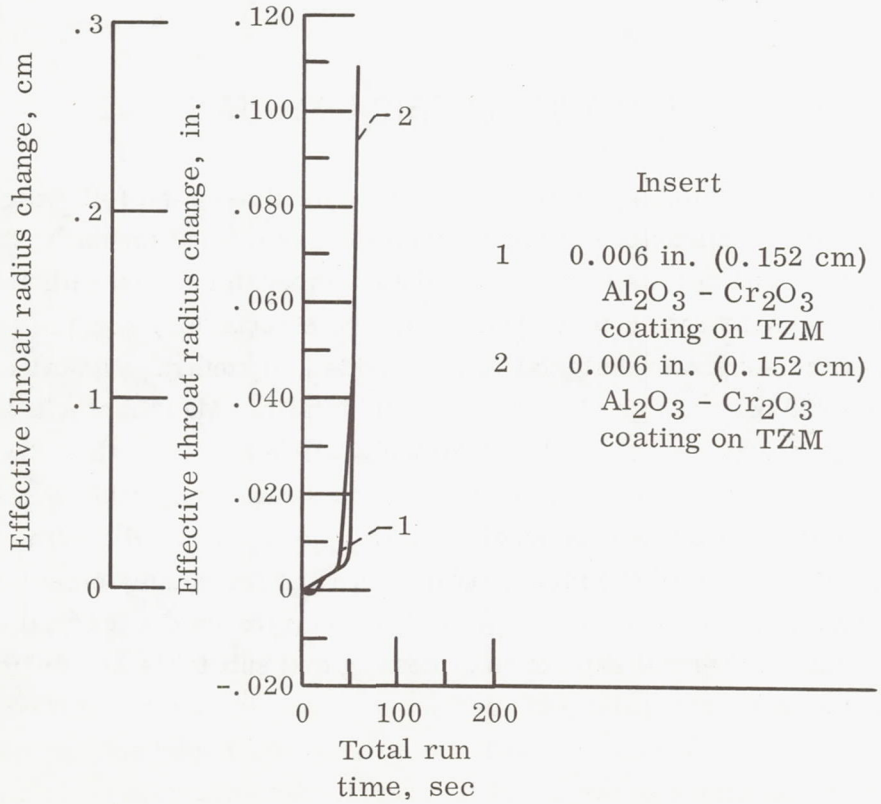

Figure 6. - Throat erosion for aluminum oxide - chromium oxide coated TZM inserts.

in figure 6, was caused by loss of the aluminum oxide - chromium oxide (Al_2O_3 - Cr_2O_3) coating followed by rapid oxidation of the unprotected TZM. Failure was primarily due to melting of the aluminum oxide layer. The coatings appeared to have adequate adhesion to the substrate. Unfortunately, the inserts were not run long enough to assess the suitability of the intermediate chromium layer at high-temperature, steady-state operation (because the aluminum oxide layer melted). Included in table VI(1) is a photograph of the fired insert number 1. The film supplement illustrates this type of failure.

Hafnium oxide - zirconium oxide on TZM. - A 0.006-inch (0.0152-cm) thick coating of hafnium oxide (HfO_2) and zirconium oxide (ZrO_2) over an intermediate layer of ZrO_2 and chromium was also applied to a TZM substrate by the plasma arc spraying and gas-pressure bonding techniques. The firing data for inserts 3 and 4 are presented in figure 7. Failure of the coating was apparently due to vaporization of the chromium in the intermediate ZrO_2-Cr layer. This indicates that a more refractory material than chromium should be used for an intermediate layer. The film supplement also shows this failure.

Hafnium - tantalum - molybdenum on TZM. - Insert 5 was a composite coating of hafnium, tantalum, and molybdenum on a TZM substrate. The coating was prepared by

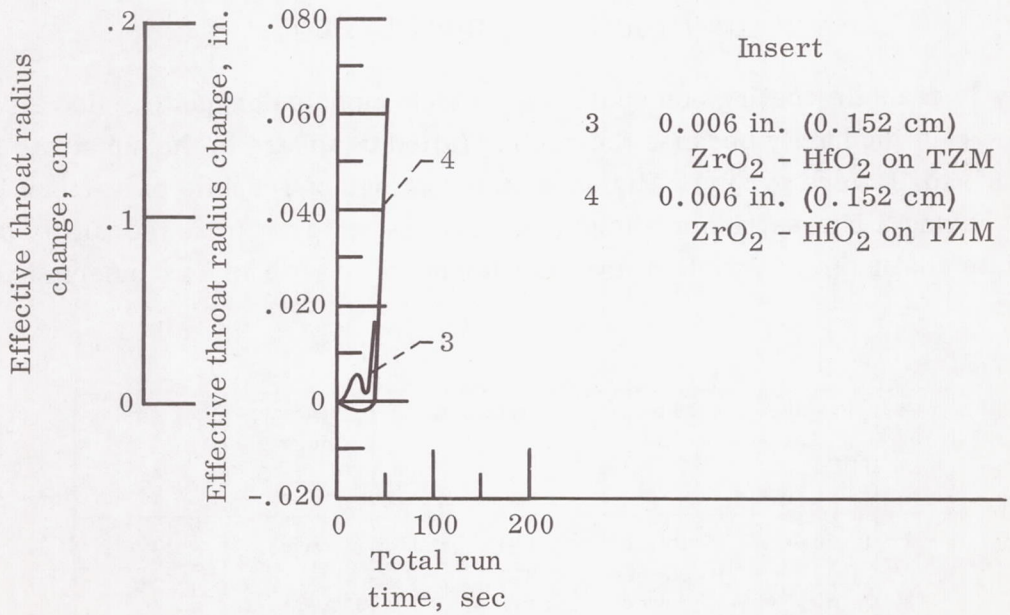

Figure 7. - Throat erosion for zirconium oxide - hafnium oxide coated TZM inserts.

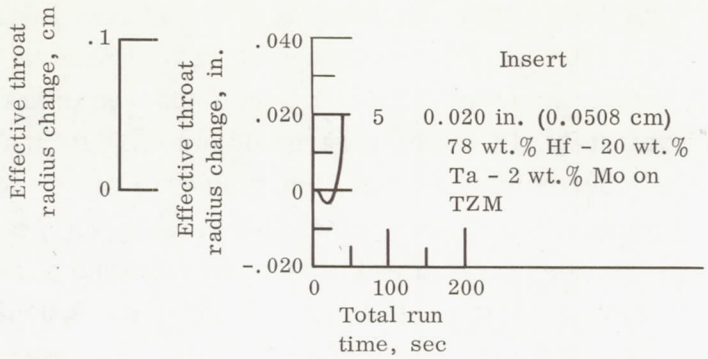

Figure 8. - Throat erosion for hafnium - tantalum - molybdenum coated TZM insert.

a plasma spray and sintering process. The firing data for insert 5 are presented in figure 8. Coating removal was caused by thermal stress, which allowed oxidation of the substrate and caused an erosion failure at about 40-seconds firing duration.

Iridium rhenium on tungsten: This insert will be discussed in a later section along with other iridium coatings.

Low-Modulus Graphite Substrates

Pyrolytic graphite coatings on conventional high-modulus graphite substrates have failed in the past primarily because the coating failed to adhere to the substrate adequately. Inserts 7 to 10 were pyrolytically deposited coatings of graphite on various low-density substrates having a low-section modulus and were tested to evaluate the ability of a pyrolytic graphite coating to adhere to a low modulus substrate. The four inserts are described as follows.

Insert	Coating thickness		Material	Substrate	Upstream liner	Configuration
	in.	cm				(a)
7	0.060	0.152	Pyrolytic graphite	Pyrolyzed graphite cloth	Ablative	a
8	.010	.0254	Pyrolytic graphite	PT 0114	JTA graphite	b
9	.040	.1015	Pyrolytic graphite with boron	Pyrolyzed graphite cloth	Zirconium oxide	b (modified)
10	.040	.1015	Pyrolytic graphite	Pyrolyzed graphite cloth	JTA graphite	b (modified)

[a]See fig. 5.

All the substrates were basically a pyrolyzed form of graphite cloth and phenolic. Insert 7 had a coating thickness of 0.060 inch (0.152 cm) and was used with an ablative liner upstream. The coating of insert 8 was only 0.010-inch (0.0254-cm) thick and also contained approximately 0.5 percent boron which was codeposited with the graphite. JTA graphite was used as the upstream liner for insert 8. Inserts 9 and 10 both had 0.040-inch (0.1015-cm) coatings; however, insert 9 used a ZrO_2 liner upstream, while insert 10 used the JTA material as a liner. After fabrication of insert 9, the coating was found to be defective in the area upstream of the throat and remachining of the insert face was necessary to remove this area. This machining of configuration B decreased the insert length, which, in turn, decreased the leading-edge diameter from the normal 2.08 inches (5.28 cm) to approximately 1.70 inches (4.32 cm). It was felt that the gas-stream velocity at this new contraction ratio would be too high and that the JTA liner would erode, exposing the insert leading edge to the high shear forces of the combustion gases; therefore, a ZrO_2 liner was used in place of JTA. Insert 10 used a JTA liner because the entrance diameter was 1.81 inches (4.60 cm). In addition, insert 10 had a simple 2.0-inch (5.08-cm) radius of curvature instead of the standard compound curvature used on all other inserts. This was done to eliminate the coating discontinuity and hopefully to prevent thermal-stress cracking.

The firing results for all four inserts are presented in figure 9. Although insert 8 has only an 0.010-inch (0.0254-cm) thick coating compared with 0.060 inch (0.152 cm) for insert 7, the extended time (50 sec compared with only 20 sec) for throat erosion to

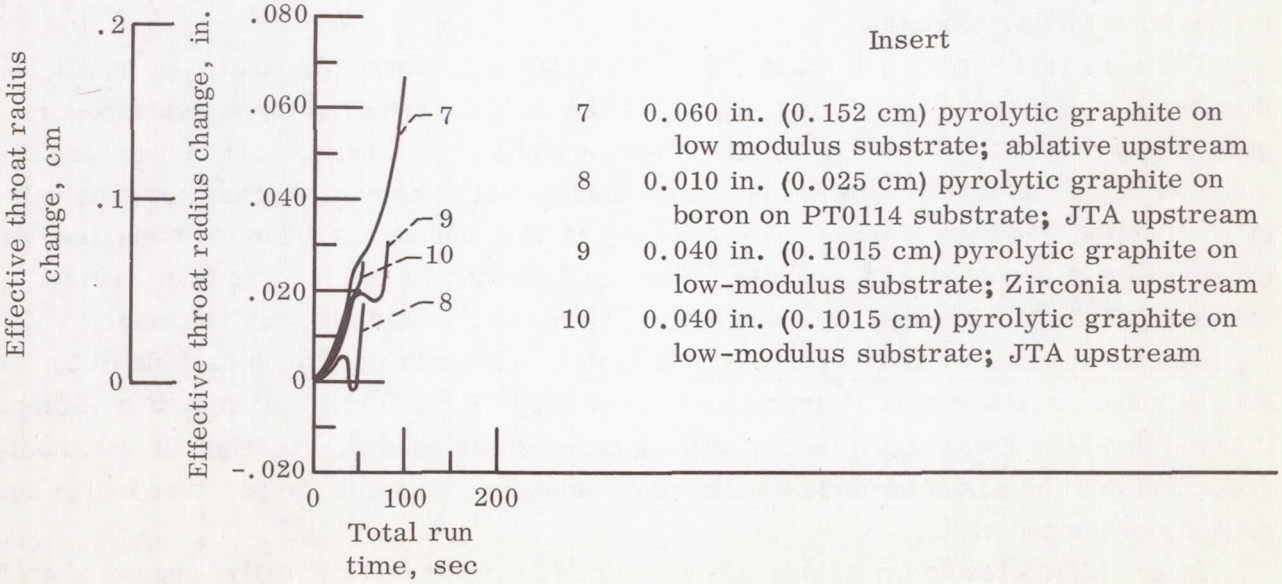

Figure 9. - Throat erosion for graphite-coated low-modulus-graphite-substrate inserts with upstream liners.

initiate in insert 8 was apparently a result of the increased oxidation resistance of the boron codeposition. Both coatings, however, lost adhesion at the leading edge as a first step to failure. For insert 7, the erosion of the upstream material (silica-phenolic) at the insert interface exposed the coating edge to the high-velocity gas stream with subsequent undercutting and attack on the substrate. When the upstream silica-phenolic material was replaced with a JTA liner for insert 8, undercutting at the insert interface did not occur. Both the coating and substrate for insert 8 cracked (see table II(8)), however, which led to oxidation of the substrate and subsequent failure of the coating. The high gas velocity experienced for insert 9 undoubtedly contributed to the premature removal of the coating in the upstream area.

The erosion rate for insert 10 was approximately 0.0005 inch per second (0.00127 cm/sec), and the firing was proceeding smoothly until the substrate cracked after about 50 seconds. Table VI(10) shows the cracked substrate and ablative holder. The coating was still well bonded to the substrate, however. The film supplement illustrates the coating loss, starting at the leading edge and progressing through the throat plane, primarily due to oxidation.

High-Modulus Graphite Substrates

Zirconium carbide on ATJ graphite. - Zirconium carbide (ZrC) will react quite rapidly in an oxidizing environment to form ZrO_2. It was hoped that the inplace formation of ZrO_2 would produce an adherent surface oxide layer that would protect the coating underlayers from further oxidation.

The very rapid erosion of the 0.020-inch (0.0508-cm) thick ZrC coating of insert 11 may be seen in figure 10. Approximately 20 seconds were required for the surface temperature to exceed the oxidation threshold temperature of the coating. The adherence of the resulting ZrO_2 formation was apparently insufficient to prevent mechanical removal by combustion-gas shear forces. A second run of 72 seconds was made to determine the erosion rate of uncoated ATJ graphite. The rapid erosion (0.004 in./sec or 0.01015 cm/sec) illustrates the need for a protective coating in the oxidizing environment.

Silicon carbide on various graphite substrates. - Monolithic silicon carbide (SiC) has good oxidation resistance at temperatures below 3500° F (2200° K), but generally fails by thermal stress. It was hoped that, if silicon carbide was used as a coating, it would not crack and that the surface could be maintained below the oxidation temperature by the heat capacity of the substrate.

Insert 12 was tested for 12 seconds when the run was ended manually because of a sudden increase in flow rate. No erosion data are plotted because of the short firing time. The coating (0.050-in. (0.127-cm) thick on insert 12) cracked as a result of ther-

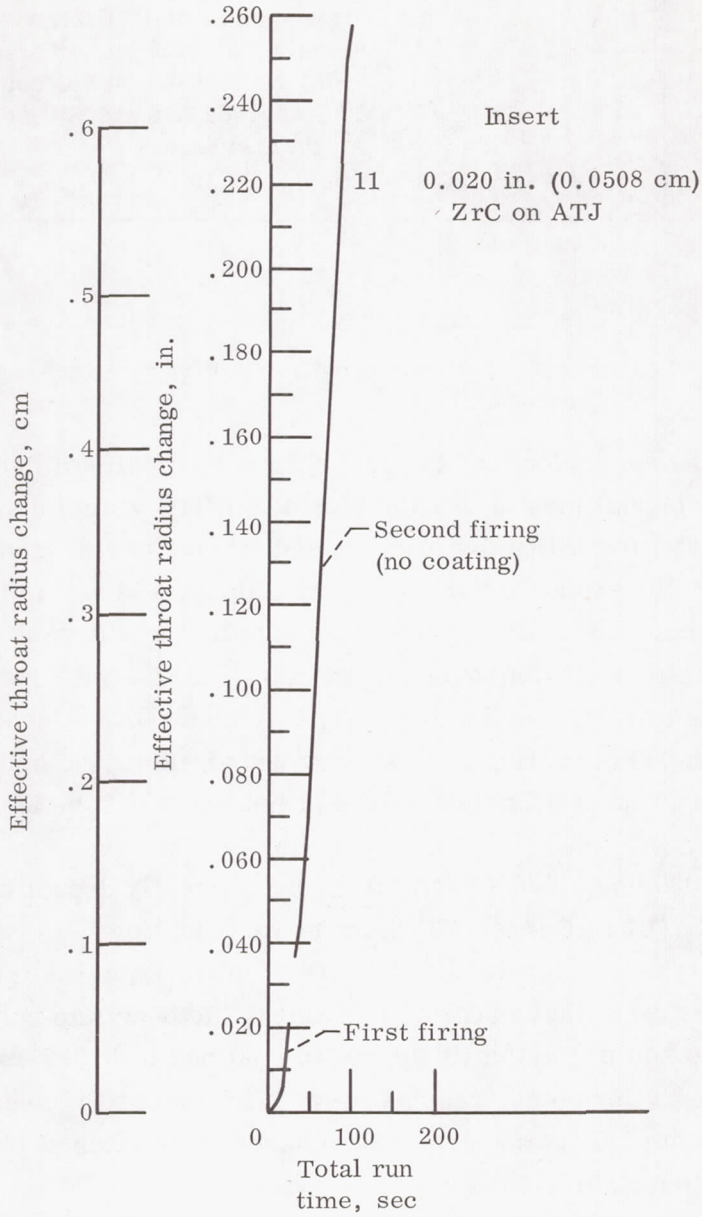

Figure 10. - Throat erosion for zirconium carbide coated AJT graphite inserts.

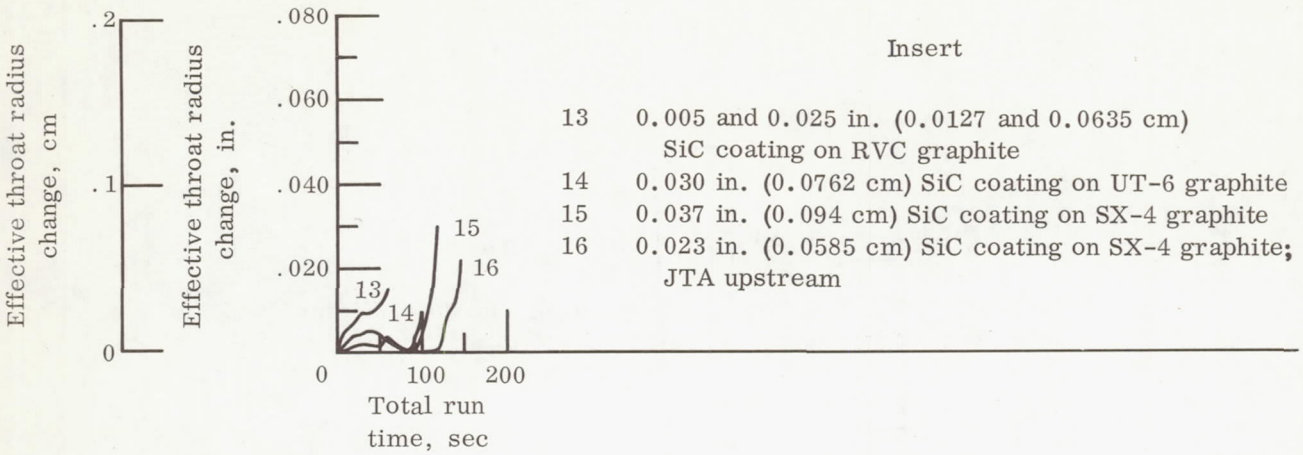

Figure 11. - Throat erosion for silicon carbide coated graphite inserts.

mal stress, and it was concluded that the upper limit for coating thickness was exceeded, at least for pyrolytic depositions of silicon carbide on UT6 graphite substrates.

Data for four additional silicon carbide coated inserts are presented in figure 11.

Insert 13 ran for 60 seconds prior to coating failure, which was thought to be due to oxidation of the coating. The silicon carbide was applied by the pack cementation process, which resulted in a diffusion zone approximately 0.025-inch (0.0635-cm) thick into the RVC graphite substrate and a dense layer of about 0.005 inch (0.0127 cm) SiC on the inside surface. This coating method provided an improved bond between coating and substrate but did not prevent oxidation possibly because of the high porosity of the surface layer.

Insert 14, an 0.030-inch (0.0762-cm) thick pyrolytically deposited coating of SiC on an isotropic substrate (Ultra Carbon UT-6) failed by oxidation after approximately 90 seconds. The oxidation was accelerated by the flow of silica from the upstream silica phenolic liner. In those areas where coating remained, the bond was adherent.

Inserts 15 and 16 had pyrolytically deposited coatings of 0.037-inch and 0.023-inch (0.094- and 0.0589-cm) thickness, respectively. The substrate used for both inserts was Speer SX-4 graphite. This substrate was chosen in an attempt to match the thermal expansion of the silicon carbide coatings during firing.

An upstream liner of JTA graphite was used for insert 16 to eliminate that portion of the oxidation potential caused by the silica flow. Insert 16 was also tested at an oxidant to fuel mixture ratio O/F of 1.6 to further decrease potential oxidation. The results of the firing shown on figure 11 indicate that the oxidation rate for insert 16 was appreciably lower than for 15 because of the JTA liner and the reduced O/F. Insert 16 ran for an additional 25 seconds or roughly 20 percent longer than 15. Matching the thermal expansion of the coating and substrate was successful in preventing thermal stress fail-

ure for these inserts. The firing of the insert is shown in the film supplement.

Iridium coatings. - Work by Englehard Industries and Union Carbide Corporation has established that iridium has excellent resistance to oxidation from 2000° F (1365° K) to its melting point, approximately 4400° F (2700° K). It was, therefore, decided to test iridium as a coating on two different substrates to determine its applicability in this test environment.

Inserts 17 and 18 were prepared by coating 0.005 and 0.003 inch (0.0127 and 0.0076 cm), respectively, of iridium metal on a proprietary graphite substrate. The substrate was compounded to approximately the high thermal expansion of iridium (3.8 (μin./in.)(°R) or 2.1(mm/km)(°K)). The coating was applied by the slurry dip process, which involved many separate operations to build up the required thickness. After application of the slurry and volatilization of the vehicle, each layer, approximately 0.0005-inch (0.00127-cm) thick, was sintered in preparation for the succeeding layer.

The firing data are plotted in figure 12. The firing of both inserts was stopped when a rapid increase in the throat area (see fig. 12) was observed. The type of failure for

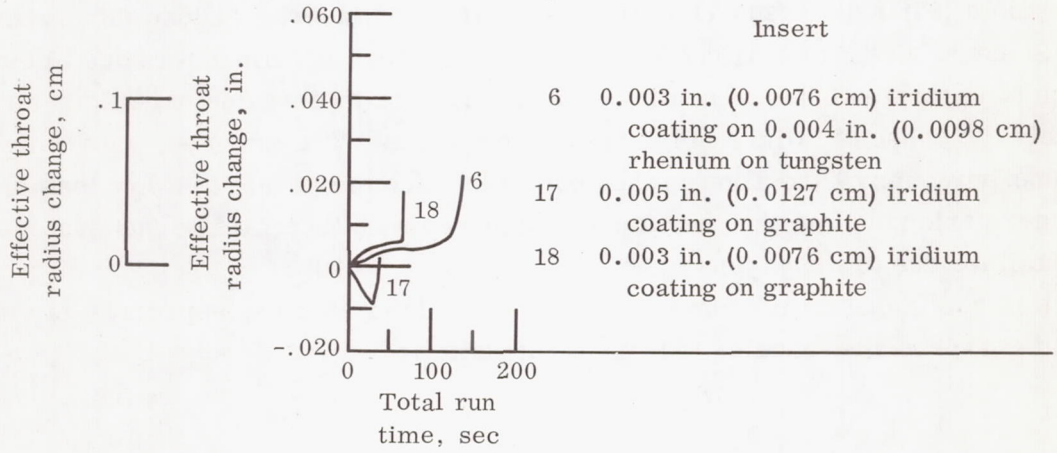

Figure 12. - Throat erosion for iridium coated substrate (graphite or tungsten) inserts.

insert 17 is illustrated in table VI(17). Failure could be assigned to thermal stress due to a mismatch of thermal expansion or by diffusion oxidation. The negative slope recorded for insert 17 during the run could be explained by diffusion oxidation of the graphite substrate, causing carbon dioxide (CO_2) gas pressure buildup between the coating and the substrate. The relatively porous structure of the iridium, inherent with the slurry dip process, may have allowed oxygen to diffuse through the coating, react with the graphite substrate to form volatile CO_2, which caused the coating to lose support, expand outward and finally burst. This would explain the rapid area change. Because the graphite

substrate had been sintered at temperatures in excess of 5000° F (3030° K), it can be safely assumed that residual volatiles were not present in the substrate at the temperature encountered during the firing.

It appears the same process of diffusion was involved in the failure of insert 18, because a thinner coating would tend to decrease the chances of failure by thermal stress. Coating loss was in progressive stages until the throat plane was affected and oxidation of the substrate increased the throat diameter. The coating was probably not strong enough (0.003-inch (0.0076-cm) thick) to remain intact after rupture. This may be seen in the film supplement.

No indication of melting or oxidation of the iridium coating was observed from the previous firings. This leads to the conclusion that an impervious layer of iridium intimately bonded to a suitably high-thermal-expansion graphite would perform satisfactorily in a number of duty cycles. A third insert (6) was prepared by coating approximately 0.003 inch (0.0076 cm) of iridium over a 0.004-inch (0.01015-cm) intermediate layer of rhenium on a tungsten substrate. Because coating techniques were perfected on a tungsten substrate, it was not possible at that time to coat the iridium-rhenium on the high-expansion graphite. Figure 12 shows the erosion data for insert 6. Approximately twice the firing time (136 sec versus 71 sec) was required for insert 6 to lose the coating at the throat. Since no melting or oxidation was noted, the coating failure was due to either a mismatch of expansion between coating and substrate or to diffusion oxidation, as was most likely the cause of failure in the prior two inserts. The tungsten, with a high thermal conductivity, may have allowed the coating surface to operate at a low temperature for a longer period of time than would have occurred with the graphite substrate, thereby delaying failure due to the expansion mismatch.

Work is continuing on iridium coatings at many laboratories, especially in plasma spray and gas-pressure-bonding techniques at Battelle.

Summary of Refractory Coating Systems

The firings showed that oxidation, thermal stress, and loss of coating adhesion are problems that were solved singly but not in combination for the required duty cycle.

The coatings applied by the gas-pressure-bonding technique appeared to be quite dense and fairly adherent in those areas that remained after the firing. The choice of chromium as an intermediate layer was unfortunate. Future work on gas-pressure-bonded coatings appears warranted, particularly the HfO_2 - ZrO_2 system, even though the results were only partially successful.

The use of low-modulus substrates were generally successful in preventing thermal stress failure and loss of adhesion of pyrolytic graphite coatings. A simple radius of

curvature rather than a compound curvature appreciably decreased failure of these coatings by loss of adhesion. The thermal stress failure of silicon carbide coatings can also be prevented by matching the thermal expansion of the coating and the substrate. Coatings less than 0.050-inch (0.127-cm) thick are required for the UT-6 substrate, however.

The oxidation resistance of silicon carbide coatings may be improved by increasing the substrate heat-sink capacity, which would improve coating lifetime.

The iridium metal was very successful in resisting oxidation. The coating also did not melt. Failure, most likely caused by combustion gas diffusion through the relatively porous coating, might be avoided by using an impervious oxidation resistant intermediate layer or by making the iridium itself impervious to the combustion gases.

REFRACTORY COMPOSITES

There are many refractory materials that meet the temperature requirements of the test environment. The difficulty is to find a refractory material or combination of materials that will eliminate or reduce both chemical reactivity and thermal stress to provide throat insert integrity for the required duty cycle.

Graphites, in general, have the necessary structural properties but require combination with other materials to provide oxidation resistance. Unique designs that take advantage of the conductivity of pyrolytic graphite might be used to keep the surface of the insert below the oxidation temperature.

Carbides generally require modifications such as graphite addition or segmenting to prevent thermal stress failure. Oxidation products that remain to protect the surface from further oxidation are desirable to eliminate excessive erosion.

Oxides can withstand the high temperatures and are oxidation resistant but generally require modification to maintain structural integrity. The modification can take the form of segmenting or precracking, addition of refractory-metal reinforcement, or oxide combinations that prevent or minimize cracking by lowering the thermal expansion coefficient.

Graphites

Graphite coated with silicon carbide and zirconium carbide. - A unique technique for improving oxidation and erosion resistance of graphite involved the coating of discrete graphite particles with various carbides. The composite is then compacted to shape with the aid of an inorganic binder.

Inserts 19 and 20 were both proprietary composites consisting of a mixture of sili-

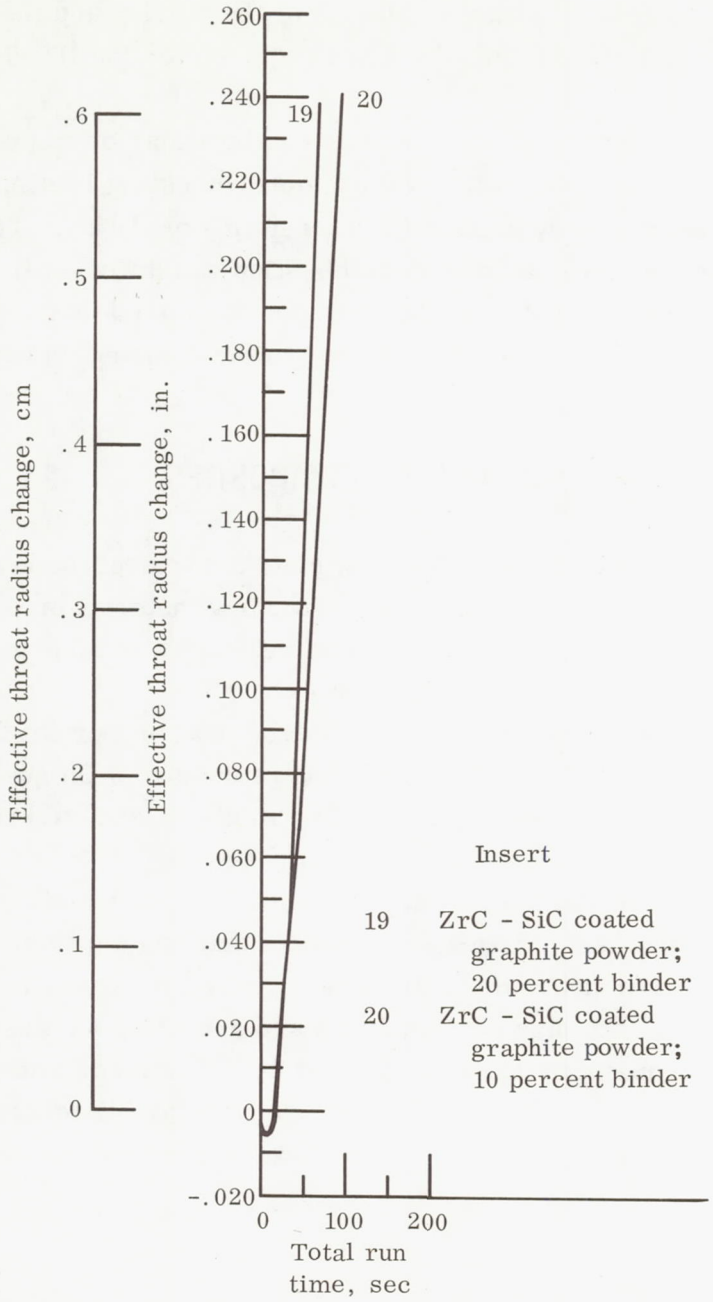

Figure 13. - Throat erosion for zirconium carbide - silicon carbide coated graphite powder inserts.

cone carbide (SiC) coated graphite powder and zirconium carbide (ZrC) coated graphite powder with an inorganic binder. Insert 19 contained 20 percent binder compared with 10 percent binder for insert 20. According to the supplier, the binder was a zirconia-base resin. Figure 13 presents the firing data for both inserts. Very high erosion rates were recorded and were due primarily to physical erosion of discrete particles rather than oxidation, which would be more time-temperature dependent. The lower binder content of insert 20 provided some improvement in erosion resistance over the higher binder content of insert 19. However, these materials apparently could not meet the necessary structural requirements of the high-shear, rocket-nozzle environment.

JTA graphite (carbon, silicon carbide, and zirconium bromide). - JTA is a commercial grade of graphite. It has been compounded to provide oxidation resistance while maintaining high resistance to thermal stress.

Figure 14 compares the erosion resistance of inserts 21 and 22, both JTA graphite material. The first comparison is the effect of oxidant-to-fuel mixture ratio. The time at which significant erosion was first detected was increased from 75 seconds at an O/F of 2.0 to 120 seconds at an O/F of 1.6. Operation at the lower O/F would give

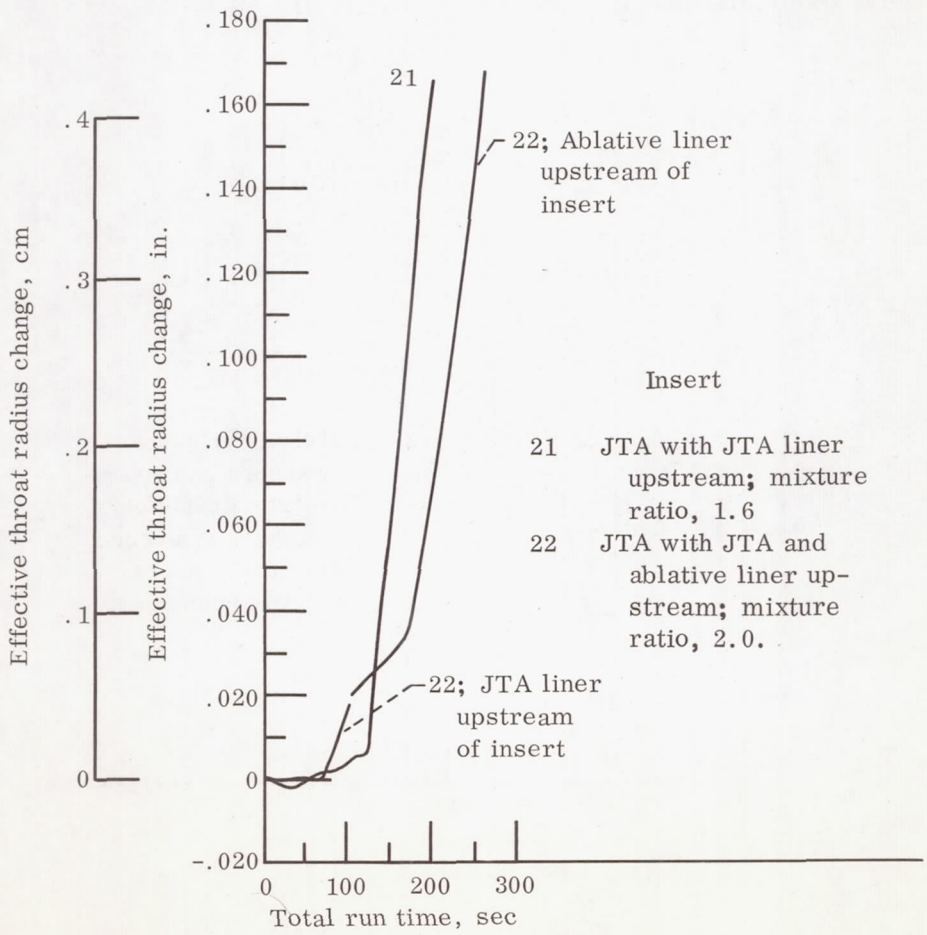

Figure 14. - Throat erosion for JTA graphite inserts.

a 60-percent increase in useful lifetime.

A second firing was made on insert 22 with an ablative liner substituted for the JTA liner upstream of the insert. It was hoped the ablative gases would provide significant cooling for the throat insert and increase the useful life of the insert. The curve on figure 14 indicates that the ablative liner did not significantly improve the erosion resistance of this particular JTA insert.

The oxides formed on the surface of the JTA inserts by the oxidizing combustion gases were not adherent enough to provide erosion protection and were removed rapidly in the high-velocity, high-shear, rocket-throat environment. However, JTA graphite performs satisfactorily as a chamber liner where a Mach number approximately 0.2 produces lower velocity-shear forces from the combustion gases.

Pyrolytic graphite. - The erosion rate of pyrolytic graphite, due primarily to oxidation, is a function of temperature. Orientation also has a minor effect on the erosion rate because of the low shear strength of the basal planes. Orientation of the layer planes preferentially to improve heat transfer from the surface may result in a surface temperature that is below the oxidation threshold for pyrolytic graphite.

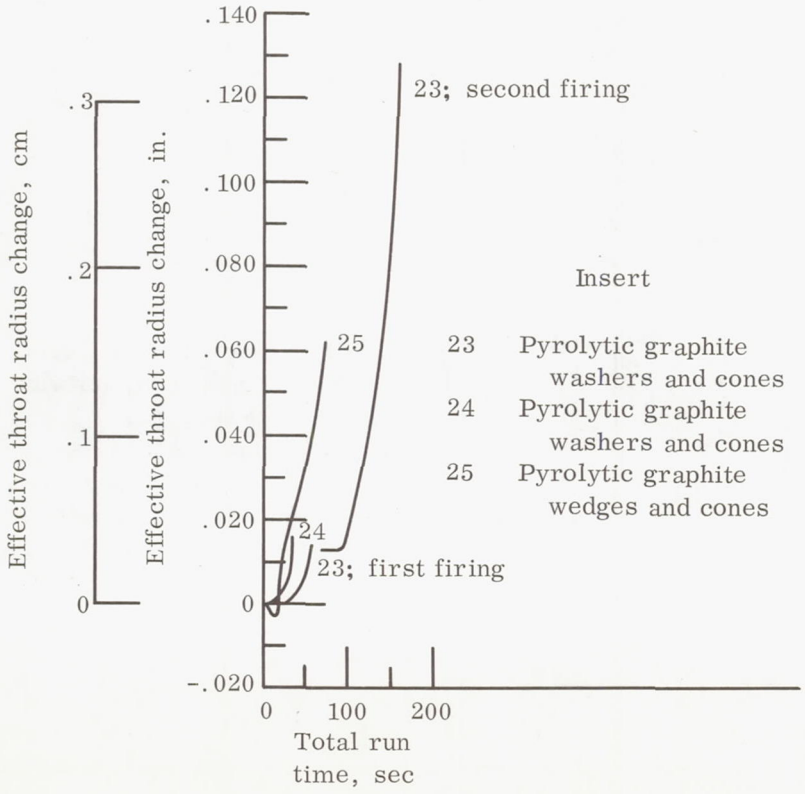

Figure 15. - Throat erosion for pyrolytic graphite inserts.

Inserts 23, 24, and 25 were fabricated from monolithic sheets of pyrolytic graphite. The sheets were machined into washers and were axially stacked for inserts 23 and 24. Wedges were machined and arranged circumferentially for insert 25. The ab (high conductivity) plane was radial and circumferential for the washers and radial and axial for the wedges. All three had a cone of pyrolytic graphite which slipped over the outside diameter of the washers or wedges. The cone had the ab plane oriented axially and circumferentially to provide an insulating layer on the insert outside diameter and also to conduct heat away from the throat region. Figure 15 is a plot of the erosion for the three inserts. All runs required approximately 25 seconds before the surface temperature was sufficiently high to initiate erosion. It was concluded that the temperature and oxidation potential of the test environment were too high to allow use of pyrolytic graphite in these design configurations. Insert number 23 was run an additional 100 seconds to confirm the time-temperature dependency of pyrolytic graphite oxidation. Approximately 25 seconds were required for the surface to reach a temperature at which oxidation was most rapid. The time-temperature dependency was, therefore, confirmed.

Carbides

Silicon carbide, segmented. - Three segmented silicon carbide (SiC) inserts were fired to evaluate thermal shock and oxidation resistance. Insert 26 was an assembly of three stacked washers. The washers of insert 27 were cut into 180° segments and were contained by a 0.250-inch (0.635-cm) thick SiC sleeve. Insert 28 was the same as insert 27 except that the three washers were cut into 120° segments and bonded together with a low-modulus sealer. An ablative material was used upstream for inserts 26 and 27, and a JTA liner was used for 28.

Figure 16 presents the firing data for the three inserts. The improved erosion resistance of insert 27 over that of insert 26 was probably due to the addition of the SiC sleeve, which provided greater heat-sink capacity and also retained the segmented washers more securely.

The substitution of the JTA liner upstream together with the increased number of segments apparently decreased the oxidation resistance of insert 28 as seen by comparing the erosion of insert 28 with that of insert 27 (fig. 16). The JTA liner could have increased oxidation by keeping ablative cooling gases out of the boundary layer and thereby increasing the surface temperature more rapidly. Close inspection of the insert indicated more oxidation at the axial interfaces of the segments; thus, more segments may mean more oxidation.

Hypereutectic carbides. - Hypereutectic carbides containing excess primary graphite were developed to minimize thermal-stress cracking by providing a low-modulus, crack-

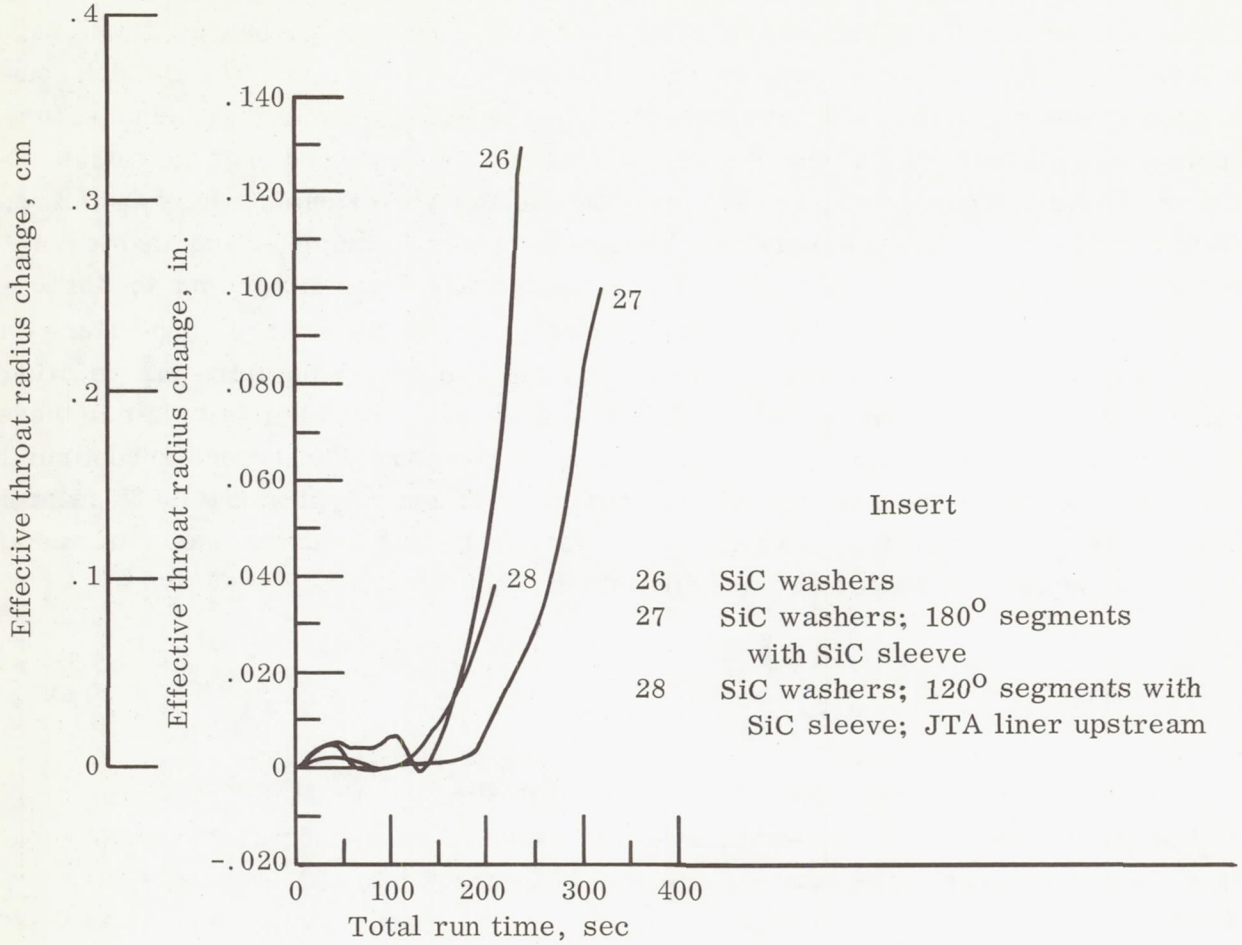

Figure 16. - Throat erosion for segmented silicon carbide inserts.

arresting material within the crystalline structure of the carbides. An increase in the erosion resistance with time was also expected because of the formation and retention of a surface oxide layer.

The firing data are presented in figure 17 for inserts 29 (ZrC plus graphite) and 30 (hafnium carbide (HfC) plus graphite). The first run of 25 seconds for insert 29 (ZrC plus graphite) was aborted because of a gas leak in the combustion chamber. The formation of an oxide layer reduced the measured throat radius approximately 0.025 inch (0.0635 cm). A second run was made for about 153 seconds at which time small pieces of the oxide layer came off at the throat. Excessive erosion at the upstream interface between the insert and the ablative material caused gas to flow around the outside diameter of the insert resulting in test termination (rapid area increase is shown in fig. 17). The final appearance of this insert (table VI(29)), however, indicates that the material has promise. No cracking or rapid removal of the oxidation products was experienced.

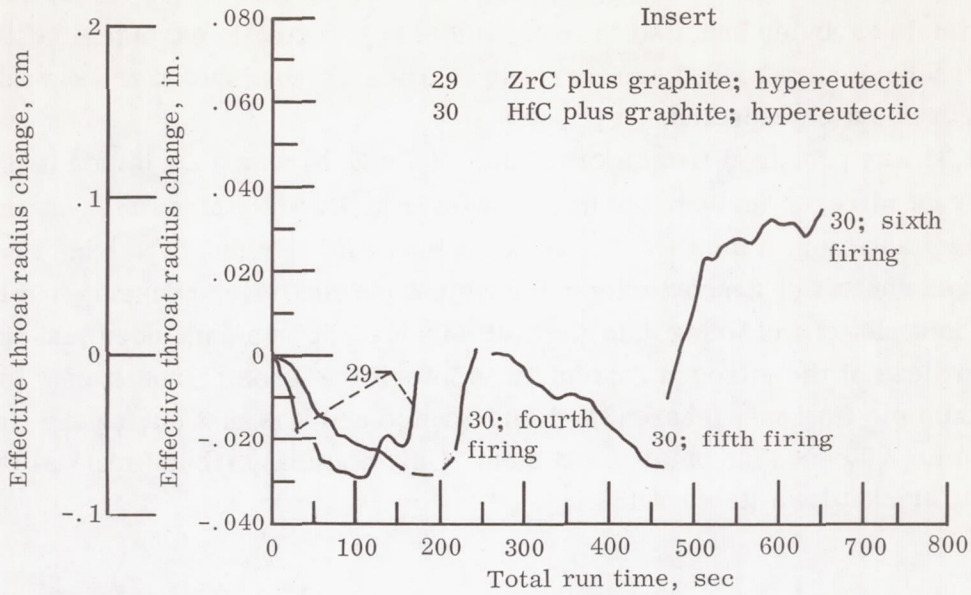

Figure 17. - Throat erosion for hypereutectic carbide inserts.

Insert 30 (HfC plus graphite) was run initially for 159 seconds with no erosion. When a gas leak occurred, the test was stopped. The formation of an oxide layer reduced the measured throat radius approximately 0.041 inch (0.104 cm). The second and third firings were aborted because of water leakage in the combustion chamber. The fourth firing of 51 seconds was shut down because of apparent erosion as shown in figure 17. The erosion was caused by partial loss of the oxide layer. The oxide layer that remained at this stage, although somewhat rough, seemed adherent enough to permit further testing. Two additional 200-second firings were made. The overall erosion shown in figure 17 was partly due to oxidation and subsequent removal of the oxide layer. Also contributing to erosion was loss of the trailing edge of the insert due to insufficient throat support (see table VI(30)). The number of cycles (6) and the total firing duration (655 sec) indicate the suitability of this material for application in the test environment. In addition, a substantial reduction of the upstream erosion for insert 30 was obtained by using a zirconia liner in place of the JTA of insert 29 (see tables VI(29) and (30)). Unfortunately, because of fabrication facility size limitations, inserts 29 and 30 were unavoidably fabricated to the configuration shown in figure 5(c), which undoubtedly contributed to leading and trailing-edge failure problems. A further improvement in overall performance would be expected if configuration B (fig. 5(b)) were used to provide an insert with higher contraction and expansion ratios.

Hypereutectic carbonitrides. - Proprietary compositions of hypereutectic carbides, which included small amounts of nitrogen were prepared. An excess amount of graphite

was also used. The purpose was to improve the thermal-stress and oxidation characteristics of simple carbides and also to improve the hypereutectic carbides. If the nitrogen were electrochemically bonded, an increase in oxidation resistance and overall composite strength would be expected.

Insert 31 was prepared from a cast billet of Zr(C, N) which contained less than 0.10 weight percent nitrogen (private communication from Battelle Memorial Institute). Insert 32 was made from a mixture of ZrC and zirconium nitride (ZrN) which resulted in a final nitrogen content of approximately 1.0 weight percent after pressing and sintering. Figure 18 is a plot of the firing data for both inserts. It was concluded that the case insert, regardless of the nitrogen content, was inferior in erosion resistance to the hot-pressed sample. The cast insert (31) disintegrated and was lost during the firing. Insert 32 ran for 200 seconds prior to erosion. Only nominal circumferential cracking was observed after shutdown (table VI(32)).

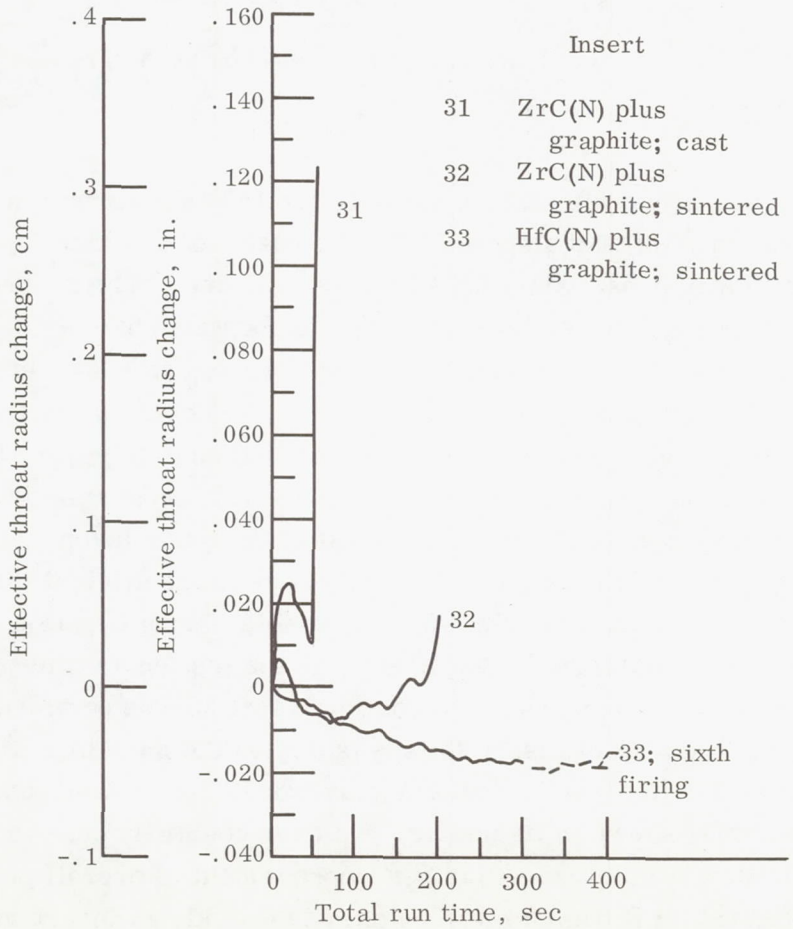

Figure 18. - Throat erosion of hypereutectic carbonitride inserts.

To assess the advantage of a more refractory hypereutectic carbonitride, insert 33 was fabricated of hafnium carbonitride (Hf(C, N). The firing data, presented in figure 18, suggest that the substitution of hafnium for zirconium is highly beneficial. A sintered hafnium carbonitride ran for 300 seconds followed by five 20-second runs. No erosion was observed; however, a distinct oxide layer formed on the inside surface during firing (table VI(33)). The oxide layer (about 0.100-in. (0.254-cm) thick) was weak and nonadherent, so further testing was not done. A postfiring analysis on this layered material indicated the white layer on the inside surface was hafnium oxide with some carbon.

The surface layer contained many small fissures or checks which did not extend into or degrade the primary material structure. Surface checking is caused by thermal stresses in the relatively weak chemical reaction zone which is formed in place during rocket firings. Mechanical erosion could result from spallation of surface particles when the local shear forces exceed the shear strength in the reaction zone. The difference between the oxidized layer and the material underneath is shown in figure 19. The bond between the two materials was weak with an excess of carbon in the area. Further development should be concentrated on strengthening the oxide layer and eliminating the cause of

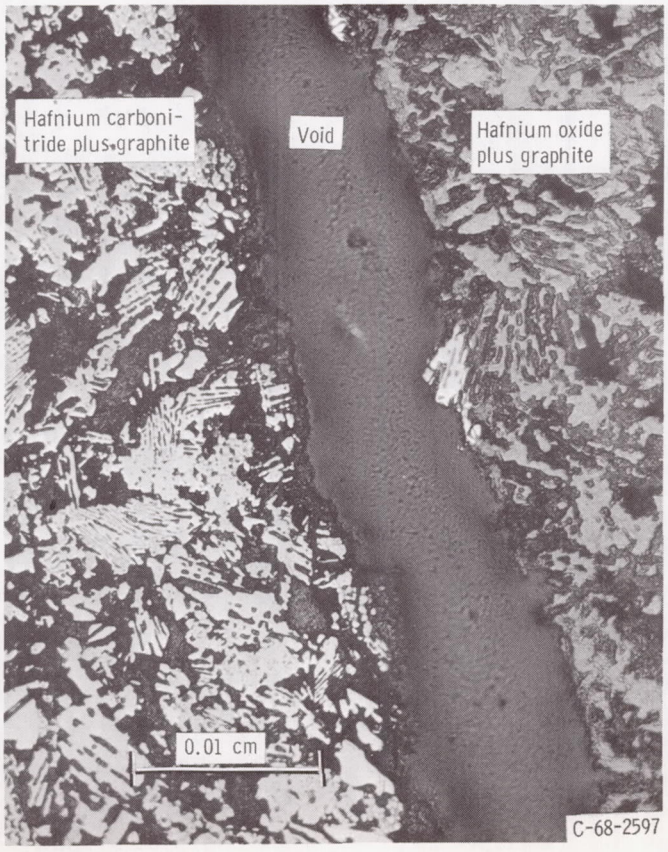

Figure 19. - Postfiring photomicrograph of hafnium carbonitride insert (33).

the bond weakness between the two zones.

JT0981 (zirconium carbide - silicon carbide - graphite). - Insert 34 was a composite material of ZrC and SiC with about 35-weight-percent excess graphite. An upstream liner of the same material was used. The throat erosion of insert 34 is plotted in figure 20. The relatively low erosion resistance was probably due to the poor adhesive qualities of the ZrO_2 and the possible formation of low-melting-temperature silica eutectics. The severe erosion at the leading edge is indicative of the low shear force resistance at this Mach number.

JT0992 (hafnium carbide - silicon carbide - graphite). - Inserts 35 to 37 were composites of HfC and SiC with about 25-weight-percent excess graphite. Inserts 35 and 36 both used an ablative liner upstream, and number 37 had the same composite material

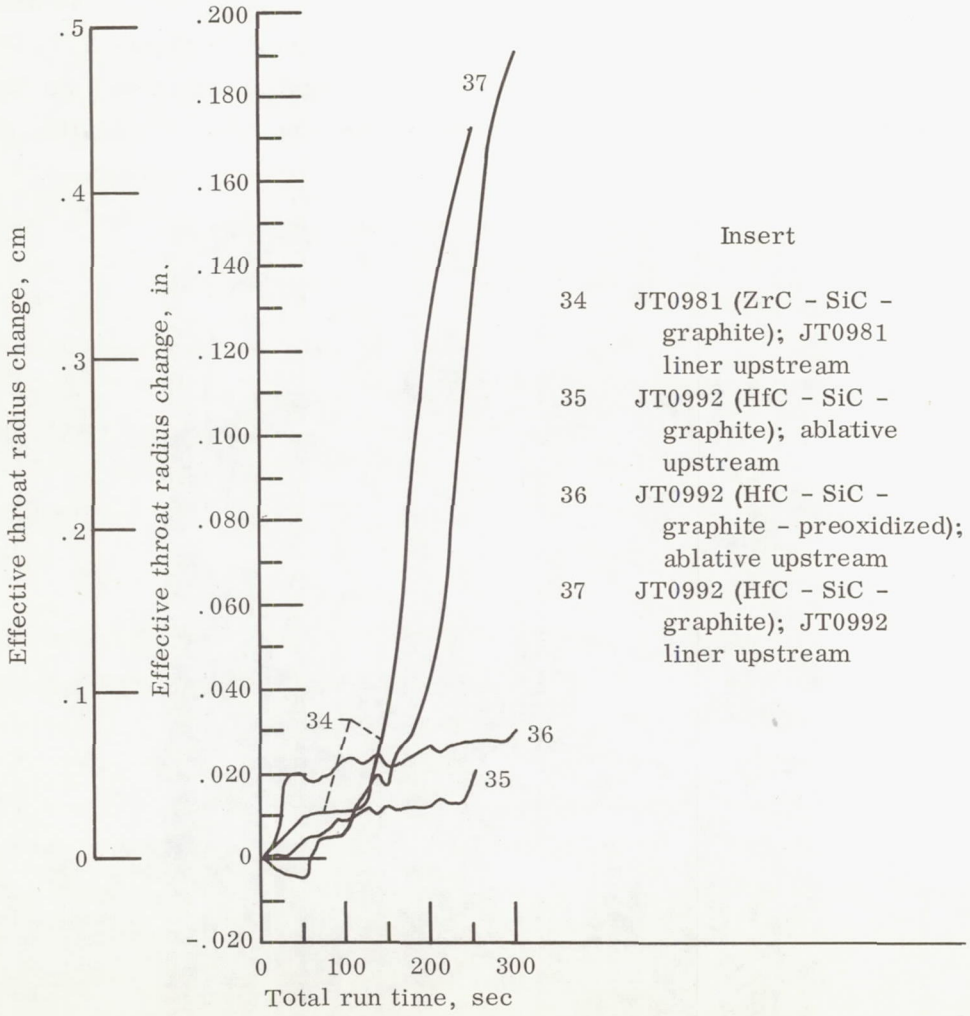

Figure 20. - Throat erosion for graphite - carbide composite inserts.

upstream as was used for the throat insert. The material used for insert 36 was preoxidized to evaluate the effect of a surface oxide layer prior to the firing.

The firing results for all three inserts are plotted in figure 20. The steady-state erosion was approximately equal for inserts 35 and 36. However, there was a large initial increase in the throat area of insert 36, obviously caused by the physical removal of the preoxidized surface layer. Both inserts were in excellent condition after the firing; however, ablative char-through made further testing impractical. No cracking or spalling was observed (see tables VI(35) and (36)). The inferior erosion resistance of insert 37 was probably due to the JT0992 liner material upstream, which did not contribute to boundary-layer cooling as the ablative material apparently did for inserts 35 and 36. The results of spalling and a rough oxide layer can be seen in table VI(37).

Oxides

Silicon dioxide, graphite. - Insert 38, an 80-weight-percent-silicon dioxide (SiO_2) - 20-weight-percent-graphite composite, experienced severe erosion. The run data are plotted in figure 21. Even though the chamber pressure was accidently low (45 to 61 psia or 310 to 420 kN/m^2), failure indicated the unsatisfactory nature of this material in the test environment, due to its relatively low melting point and lack of composite strength.

Zirconium oxide foam, phenolic resin. - The run data for insert 39, a composite of 56-weight-percent ZrO_2 foam with a 44-weight-percent phenolic resin binder, are plotted in figure 22. Very rapid and severe physical erosion was experienced because the foam lacked strength and the phenolic decomposition products did not provide sufficient protection.

Zirconium oxide-yttria stabilized. - Zirconium oxide is a very interesting material for use in the storable-propellant environment. Its melting temperature in excess of 4500° F (2750 K) and its high resistance to oxidation together with high strength make it very attractive. Unfortunately, unalloyed ZrO_2 is highly susceptible to thermal stress cracking. When unstabilized pure ZrO_2 is heated, the crystalline structure changes from monoclinic to tetragonal, which results in a volume decrease. To prevent cracking, which is associated with this volume change, from taking place, various stabilizing agents have been tried. Calcium oxide is one of the most commonly used stabilizers and has been effective for low heat-flux environments. It has not proved successful where the heat flux has been large, as is typical in a rocket engine. The Air Force has experimented with the use of rare earth oxides as stabilization agents for ZrO_2 (ref. 5). Recently, yttria (Y_2O_3) was shown to be quite promising. Four yttria-stabilized inserts were evaluated (inserts 40 to 43). Inserts 40 and 41 were compacted to approximately 75 percent theoretical density, and inserts 42 and 43 had a density of 90 percent. The low-density

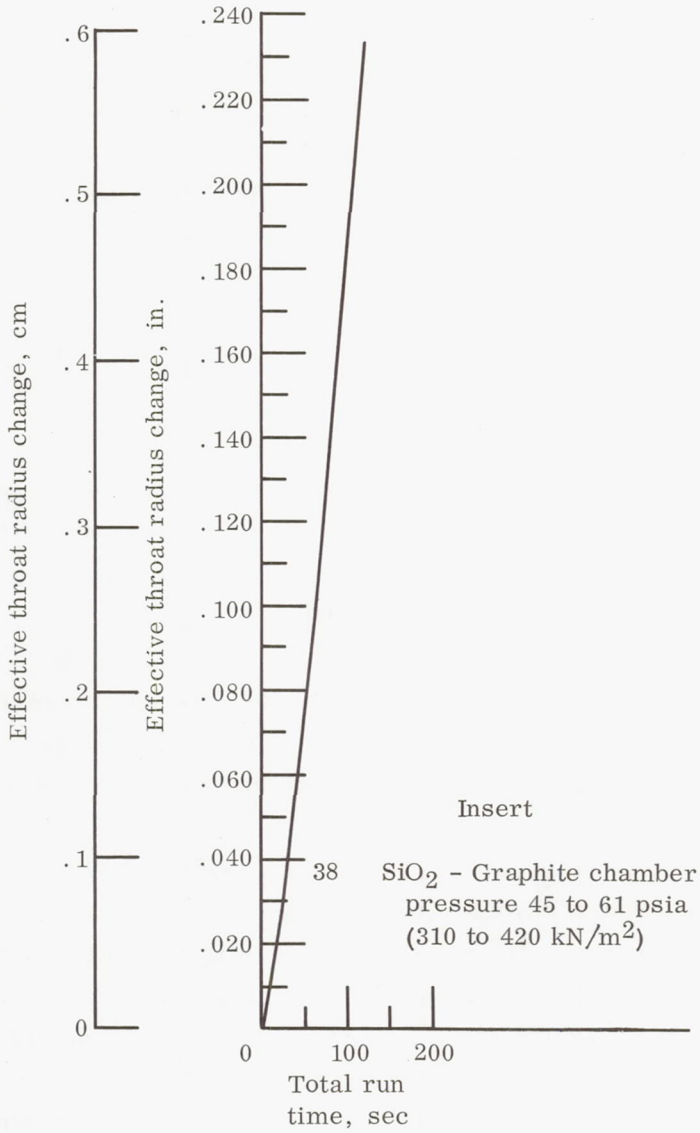

Figure 21. - Throat erosion for silicon dioxide-graphite composite insert.

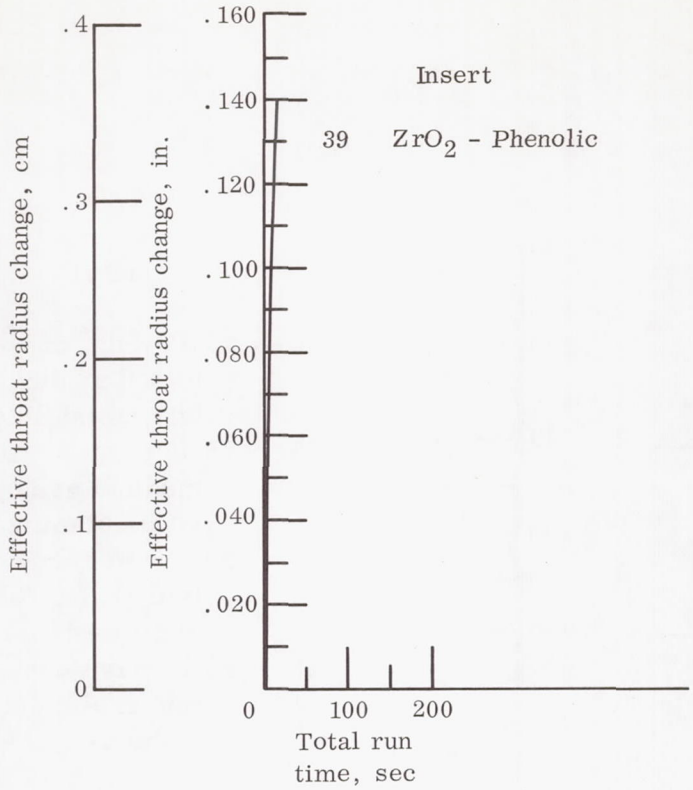

Figure 22. - Throat erosion for zirconium oxide foam and phenolic resin binder composite insert.

material used relatively coarse grain; whereas the higher density inserts were made from a finer grain material. The two high-density inserts (42 and 43) were obtained from different suppliers to measure the effect of manufacturing technique. Figure 23 shows the firing results of the four inserts. All were severely cracked after firing (see tables VI(40) to (43)). It was not determined why these yttria-stabilized inserts eroded so rapidly and were so weak after firing. Possible sources of failure may be found in the material and process control records.

Zirconium oxide, sintered, mixed grain size. - The firing data for three ZrO_2 inserts (44 to 46) are presented in figure 24. All three inserts were hot pressed from a mixed-grain-size, magnesia-stabilized mix. The outside of insert 44 was machined to have approximately one-half the wall thickness of the other two inserts in an attempt to minimize thermal stresses. A 0.250-inch (0.508-cm) thick RVC graphite sleeve was used as a backup material for insert 44. Slight axial and circumferential cracks were observed on the inside surface after the initial 60-second firing. The second firing of insert 44 resulted in loss of the insert throat section. Note the rapid increase in throat radius shown

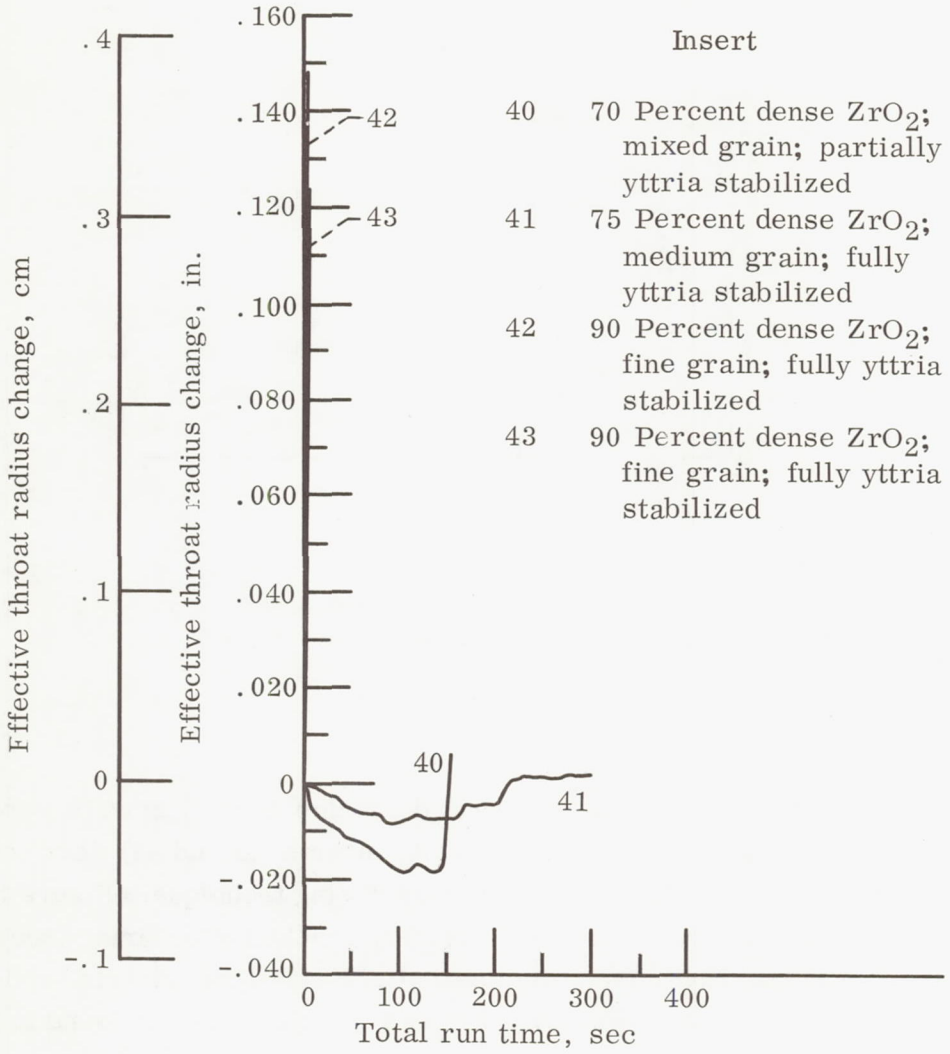

Figure 23. - Throat erosion for yttria stabilized zirconium oxide inserts.

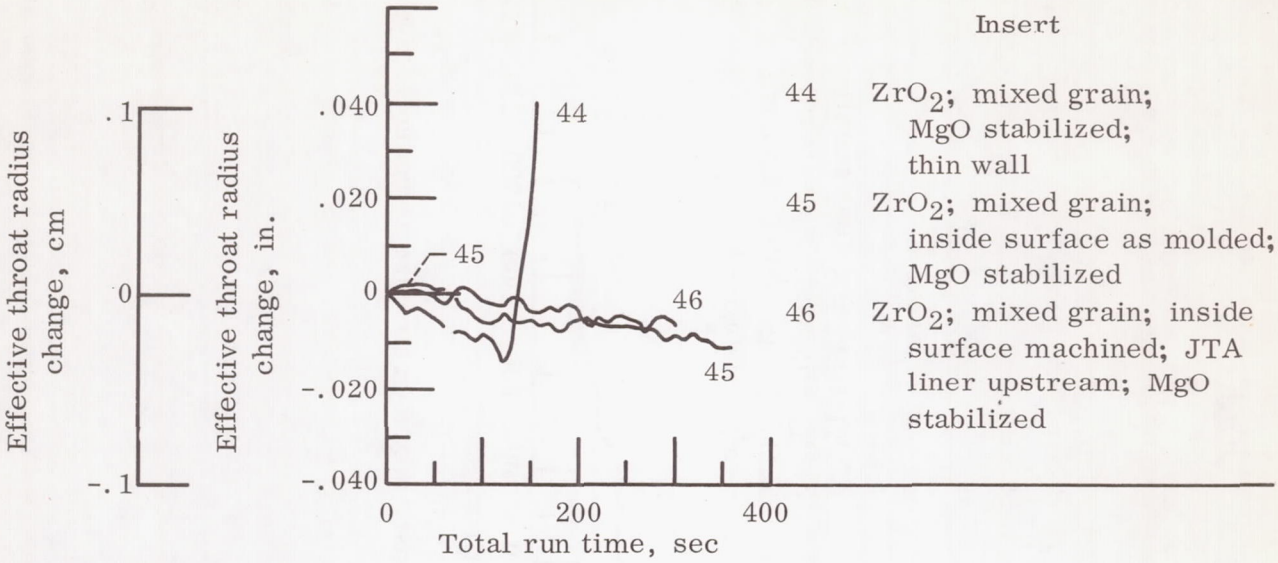

Figure 24. - Throat erosion for sintered, mixed-grains size zirconium oxide inserts.

in figure 24 and the post-test photograph in table VI(44). This is also the type of catastrophic failure observed when structural failures occur in larger throat sizes (ref. 2).

Insert 45 also was slightly cracked on the inside surface after the initial 60-second firing. A subsequent 300-second firing produced further cracking and some loss of material downstream of the throat. Table VI(45) illustrates loss of material as well as the reaction of the insert with molten SiO_2. The formation of low-temperature melting point silicates should be avoided.

Insert 46 was fired for 300 seconds continuously with no throat erosion and only minor axial cracks. A small piece of material was lost downstream of the throat (table VI(46)). Use of the JTA liner upstream of the throat insert eliminated the effect of silica attack on the insert leading edge. Comparison of table VI(45) and (46) illustrates the advantage of the JTA liner in preventing silica attack. No significant difference in structural behavior was noted between inserts 45 and 46 as a result of machining the inside surface of insert 46 compared with leaving the inside surface of insert 45 as molded. Both inserts were capable of being rerun and show considerable promise. Running was terminated because of complete char-through of the ablative holder.

Zirconium oxide, slip cast mixed-grain size. - Insert 47 was prepared from slip-cast ZrO_2 stabilized with calcium oxide (CaO); the stabilization agent used for 48 and 49 was magnesium oxide. The importance of stabilizing ZrO_2 is due to the volume change

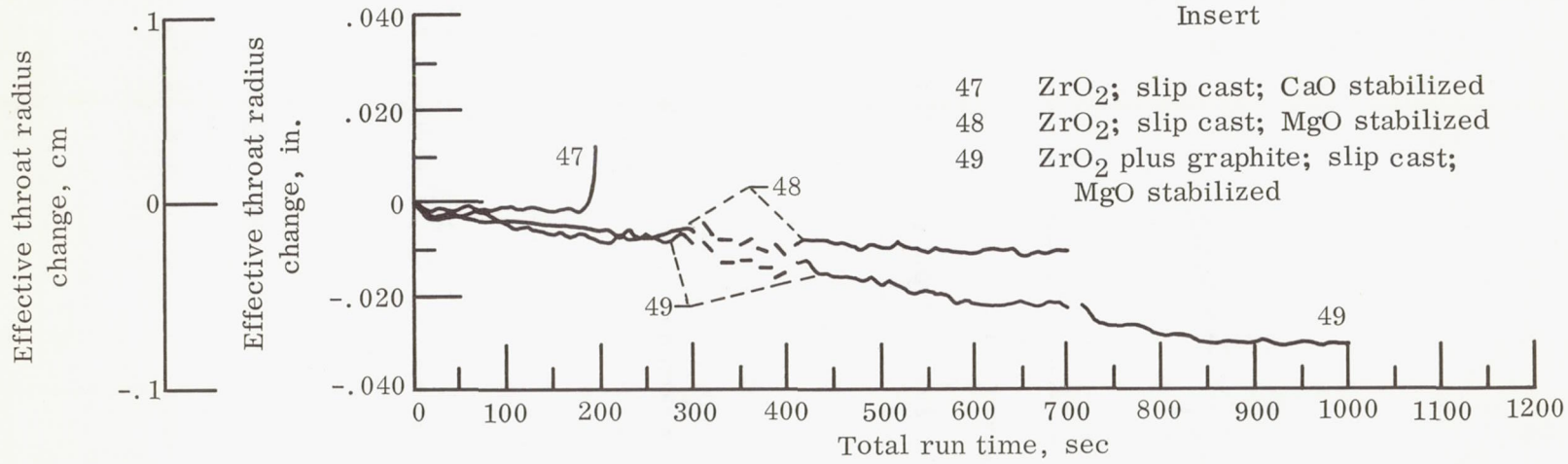

Figure 25. - Throat erosion for slip-cast, mixed-grain-size zirconium oxide inserts.

associated with the phase change from monoclinic to tetragonal. Insert 49 also contained a small amount of carbon powder as an aid in crack prevention. Mixed-grain-size ZrO_2 was again used because of its past performance and to compare directly with pressed and sintered inserts 44 to 46. Figure 25 compares the erosion results for the three inserts. The failure mechanism of insert 47 was severe cracking and spallation possibly due to the inability of calcium oxide to adequately stabilize zirconium oxide in the test environment.

Inserts 48 and 49 were both run for the entire duty cycle of 300 seconds followed by five 20-second firings and ending in a final 300-second run. These inserts were slightly cracked axially during the initial firing in a manner similar to the hot pressed inserts (44 to 46). Subsequent firings caused no substantial loss of material even through the inserts were cracked. No significant difference in behavior was noted due to the addition of carbon to the ZrO_2 of insert 49. In order to establish the design limits, this particular insert was run for an additional 300 seconds with no significant change. The throat radius decrease observed could have been due to the volume change associated with the phase change from monoclinic to tetragonal, typical of ZrO_2 material when not fully stabilized. The throat radius change was linear even beyond the 700-second design point. The lower cost of the slip-cast material relative to the sintered material appears attractive for large-scale application if the structural cracking can be controlled.

Zirconium oxide-copper (anion deficient). - Five proprietary (unpublished data from S. Brown, Rocketdyne Div. of North American Aviation Corp.) anion deficient ZrO_2 inserts were test fired. Copper was added to the ZrO_2 matrix to increase the thermal shock resistance. The variables investigated were copper content and insert wall thickness. Firing data for inserts 50 to 54 are presented in figure 26.

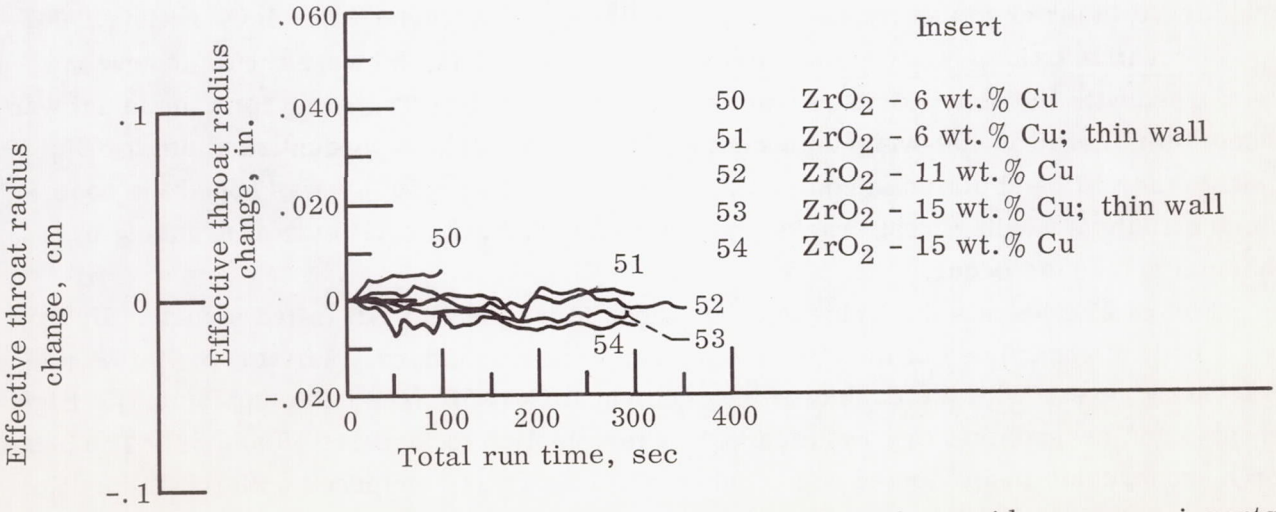

Figure 26. - Throat erosion for zirconium oxide - copper inserts.

Insert 50 (6 wt. % Cu, 0.53-in. (1.345-cm) wall thickness) was run for one continuous firing of 100 seconds. The run was terminated because of a propellant leak, and the insert was examined at the time. Several severe circumferential cracks were observed (see table VI(50)). Insert number 51 (6 wt. % Cu, 0.30-in. (0.762-cm) wall thickness) was of thin-wall construction. The insert was tested for 300 seconds and examined. Although both axial and circumferential cracking was observed, the nature and extent of the cracks were less than in the thicker (0.53 in. (1.345 cm)) wall of insert 50.

The results of the preceeding tests proved that structural failure was the problem to attack. Subsequent firings were eliminated, so that cracking severity could be compared after a single firing. The 300-second firing time was selected to establish erosion resistance of the ZrO_2-copper composite. To improve the crack resistance of insert 52 over that of 50 and 51, the copper content was increased from 6 to 11 weight percent. The insert was tested for 357 seconds and examination revealed moderate axial cracking, but the circumferential cracks were eliminated. The film supplement shows this firing. Based on these firing data, the copper content for inserts 53 and 54 was increased to 15-weight-percent copper. Two wall thicknesses were tested at the 15-weight-percent copper concentration for 300 seconds. Circumferential cracking was more severe for the 0.53-inch (1.345-cm) wall than the 0.38-inch (0.966-cm) thin-wall design. The thick-wall 15-weight-percent copper insert was severely cracked circumferentially compared with less severe axial cracks for the thick-wall 11 weight percent copper insert 52. If further tests were to be made, the composite could be a thin-walled (0.38 in. (0.966 cm)) design containing approximately 11-weight-percent copper. Tables VI(50) to (54) show post-test photographs of all the inserts.

This concept showed considerable merit. A segmented design might solve the cracking problem. However, special attention to processing parameters would also have to be considered in order to assure even copper distribution throughout the ZrO_2 matrix.

Zirconium oxide, honeycomb reinforced. - Inserts 55 to 58 were metal-honeycomb reinforced with the honeycomb cell walls oriented radially. The honeycomb material was Inconel for insert 55, 50-weight-percent platinum - 50-weight-percent rhodium for 56, tungsten for 57, and platinum coated molybdenum for insert 58. It was hoped the honeycomb structure would arrest cracks and retain the ZrO_2 material even if cracking by thermal stress did occur.

Figure 27 presents the firing data for these four inserts. All failed structurally to some degree regardless of the reinforcing honeycomb employed. Surface spallation was extremely severe with the Inconel reinforcement (insert 55) (see film supplement). High erosion and severe cracking resulted in test termination for inserts 56 and 58. The best ZrO_2-honeycomb insert tested was number 57, which was reinforced with tungsten. No throat erosion was measured but cracking and loss of material downstream of the throat precluded further testing (table VI(57)).

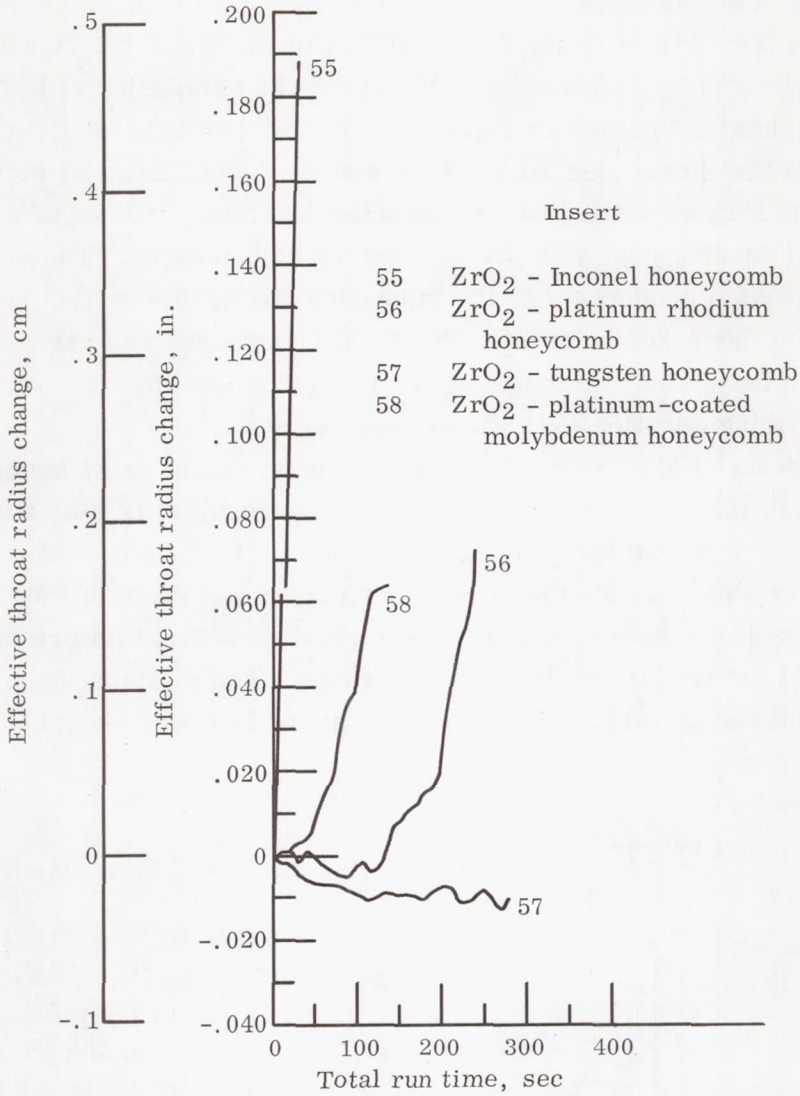

Figure 27. - Throat erosion for honeycomb reinforced zirconium oxide inserts.

The wide range of behavior between these inserts indicates the need for careful matching of the ceramic with the honeycomb reinforcing material with regard to chemical compatibility, melting point of the honeycomb, and relative thermal expansion coefficients.

Magnesium oxide, honeycomb reinforced. - Insert 58 was magnesium oxide (MgO) reinforced with mild steel honeycomb, and insert 60 was MgO reinforced with Inconel honeycomb. They were tested to evaluate the suitability of the MgO, the relative merits of Inconel and steel reinforcing, and the compatibility of the composite with the test environment. The firing data are plotted on figure 28. Both inserts failed structurally upstream and downstream of the throat (see table VI(59) and (60)). Although no significant throat erosion was noted, further testing was not practical because erosion of the ablative material at the insert leading edge was pronounced for both inserts. The chemical reactivity effects of ablation products with the insert leading edge was also noticeable, particularly for the steel honeycomb insert. The steel honeycomb was rated superior to the Inconel honeycomb because of its longer total firing duration (321 sec versus 209 sec) and the longer single firing duration (261 sec versus 141 sec).

Additional inserts of MgO reinforced with platinum coated steel honeycomb (61) and platinum honeycomb (62) were fabricated. The firing results are also shown in figure 28 and the post-test photographs are in table VI(61) and (62). Leading-edge failure and chemical reactivity was alleviated by using a JTA liner upstream of the throat insert. The platinum-coated steel honeycomb did not prevent structural failure of the ceramic matrix of insert 61 but throat erosion was prevented. The platinum honeycomb reinforced MgO (insert 62) showed no failure over the run time of 143 seconds. Unfortunately, fail-

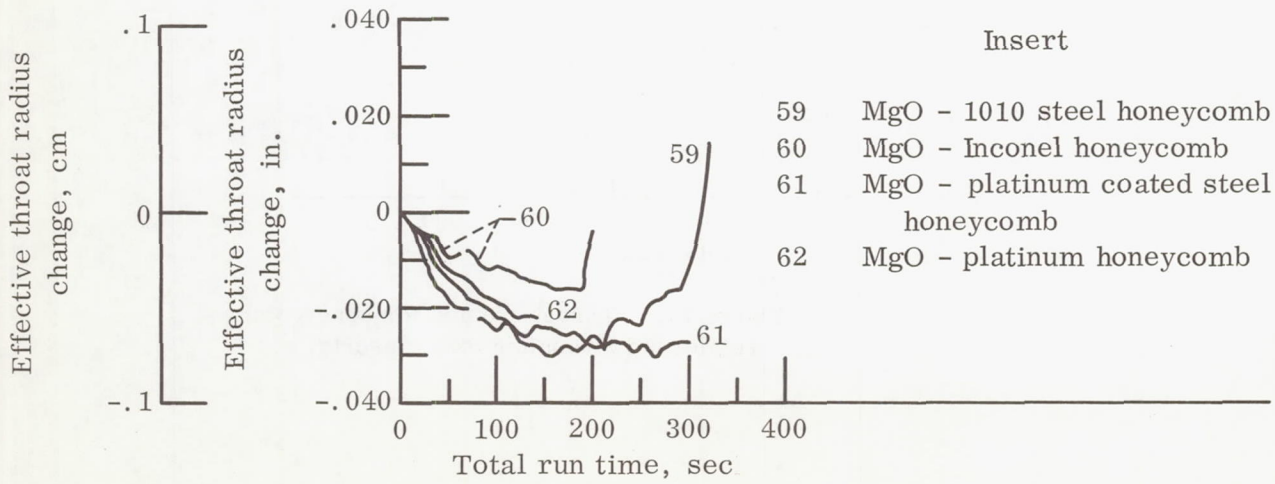

Figure 28. - Throat erosion for honeycomb reinforced magnesium oxide inserts.

ure of the ablative envelope seal precluded further testing. Additional testing of platinum honeycomb reinforced MgO is required to establish performance limits. Variation in honeycomb geometry might be used to prevent structural failure with other material combinations.

Magnesium oxide, fiber reinforced. - Metal fibers (5 vol. %) were added to MgO in order to minimize thermal stress cracking. It was desired to obtain inserts with a uniform, random dispersion of metal within the ceramic matrix. However, examination of the completed inserts revealed the presence of stratified layers of circumferentially oriented fibers. It was decided, nevertheless, to test the inserts to see whether the stratified layers with specific fiber orientation would perform satisfactorily.

Figure 29 presents the firing data for the three inserts - insert 63 was MgO with 0.0003-inch (0.00076-cm) diameter Inconel fibers, insert 64 was MgO with 0.005-inch (0.0127-cm) diameter Inconel fibers, insert 65 was MgO with 0.0003-inch (0.00076-cm) diameter tungsten fibers. The results indicate superior performance for the smaller diameter fibers. Inconel was also found to be superior to tungsten as a reinforcement, probably because of the high susceptibility of tungsten to oxidation and also the superior ductility of the Inconel.

Post-test inspection (see table VI(63) to (65)) indicated that the erosion was due to structural failure and rapid loss of surface layers. Cracking was largely circumferential and located where the fiber stratification was greatest. An improvement in the inserts structural strength and erosion resistance might be expected if a uniform dispersion and random orientation of the metal fibers could be procured.

Beryllium oxide, prestressed. - Insert 66 was prepared by hot pressing and sintering BeO powder. After machining to shape, a 0.125-inch (0.318-cm) thick steel sleeve was interference fitted to the outside diameter. The prestress was intended to apply compres-

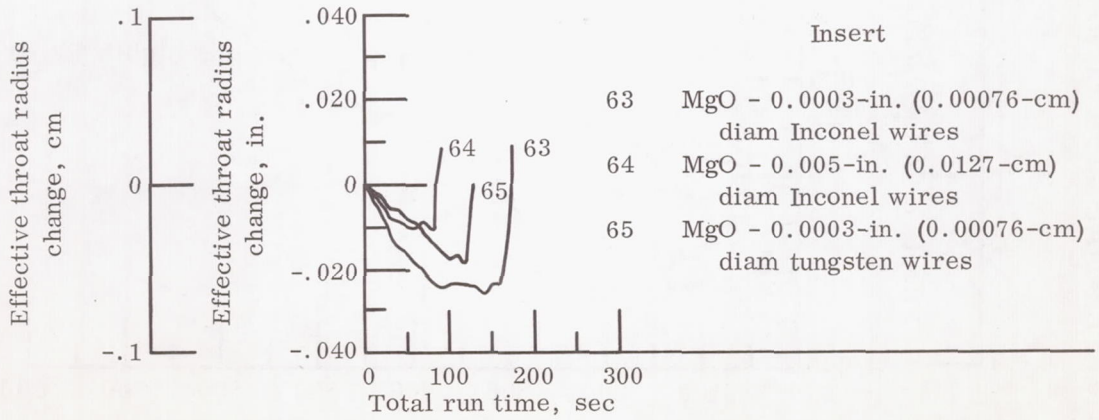

Figure 29. - Throat erosion for fiber reinforced magnesium oxide.

sion to the outside surface of the insert. Given a compressive prestress, the test firing could produce lower net tensile stress on the outside surface of the insert. It was postulated that a proper amount of prestress would prevent thermal stress failure of the insert. The small insert of configuration c was used to expedite fabrication and delivery. A 0.005-inch (0.0127-cm) interference fit was calculated to give the required compressive strength. After delivery, it was noted that the interference was only 0.003 inch (0.0076 cm).

Figure 30 is a plot of the firing data for this insert. Insert 66 was severely cracked circumferentially just upstream of the throat because of a lack of adequate prestress from the steel ring. Further testing was not necessary because the design was inadequate for extended firing durations.

Another approach to prevent structural failure is to segment the BeO, which was done for insert 67. The design consisted of three washers, each segmented every 120°, and held in a conical tantalum sleeve. Figure 30 also presents the erosion curve for the segmented design. Failure was in the tantalum sleeve at the insert leading edge (table VI(67)), possibly caused by a reaction between the BeO and the tantalum.

In order to prevent a tantalum-BeO reaction, another insert was designed with a 1/4-inch (0.635-cm) thick conical BeO sleeve on the outside to retain the segments. This insert (number 68) was tested for 691 seconds with structural cracking of the segments leading to the erosion shown on figure 30. Structural problems were first noticed after

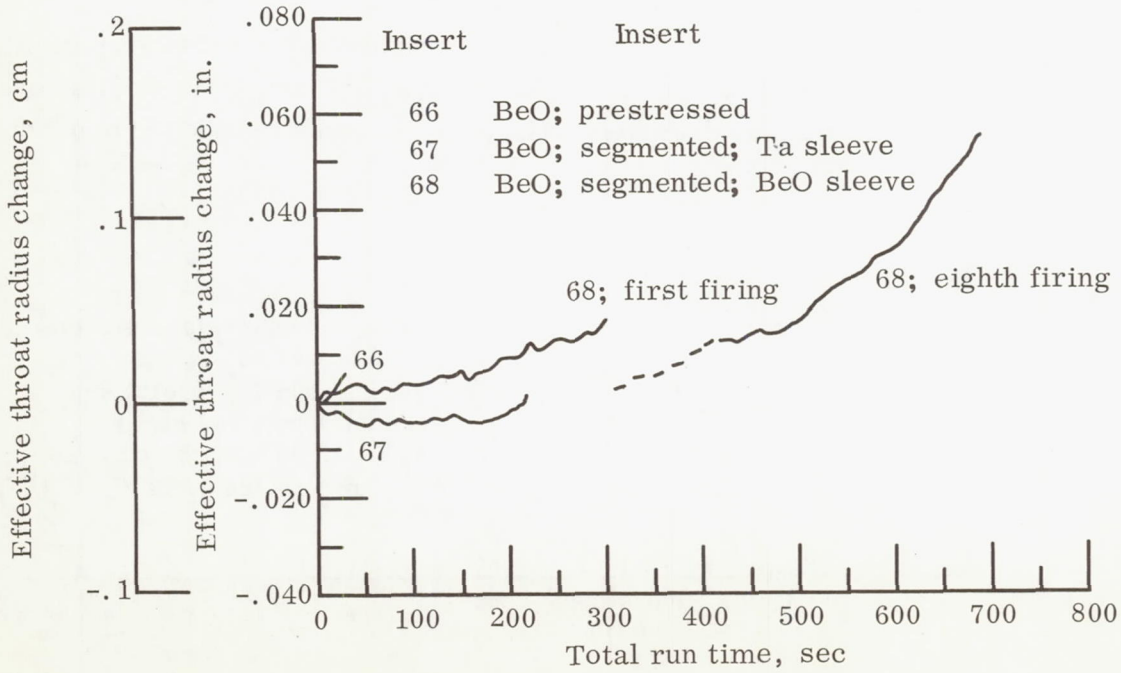

Figure 30. - Throat erosion for beryllium oxide inserts.

the first 300-second firing when cracking of some segments occurred. Loss of material due to cracking and spalling occurred during subsequent firings. An elastic bonding agent could be used between the segments to prevent structural failure of the segments. A material which would remain in place during cycling firing would be required.

Tungsten coated beryllium oxide spheres. - Inserts 69 and 70 were fabricated as modified cermets to prevent cracking of an all-ceramic structure. Beryllium oxide microspheres were coated with tungsten, then the coated BeO was pressed and sintered to form a composite throat insert. Insert 69 contained 68 weight percent tungsten. The tungsten was only 25 volume percent, however, and only a small percentage of the insert surface was tungsten. Figure 31 presents the throat erosion data. Rapid throat erosion occurred after 170 seconds. This rapid erosion is typical of a tungsten oxidation failure. Pre- and post-test photomicrographs of insert 69 are shown in figure 32(a). Loss of the tungsten due to oxidation left a weak agglomerate of BeO particles. The erosion failure due to loss of the unsupported particles was governed by the oxidation rate of the tungsten matrix.

The tungsten content for insert 70 was reduced to 25 weight percent. The throat erosion shown on figure 31 was not significantly improved over the erosion of insert 69. Pre- and post-test photomicrographs of insert 70 are shown in figure 32(b). The tungsten matrix is no longer continuous and a large number of voids are seen. The erosion failure of insert 70 was thought to be due to structural failure of the relatively porous BeO accentuated by oxidation of the tungsten.

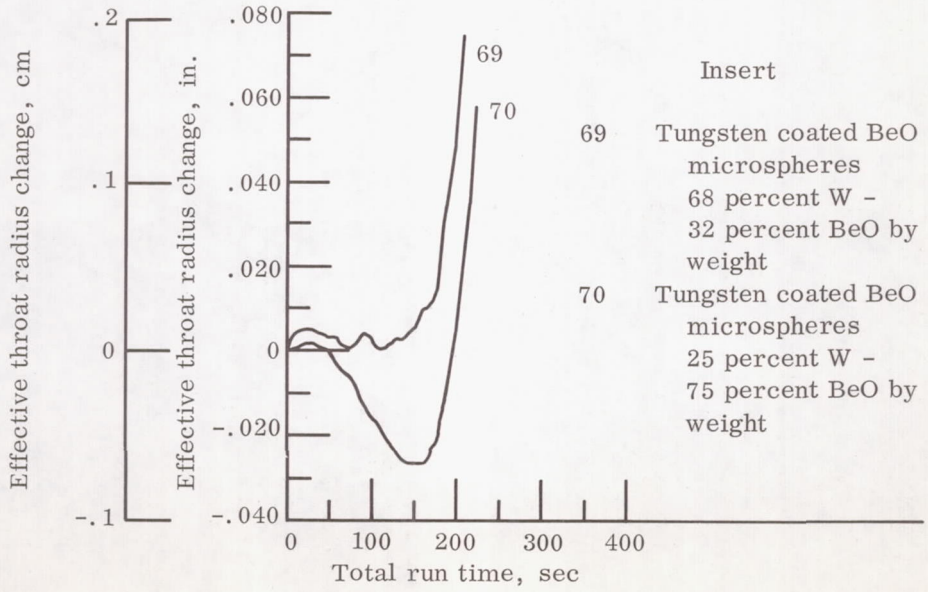

Figure 31. - Throat erosion for tungsten coated beryllium oxide microspheres.

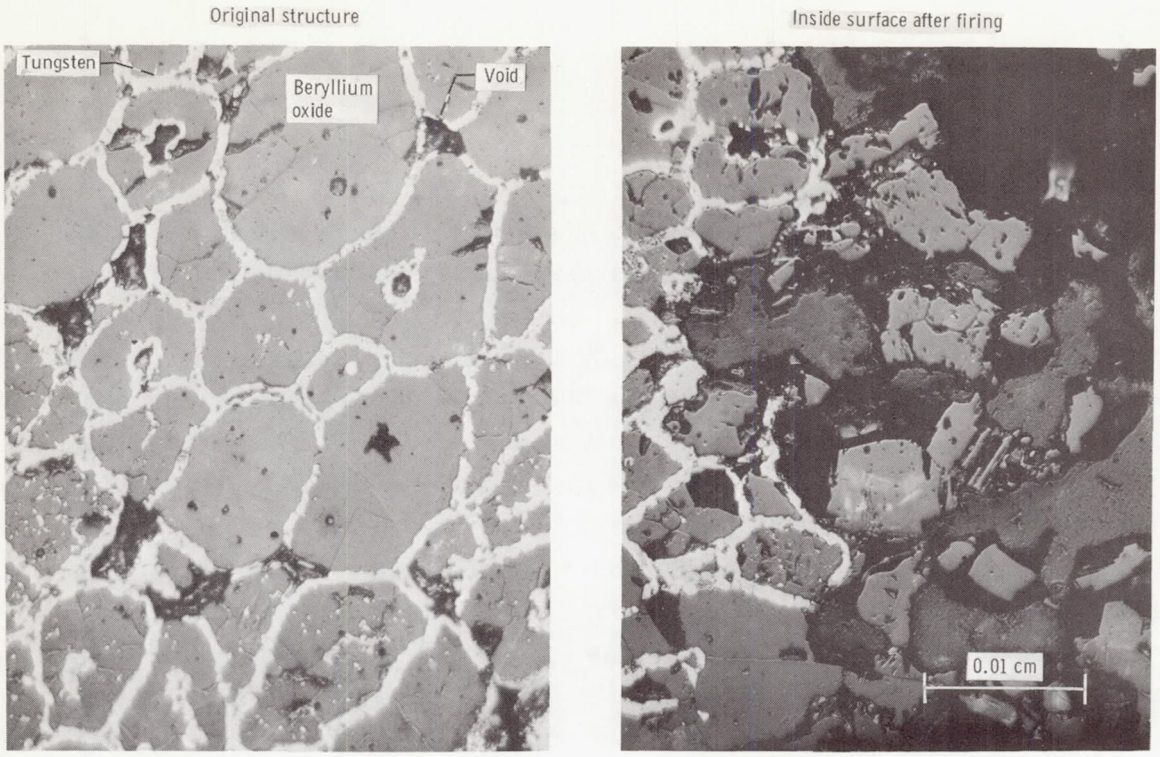

(a) Tungsten content, 68 weight percent; insert 69.

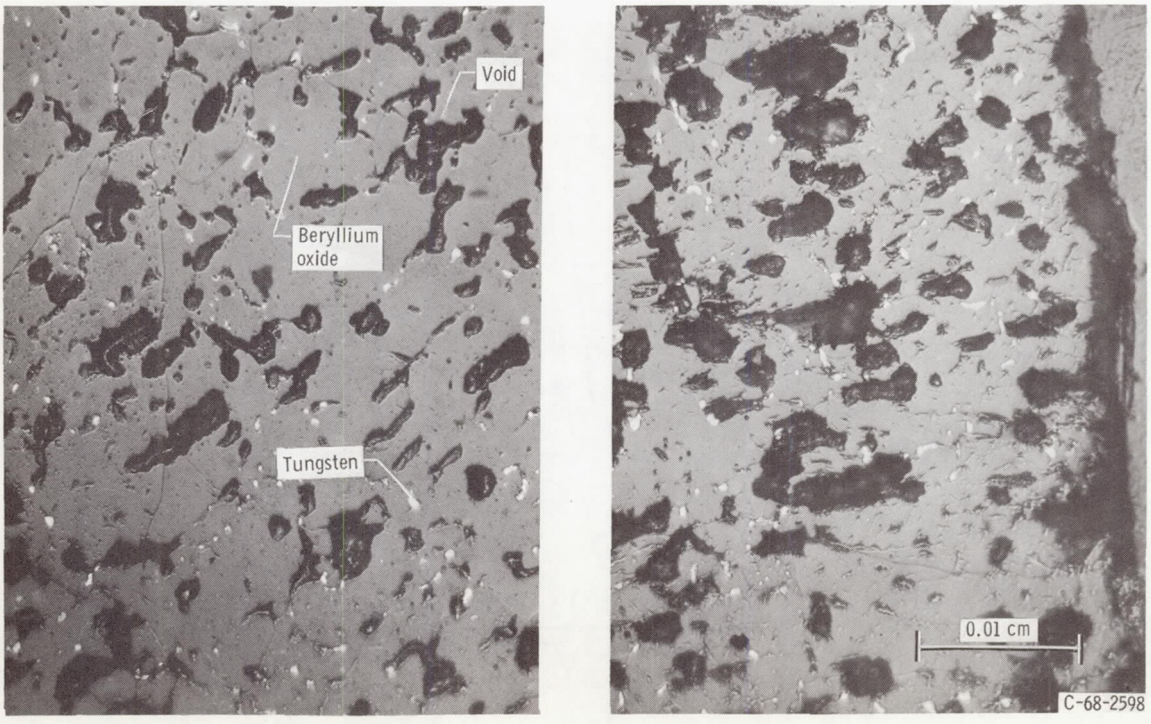

(b) Tungsten content, 25 weight percent; insert 70.

Figure 32. - Photomicrographs of tungsten coated beryillium oxide mocrospheres.

Improvement of the beryllium oxide - tungsten (BeO-W) composite should be concentrated on decreasing the voids and determining the optimum tungsten content to eliminate erosion and still maintain resistance to thermal stress cracking.

Hafnium oxide - zirconium oxide - titanium oxide. - By introducing the relatively small titanium ion into the HfO_2 and ZrO_2 matrix, it was hoped to achieve a thermal expansion coefficient of approximately zero. If this could be done, the thermal stress would be negligible and the insert highly crack resistant.

Figure 33 presents the firing data for inserts 71 to 74. The inserts were prepared by mixing HfO_2, ZrO_2, and TiO_2. The mixture was pressed, reaction sintered and pulverized, then isostatically pressed and resintered. Because of a firing malfunction during the scheduled 300-second run of insert 71, the run was terminated after only 229 seconds. It was decided to section the insert at this time in order to make a decision as to what composition would be best for insert 72. No cracks, melting or erosion were observed, and insert 72 was made identical to insert 71. To assess the long-term capabilities, an initial run of 358 seconds was made. Again, no cracking, melting or erosion was observed and a second firing was made for 365 seconds. After a total firing time of 723 seconds, a few minor surface fissures were noted. Three 20-second runs were then made, but the insert was not inspected between runs. After the fourth and fifth 20-second runs, the insert was inspected in the test cell. The six axial cracks which appeared after the fourth 20-second run were more severe and accompanied by some circumferential

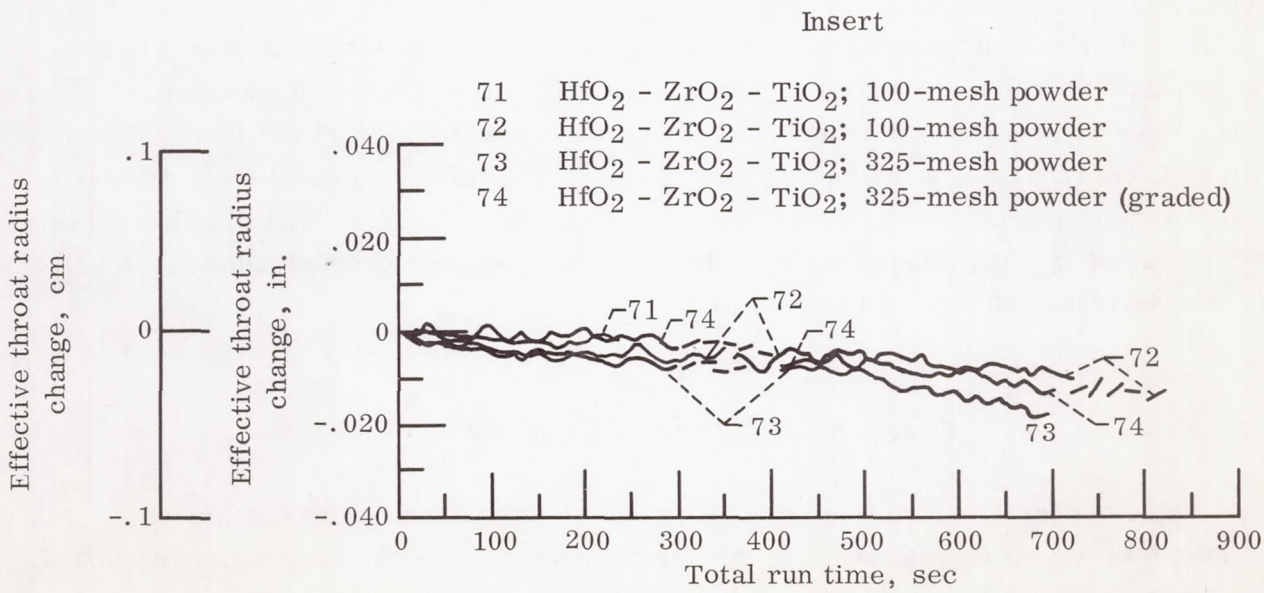

Figure 33. - Throat erosion for hafnium oxide - zirconium oxide - titanium oxide inserts.

cracking after the fifth 20-second run. During disassembly of the nozzle, the insert broke into several pieces.

The last two inserts in this series (73 and 74) were prepared from -325 mesh powders compared with -100 mesh powders used for the preceding inserts. In addition to the finer grain size, insert 74 contained more HfO_2, with correspondingly less TiO_2, on the inside diameter half of the insert. The outside half of the insert contained an increased TiO_2 and decreased HfO_2 content. Both inserts were coated on the outside diameter with approximately 0.005-inch (0.0127-cm) thick nickel metal to prevent reaction with the pyrolized resin gases from the ablative backup material.

Both inserts were fired for the specified seven cycles (300-sec, five 20-sec, and 300-sec firings). For insert 73, there was one well-developed circumferential crack lying in a plane normal to the axis of the insert which started at the back wall of the insert and penetrated two-thirds of the distance to the inner surface near the leading edge (table VI(73)). The cracking that developed was probably the combined result of thermal cycling through the monoclinic-tetragonal phase transition and thermal stress. Loss of material was probably due to imperfect manufacturing techniques during the sintering operation as the appearance of the void showed signs of adhesive failure (table VI(73)).

Throat insert 74 (graded) developed a circumferential crack on the outside surface of the insert, probably during the initial firing. The circumferential crack was not as deep as the one for insert 73. Four hairline surface fissures were noted after the first 300-second firing. The network of surface fissures did not lead to material loss during the rest of the duty cycle nor lead to a degradation in structural integrity. No melting, erosion or change in dimension was detected (see table VI(74)).

The difference in behavior between 74 and 73 was probably due to a slight change in the thermal expansion characteristics and a slight difference in the temperature of the monoclinic-tetragonal phase transition of the two layers of insert 74 (graded). Optimization of this type or insert would require some additional development work centered around very fine grain size and modified composites to enhance the stabilization during cyclic operation. The results strongly indicate that the basic concept holds merit and additional development would be worthwhile.

Refractory Macrolaminate

Another concept, which was intended to combine the oxidation resistance of a ceramic with the thermal shock resistance of a refractory metal, was the macrolaminate insert. The macrolaminate differs from an ordinary cermet in that a cermet is composed of randomly oriented ceramic and metal particles, but the macrolaminate is made from particles, each containing alternate layers of ceramic and metal. The layered particles are

compacted and sintered into a composite structure. A high degree of thermal shock resistance was expected together with adequate oxidation resistance.

Nozzle 75 was composed of a macrolaminate structure of molybdenum and HfO_2 with cesium oxide (CeO) added as a bonding agent. The composite consisted of discrete layers of HfO_2 and molybdenum within each macroparticle. The firing results are shown on figure 34. This insert was the only one tested that survived the 700-second duty cycle with neither cracking nor appreciable erosion. A final 300-second firing produced the erosion

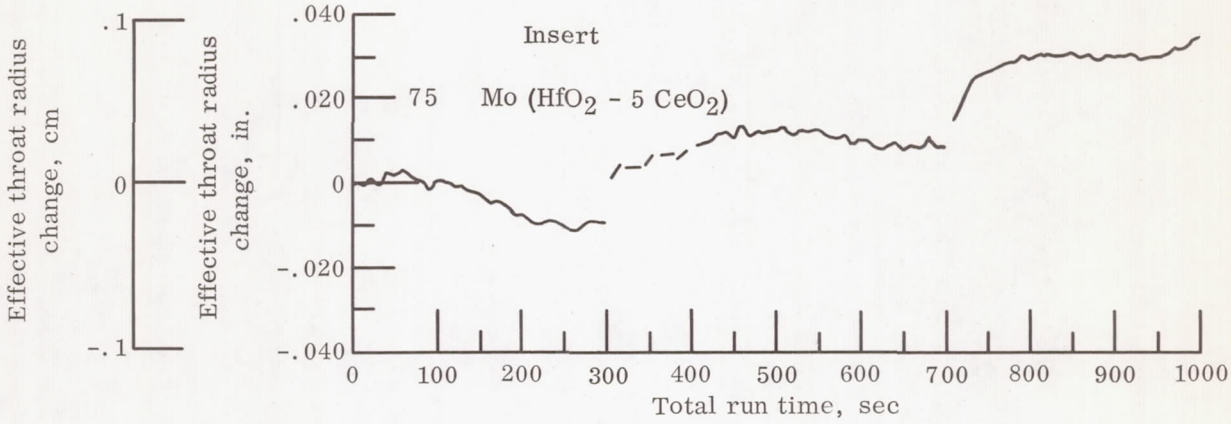

Figure 34. - Throat erosion for macrolaminate insert.

of 0.035 inch (0.089 cm), which is indicated in figure 34. During each of the longer firings, a thin, weak, porous coating formed and was removed on subsequent firings. This action is illustrated by the 0.020-inch (0.0508-cm) offsets in the erosion curve after 300 seconds and after 700 seconds.

A section view of the nozzle (table VI(75)) after firing illustrates a reaction zone 0.100-inch (0.254-cm) thick with essentially virgin material behind this. The reaction zone was composed of material which was highly adherent and protective except for the 0.035-inch (0.089-cm) layer lost earlier.

The crystalline structure is shown in figure 35. Loss of molybdenum due to oxidation is illustrated along with the characteristics of the remaining HfO_2 in the protective layer.

The refractory macrolaminate may be suitable for scale up to larger sizes. Some development would be required to perfect the manufacturing processes to eliminate the voids evident in the virgin structure shown in table II(75) and also to reduce processing costs.

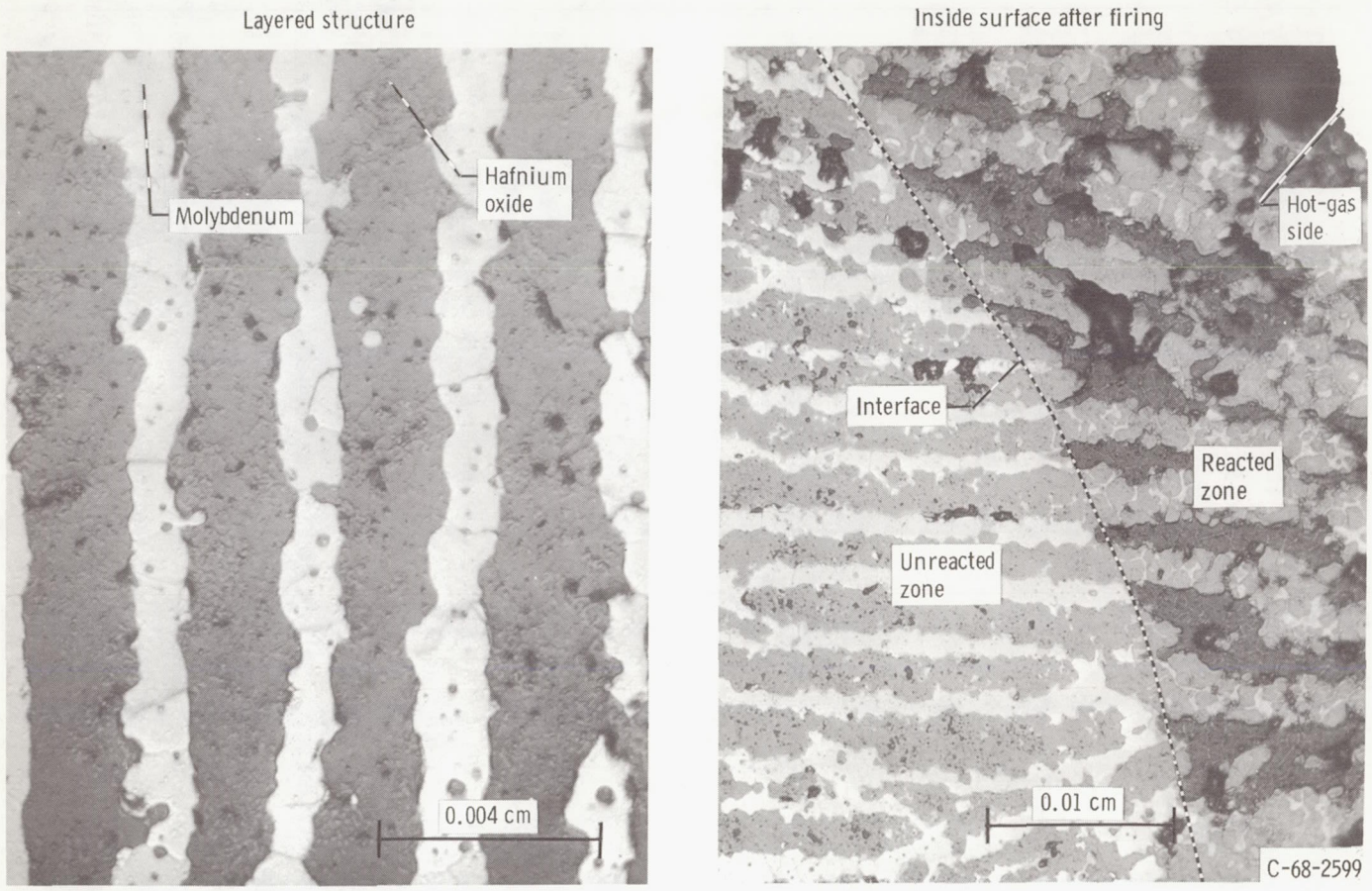

Figure 35. - Photomicrographs of hafnium oxide - molybdenum macrolaminate structure.

Summary of Refractory Composite Inserts

Test firing results show that graphite composites and pyrolytic graphite are subject to oxidation failure. The graphite composites tested were generally satisfactory structurally but oxidation protection techniques were not sufficient for the test environment.

Carbide composites designed to prevent structural failure were generally successful in this respect. Oxidation remained a problem, however. Materials that formed an adherent protective oxide in the test environment (e.g., HfC plus graphite) came the closest to meeting the required duty cycle.

Oxides generally cracked due to thermal stress. Zirconium oxide inserts stabilized with MgO were more thermal stress resistant than ZrO_2 inserts stabilized with either CaO or Y_2O_3. Various methods of adding refractory metals to the oxides were tested and the most successful was a combination of HfO_2 and molybdenum in macrolaminate form. Oxide combinations of HfO_2, TiO_2, and ZrO_2 minimized the effects of thermal stress cracking for the entire duty cycle. A system of controlling the grain-size distribution in ZrO_2 inserts also showed promise. Segmenting of beryllium oxide and other materials was generally successful in reducing cracking.

NOZZLE DESIGNS

Nine nozzle designs were tested and evaluated in this program. Complete nozzle designs were included to determine whether detailed analytical techniques could be used to select the materials and make the designs necessary to give satisfactory performance in a specific rocket-engine environment without prior engine testing. Another objective was to compare the firing results of similar materials tested in the insert configuration to the firing results of nozzle designs developed primarily with analytical techniques.

Pyroconvective

The design concept consisted of a refractory SiC coated graphite liner, grooved on the outside diameter, and backed with a gas reservoir structure. The reservoir system of nozzle design 76 was a composite of quartz and graphite fibers impregnated with a polypropylene-phenolic binder. The binder volatilized on heating and provided cooling gas which escaped through holes in the liner, located downstream of the throat plane. The reservoir system for nozzle 77 did not contain graphite fibers and was different in other respects including the elimination of the downstream holes. A comparison of configurations D and E (fig. 5(d) and (e)) illustrates the design differences between 76 and 77. Figure 36 presents the firing data for the two nozzles. Both nozzles failed by cracking of the composite liner probably within the first few seconds of firing time. Residual stresses

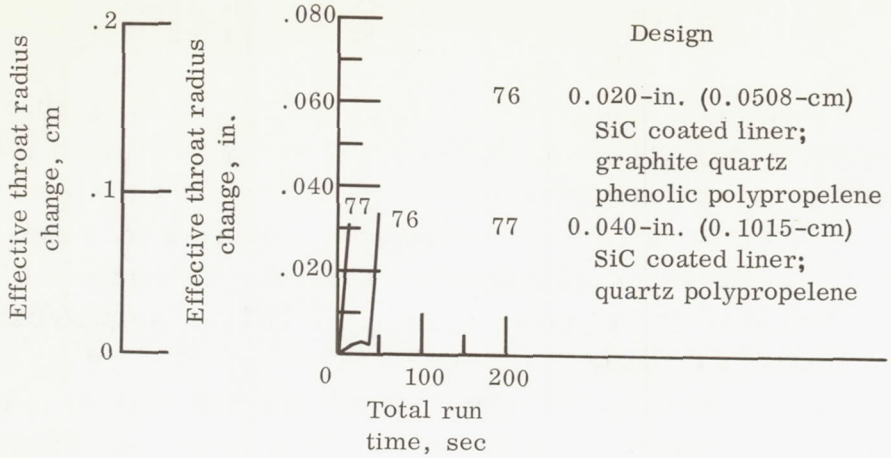

Figure 36. - Throat erosion for pyroconvective nozzle designs.

inherent in the pyrolytic deposition process contributed to the cracking as did thermal stress. The original design called for a vapor deposited free-standing silicon carbide liner, but the supplier was unable to fabricate free-standing silicon carbide in the desired configuration. A composite liner was, therefore, procured to the specification shown in figure 5(d) for nozzle 76, and, after the first firing, to figure 5(e) for nozzle 77. Neither composite provided the desired structural integrity. The analytical calculations indicated that the composite liner would have higher crack resistance than the free-standing silicon carbide liner and both would not crack. The analysis could not take into account the stresses induced during fabrication, however. In hindsight, a crack resistant liner should have been demonstrated with an ordinary ablative material as was done with the silicon carbide coated inserts 13 to 16. Once structural integrity was demonstrated, the two coolant reservoirs could have been tested to measure their influence on the oxidation rate of the silicon carbide.

Tungsten Disilicide Coated Molybdenum

The design illustrated in figure 5(f) has been used for attitude control thrusters as discussed in references 3 and 6. The propellants were the same as those used here and it was desired to compare the severity of the Lewis Research Center test engine with the environment of previous engines where the nozzle design had performed satisfactorily up to 3500° F (2200 K) inside wall temperature.

The nozzle test was terminated after 45 seconds because of a combustion gas leak. The throat erosion data are on figure 37. Inspection of the nozzle revealed partial removal of the coating by a combination of melting and oxidation. The extent of coating loss and oxidation of the molybdenum substrate may be seen in table VI(78). The failure indi-

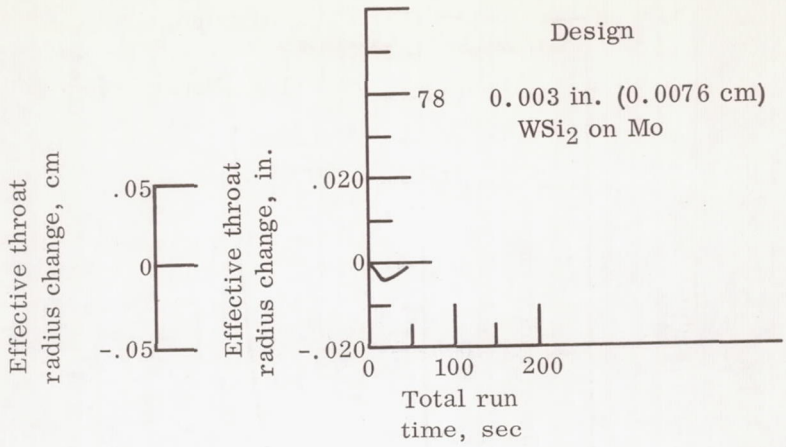

Figure 37. - Throat erosion for tungsten disilicide coated molybdenum nozzle design.

cated that the test environment was more severely oxidizing and higher in temperature than disilicide coatings could withstand.

Prestressed Tantalum Carbide

Figure 5(g) details the design configuration of nozzle 79. To compensate for the poor thermal-shock characteristics inherent in tantalum carbide structures, a ring of FS-85 columbium alloy was interference fitted around the outside diameter of the tantalum carbide insert. The prestress was intended to apply compression to the outside surface of the insert. Given a compressive prestress, the test firing would produce lower net tensile stress on the outside surface of the insert. A proper amount of prestress would prevent thermal-stress failure of the insert by reducing tensile stress on the outside of the insert, while not overstressing the inside of the insert in compression. By maintaining all the stresses within the elastic range, thermal-stress failure could be prevented during cyclic operation also.

The test firing produced throat erosion as shown in figure 38. The erosion as shown in the film supplement was due primarily to oxidation. A second firing was made to measure the oxidation rate and the effect of restart on the prestressed design. The insert was not cracked following the initial firing. After the second firing, however, axial cracks were found in the insert (see table VI(79)). The cracking illustrates the difficulty of maintaining elastic behavior of material combinations whose properties are not precisely known. The nozzle design attempted to control the oxidation of the tantalum carbide insert by keeping the surface temperature below 3700° F (2310 K) for a 300-second

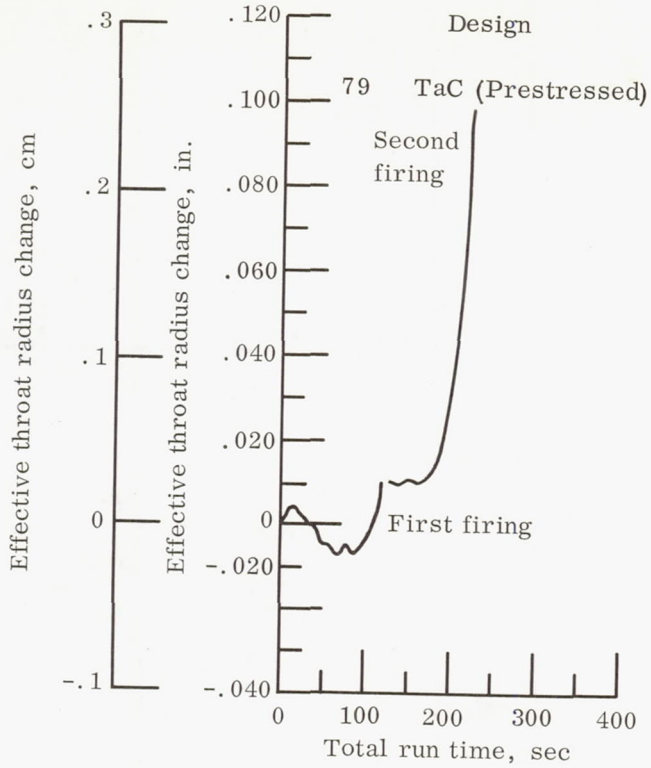

Figure 38. - Throat erosion for prestressed tantalum carbide nozzle design.

firing. Oxidation of the insert after 100 seconds of firing indicates the surface temperature or the oxidizing potential of the environment was significantly higher than the analytical calculations predicted.

Hafnium Carbide-Graded Tantalum Carbide

Figure 5(h) details the graded carbide design concept used for nozzle 80. The design consisted of four carbide layers with varying graphite content. The firing data, presented in figure 39, indicates a rapid erosion failure. Post-test inspection of the insert (table VI(80)) showed two circumferential cracks completely through the insert as well as numerous axial cracks. Although some pieces were lost from the insert during firing, the major contribution to throat erosion was oxidation of the HfC on the inside surface. The thickness of the HfC remaining at the throat was about 0.070 inch (0.178 cm). Adding the 0.035-inch (0.089-cm) erosion gives a layer 0.105-inch (0.267-cm) thick at the throat compared with the 0.100-inch (0.254-cm) design value. The other layers, however,

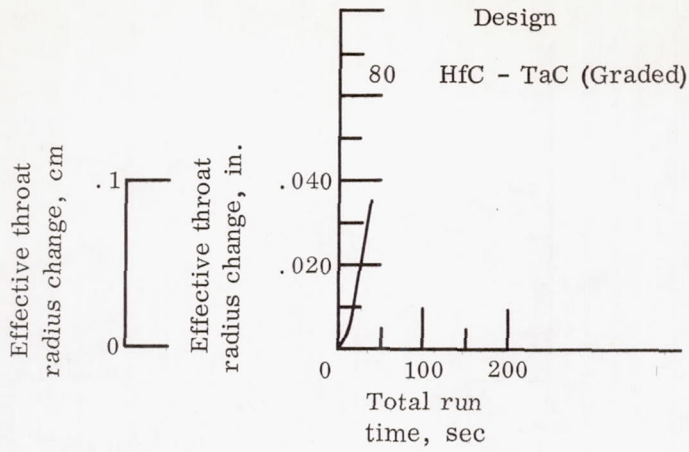

Figure 39. - Throat erosion for hafnium carbide - graded tantalum carbide nozzle design.

measured 0.070, 0.030, and 0.200 inch (0.178, 0.076, and 0.508 cm) at the throat. The design called for each layer to be 0.100-inch (0.254-cm) thick. Table VI(80) illustrates the uneven layers and indicates the difficulty of fabricating a layered composite structure. The uneven geometry and lack of high-temperature material properties hampered the temperature and thermal stress analyses. The severe cracking of all the layers indicates the difficulty of analytically designing a layered composite structure.

The rapid erosion of HfC, due to oxidation, was not anticipated. In laboratory testing with CO_2 at 4000° F (2480 K), an adherent HfO_2 scale was formed on the hafnium carbide. It was deemed likely that the protective oxide would remain in place in the rocket-engine throat environment also. Test results showed that the HfO_2 was removed from the surface as rapidly as it was formed.

The only comparison with inserts tested was the hypereutectic HfC of inserts 30 and 33. An adherent protective oxide layer did form on insert 33 during a 300-second firing. The five 20-second firings cracked and loosened the oxide layer, however. An adherent protective oxide layer on insert 30 remained in place over 655 seconds total firing duration. Although basic structural differences exist between HfC and hypereutectic HfC, the exact mechanism by which the oxide layer is retained is not known. In addition, the hypereutectic also solved the thermal cracking problem associated with carbides in general.

Zirconium Oxide-Pyrolytic Graphite Laminated Washers

Nozzle design 81 was composed of alternate axial washers of ZrO_2 and pyrolytic

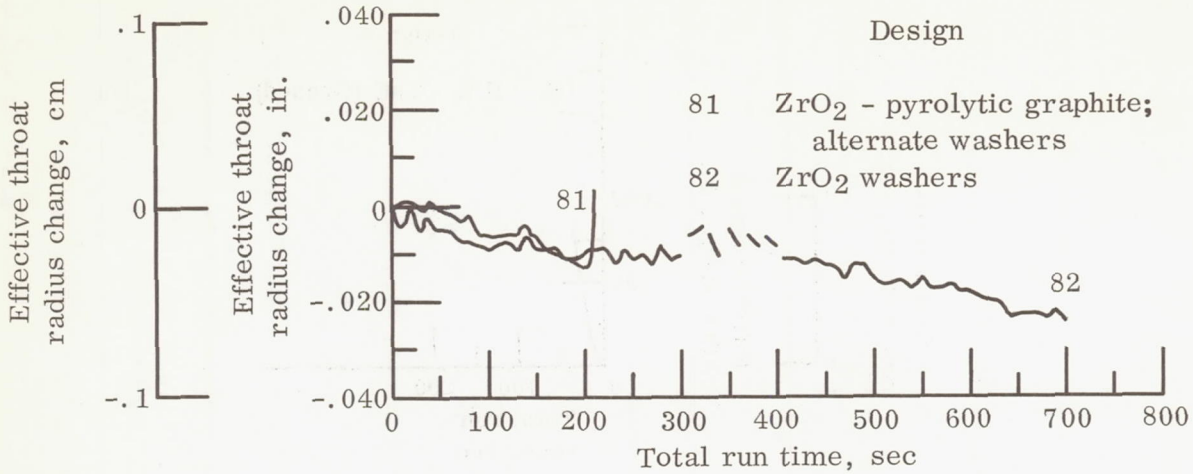

Figure 40. - Throat erosion for pyrolytic graphite laminated zirconium oxide washers.

graphite, nozzle 82 contained only the ZrO_2 washers. Figure 5(i) gives a detailed description of these designs, and figure 40 presents the firing data. The purpose of the pyrolytic graphite was to more evenly distribute the heat through the insert and to decrease thermal stress. The addition of pyrolytic graphite washers appears to have been detrimental to the ZrO_2 washers. When the pyrolytic graphite eroded due to oxidation, the exposed edges of the ZrO_2 were rapidly spalled away.

When another nozzle was designed containing only ZrO_2 washers (nozzle 82), the structural integrity was improved so that the required duty cycle was attained. Some cracking and surface spallation was apparent (table VI(82)) after shutdown. Radial segmentation in addition to the axial segmentation could possibly eliminate the cracking and spalling. The erosion resistance of nozzle 82 was similar to that of slip cast ZrO_2 inserts 48 and 49 (see fig. 25). Loss of material due to cracking was also similar (see table VI(48) and (49)). The cast ZrO_2 inserts were mainly cracked axially indicating the need for at least three radial segments for nozzle 82.

Zirconium Oxide - Tungsten Rhenium Wire Reinforced

Figure 5(j) is a sketch of the design used for nozzles 83 and 84. Nozzle 83 contained 5-volume-percent and nozzle 84 contained 7-volume-percent tungsten - 3-weight-percent rhenium wires dispersed in a ZrO_2 matrix. Wire diameter was 0.0035 inch (0.0089 cm) and wire length was nominally 3/16 inch (0.476 cm). Figure 41 presents the firing data. Both inserts survived the required duty cycle with no erosion and only minor surface spallation. However, both were cracked after the first 300-second cycle.

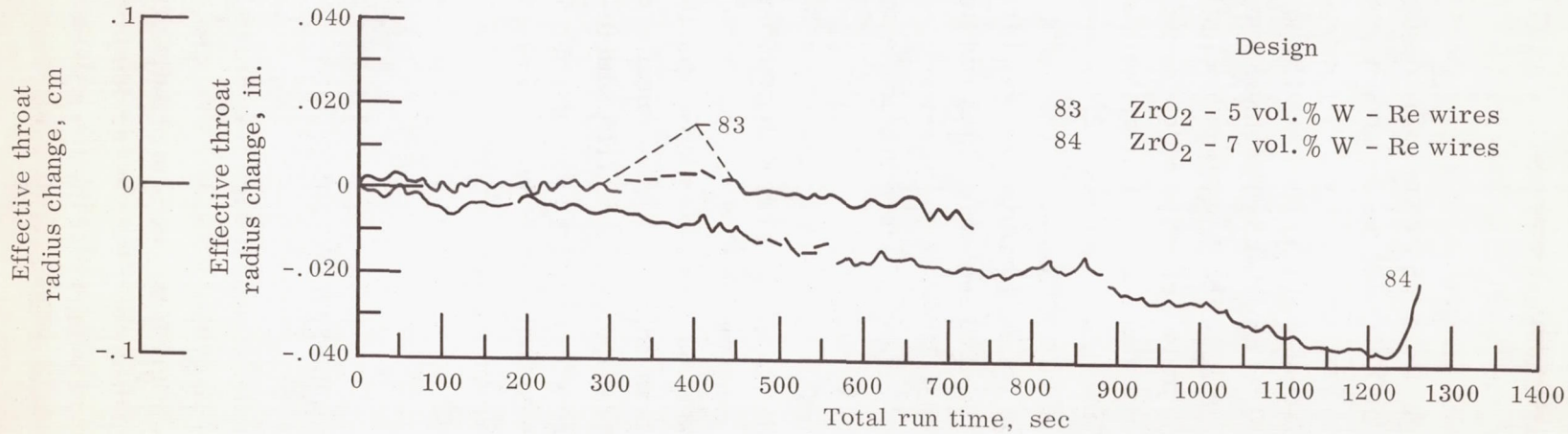

Figure 41. - Throat erosion for tungsten-rhenium wire reinforced zirconium oxide.

Nozzle 83 was X-ray inspected in an axial direction following its initial 310-second firing. Five axial cracks on the inside diameter and two axial cracks through the insert were detected. The condition of the insert after the complete firing cycle is shown in the post-test photograph (table VI(83)). It was hoped that an increase in the tungsten-rhenium wire content would provide a significant improvement in crack resistance over inserts 48 and 49 (slip-cast, mixed-grain ZrO_2) as well as an improvement over nozzle design 83.

When the insert of nozzle 84 was fabricated with 7-percent reinforcing wires, cracks became evident on the outside diameter during final machining. Because the cracks were not completely through the insert, it was decided to run the regular test series. The major difference detected during testing of the 7-percent specimen was the presence of more severe axial cracks on the insert inside diameter following the initial test firing. Insert behavior was essentially similar to the 5-percent insert with somewhat more spalling of the surface at the conclusion of the firing. An extra firing beyond the normal sequence was run to determine failure mode for the design. It was possible to run beyond the basic 700-second duty cycle because of the conservative design of the ablative envelope. Test termination, which occurred after 1258 seconds of total run time, was due to flow behind the insert caused by erosion of the JT0981 at the insert leading edge. For run durations of this magnitude (over 1200 sec), material more erosion resistant than JT0981 must be used in the converging section of the nozzle.

The only comparison with inserts that can be made is with the wire reinforced MgO inserts 63 to 65. Because all the materials were different, only general conclusions can be drawn. The uniformity and randomness of wire dispersion was much better in nozzles 83 and 84 than in inserts 63 to 65. This may have been the reason nozzles 83 and 84 did not erode even though they cracked. The improvement in crack resistance afforded by 0.0003-inch (0.00076-cm) diameter wire compared with 0.005-inch (0.0127-cm) diameter wire suggests that an improvement in the nozzle designs might be achieved by using a wire diameter less than the 0.0035-inch (0.0089-cm) diameter used here. However, a detailed knowledge of the dispersion characteristics would be required to completely define this parameter.

Summary of Nozzle Designs

The 5-volume-percent tungsten-rhenium wire reinforced ZrO_2 nozzle design had less than ±5 percent area change for the 700-second duty cycle but developed cracks.

The pyroconvective design might have performed satisfactorily if it had been possible to produce the free-standing, high-density silicon carbide liner, to the desired configuration. However, even if structural integrity of the liner were assured, further testing would be required to assure cooling of the outside surface while maintaining structural integrity of the gas reservoir system.

The prestressed design of the tantalum carbide nozzle successfully eliminated cracking by thermal stress on the first firing. However, oxidation was quite severe and thermal stress failure occurred on the second test firing. Prestressing may be useful for other carbides or oxides where the material is not subject to rapid oxidation in the test environment and provided the prestress state can be maintained to give restart capability.

The graded carbide design was inadequate both structurally and chemically.

Cracking, which is characteristic of ZrO_2 material in this environment, resulted in loss of material in both laminated designs. The pyrolytic graphite washers lowered the temperature differential across the ZrO_2 but as the pyrolytic graphite eroded, the unsupported ZrO_2 spalled from the surface. The all zirconium dioxide washers ran the full duty cycle of 700 seconds. However, spallation and cracking, particularly upstream of the throat, were fairly severe compared with monolithic ZrO_2 as used for inserts 49 and 50.

The most successful of the complete nozzle designs was the ZrO_2 nozzle reinforced with 5-volume-percent of the tungsten - 3-weight-percent rhenium wire. The insert cracked, but the throat radius change was minor over the 700-second duty cycle.

In retrospect, all the materials used in the nozzle designs should first have been tested as nozzle inserts to determine material suitability in the rocket engine environment. Then the more successful of the material candidates could have been characterized and designed in detail to optimize their performance in the test environment.

CONCLUSIONS AND RECOMMENDATIONS

Seventy-five throat inserts and nine complete nozzle designs were evaluated in a storable-propellant (nitrogen tetroxide and a 50-percent blend of unsymmetric dimethylhydrazine with hydrazine) rocket engine. The purpose was to develop materials and design concepts capable of surviving an extended duty cycle consisting of an initial 300-second firing, followed by five 20-second firings, and ending in another 300-second firing. The nominal engine operating condition included an oxidant-to-fuel mixture ratio of 2.0, a chamber pressure of 100 psia (689 N/m^2) with an initial throat diameter of 1.2 inches (3.05 cm).

All the materials, designs, or fabrication techniques which are discussed in the following paragraphs are considered worthy of future effort. Each was successful to some degree in meeting the chosen duty cycle and show promise in being optimized for a specific duty cycle.

Gas-pressure bonding of refractory coatings increased the density of plasma-sprayed oxide coatings and improved the adhesion of the coating to the underlying substrate. Unfortunately, the relatively low melting temperature and the high vapor pressure of the

chromium intermediate layer resulted in premature coating loss. The substitution of a more refractory metal such as molybdenum in the intermediate layer should prevent this type of failure.

Low-modulus, high-expansion graphitic substrates were developed to match the expansion of pyrolytic graphite coatings during the firing. In addition, the relatively porous structure of the substrate achieved a high degree of bond strength between the coating and the substrate by increasing the depth of penetration of the coating into the substrate. Addition of small amounts of boron (less than 1 percent) appreciably increased the oxidation resistance of pyrolytic graphite coatings.

Silicon carbide coatings were generally structurally sound and oxidation resistant for run durations of approximately 120 seconds. Longer runs are possible and are directly related to the substrate heat-sink capacity.

A very promising coating system was iridium-rhenium on a tungsten substrate. The iridium did not melt or oxidize during a 140-second firing. Diffusion of oxidizing combustion products through the semiporous iridium layer probably caused failure. Long runs might be possible with an impervious layer to prevent substrate oxidation. Iridium coatings for high-expansion graphite substrates are particularly worthy of future development.

Graphite composites containing zirconium, hafnium, and/or boron were developed that had increased resistance to oxidation compared with conventional grades of graphite. Hypereutectic carbides containing primary graphite were generally successful in eliminating thermal-stress cracking. The in-place formation of hafnium oxide appeared to be the most adherent of the protective oxide coatings formed during the firings and came close to meeting the required duty cycle. The addition of small amounts of nitrogen to either the zirconium or hafnium hypereutectic appeared to decrease the insert's resistance to cracking or spalling.

A slip-cast, mixed-grain-size zirconium oxide insert was the most successful of the mono-oxides tested. It was superior in performance to the sintered material and also to either 100-percent fine grain or 100-percent coarse grain zirconium oxide material. It was also determined that magnesium oxide as a stabilizing agent was much superior to calcium oxide or yttrium oxide in preventing cracking and material loss due to thermal stress.

Metal wire used to reinforce ceramics did not eliminate thermal stress cracking, but did reduce crack propagation. Small diameter wires were more successful than the larger diameter wires in minimizing thermal stress cracking. Platinum honeycomb reinforced magnesium oxide did not crack during a single 143-second firing. Other metal honeycomb-ceramic combinations were unsuccessful in preventing cracking. Further testing of the platinum - magnesium oxide combination is required. Variation of honeycomb geometry might prevent structural failure with the other material combinations.

When a silicon oxide reinforced ablative liner was used upstream of a zirconium oxide or magnesium oxide containing insert, the melted silica flowing over the insert during the firing formed low-melting-temperature compounds. An upstream liner of JTA graphite eliminated this problem and was generally successful in preventing erosion at the liner-insert interface.

Thermal stress cracking of beryllium oxide inserts was reduced by using segmented washers. Bonding the segments with an elastic material might solve the cracking and spalling problems of segmented designs

The structural integrity of a tantalum carbide nozzle design was maintained for a single firing by prestressing. However, thermal stress failure occurred during the second firing along with rapid oxidation of the tantalum carbide. Prestressing could be applied to oxides to eliminate reaction with the combustion environment.

Mixed oxides of zirconium, hafnium, and titanium provided erosion resistance and gave better crack resistance over the entire duty cycle than any of the other materials tested, except the macrolaminate concept.

The most successful of all materials tested in the program was a hafnium oxide - molybdenum macrolaminate insert which provided satisfactory erosion resistance and structural integrity over the complete duty cycle.

Insert design for larger throat sizes is a difficult problem; materials developed and tested herein can be used as a guide, however. Because thermal stress problems are more severe in larger sizes (ref. 2), only the most crack resistance materials should be considered. Production of larger inserts must be controlled to provide uniform and reproducible material properties. The larger the size, the more difficult the problems.

An analytical technique for temperature and stress analysis would be a valuable aid to insert design and scale changes. Analytical definition of the internal environment of a rocket engine is very difficult, however. Obtaining high-temperature material properties for all possible insert composites is also very difficult. Both the internal environment and suitability of materials can best be determined by actual rocket-engine testing. The more promising materials can then be better characterized and designed in detail to meet the known requirements of the actual test environment. Therefore, detailed analytical techniques for nozzle designs should be used only when adequate material properties are available and duty cycle and internal environment is known.

Lewis Research Center,
National Aeronautics and Space Administration,
Cleveland, Ohio, July 15, 1968,
128-31-03-02-22.

APPENDIX - SYMBOLS

A_B	base area of nozzle, in.^{2}; cm^2
A_E	exit area of nozzle, in.^{2}; cm^2
A_p	throat area planimeter, in.^{2}; cm^2
A_t	throat area, in.^{2}; cm^2
C^*	characteristic velocity
C_k^*	characteristic velocity determined from heat-sink calibration firings, ft/sec; m/sec
F	thrust, lb; N
F_{vac}	vacuum thrust, lb; N
g	gravitational constant, 32.174 ft/sec^2; 9.8 m/sec^2
I_{sp}	specific impulse
I_{vac}	vacuum specific impulse
O/F	oxidant-to-fuel mixture ratio
ΔP	pressure drop
P_B	pressure at nozzle base, psi; kN/m^2
P_{bar}	barometric pressure, psia; kN/m^2
P_c	chamber pressure, psia; kN/m^2
ΔR_e	effective throat radius change, in.; cm
$R_{t,0}$	initial throat radius, in.; cm
T	temperature, $^{\circ}$R; K
V	volume flow
w	weight flow, lb; kg
ηC^*	characteristic velocity efficiency
ηC_F^*	thrust coefficient efficiency
τ	firing time, sec
ρ	density, lb/ft^3; kg/m^3
φ	momentum pressure loss, percent

Subscripts:

f	fuel
f, t	fuel turbine meter
f, v	fuel venturi meter
o	oxidant
o, t	oxidant turbine meter
o, v	oxidant venturi meter
TE	theoretical equilibrium
tot	total
vac	vacuum

REFERENCES

1. Winter, Jerry M.; Plews, Larry D.; and Johnston, James R.: Experimental Evaluation of Throat Inserts in a Storable-Propellant Rocket Engine. NASA TM X-1266, 1966.

2. Winter, Jerry M.; and Peterson, Donald A.: Experimental Evaluation of 7.82-Inch-(19.8-Cm-) Diameter Throat Inserts in a Storable-Propellant Rocket Engine. NASA TM X-1463, 1968.

3. Crump, D. N.; Henderson, H. H.; and Smith, K. J.: Improved Throat Inserts for Ablative Thrust Chambers. TRW, Inc. (NASA CR-54984), 1967.

4. Diersing, R. J.; Carmichael, D. C.; and Wright, T. R.: The Gas Pressure Bonding of Protective Coatings to Rocket Nozzle Throat Inserts. Battelle Memorial Inst. (Contract NAS3-7173), 1965.

5. Fehrenbacher, L. L.; Jacobson, L. A.; and Lynch, C. T.: The Role of Rare Earth Oxides in the Stabilization of Cubic Zirconia. Presented at the USAFOSR and Arizona State University, 4th Rare Earth Research Conference, Phoenix Ariz., Apr. 22-25, 1964.

6. Anon.: Development of Ablative Thrust Chambers and Throat Inserts Suitable for Use on the Gemini and Apollo Vehicles. Rep. ER-6507, TRW Inc. (NASA CR-65055), May 28, 1965.

7. Brown, S. D.: Internal Research and Development. Rocketdyne, Div. of North American Aviation Corp.

8. Simpson, F. H.: Laminate Particle Composite Research. The Boeing Company, Oct. 1966.

TABLE I. - MEASURED VARIABLES

Variables and constants	Nominal value	Standard deviation, % nominal
Chamber pressure, P_c, psia; kN/m^2	100; 689	±1.5
Thrust, F, lb; N	100; 444	±1.0
Oxidant venturi pressure drop, $\Delta P_{o,v}$, psi; kN/m^2	25; 172	±4.0
Volume flow, oxidant turbine meter, $V_{o,t}$, ft^3/sec; cm^3/sec	0.0048; 0.0137	±1.0
Fuel venturi pressure drop, $\Delta P_{f,v}$, psi; kN/m^2	25; 172	±4.0
Volume flow, fuel turbine meter, $V_{f,t}$, ft^3/sec; cm^3/sec	0.0048; 0.0137	±1.0
Firing time, θ, sec	150	±0.3
Throat area planimeter, A_p, $in.^2$; cm^2	1.131; 7.3	±1.0
Oxidant temperature, T_o, ^oR; K	530; 289	±0.4
Fuel temperature, T_f, ^oR; K	530; 289	±0.4
Base area of nozzle, A_B, $in.^2$; cm^2	1.7; 10.90	±0.6
Pressure drop at nozzle base, ΔP_B, psi; kN/m^2	0.1; 0.689	±10.0
Exit area of nozzle, A_E, $in.^2$; cm^2	2.4; 16.1	±0.4
Initial throat radius, $R_{t,0}$, in.; cm	0.6; 1.525	±0.2
Barometric pressure, P_{bar}, psia; kN/m^2	14.4; 99.2	±0.1
Momentum pressure loss, φ, %	0.8	-----
Thrust coefficient efficiency, η_{CF}, %	95.5	-----
Characteristic velocity determined from heat-sink calibration firings, C_K^*, ft/sec; m/sec	5300; 1615	-----
Oxidant density, ρ_o, lb/ft^3; kg/m^3	91.5; 1460	-----
Fuel density, ρ_f, lb/ft^3; kg/m^3	56.8; 896	-----
Gravitational constant, g, ft/sec^2; m/sec^2	32.174; 9.8	-----

TABLE II. - INSERT TABULATION

(1) Refractory coating systems

Insert	Configuration	Coating	Coating thickness		Substrate
			in.	cm	
Refractory metal substrates					
1	A	50 wt. % Al_2O_3 - 50 wt. % Cr_2O_3	0.006	0.0152	TZM
2	A	50 wt. % Al_2O_3 - 50 wt. % Cr_2O_3	.006	.0152	TZM
3	B	50 wt. % ZrO_2 - 50 wt. % HfO_2	.006	.0152	TZM
4	B	50 wt. % ZrO_2 - 50 wt. % HfO_2	.006	.0152	TZM
5	B	78 wt. % Hf - 20 wt. % Ta - 2 wt. % Mo	.020	.0508	TZM
6	B[a]	Iridium - rhenium	[b].007	.0178	Tungsten
Low-modulus graphite substrates					
7	A	Pyrolytic graphite	0.060	0.152	Pyrolyzed graphite cloth-phenolic
8	B	Pyrolytic graphite	.010	.0254	PT 0114
9	B[a]	Pyrolytic graphite with 0.5 wt. % boron	.040	.1015	Pyrolyzed graphite cloth
10	B[a]	Pyrolytic graphite	.040	.1015	Pyrolyzed graphite cloth
High-modulus graphite substrates					
11	A	ZrC (pyrolytic)	0.020	0.0508	ATJ graphite
12	A	SiC (pyrolytic)	.050	.127	UT-6 graphite
13	A	SiC (pack cementation)	.005	.0127	RVC graphite
14	A	SiC (pyrolytic)	.030	.076	UT-6 graphite
15	A	SiC (pyrolytic)	.037	.094	SX-4 graphite
16	B	SiC (pyrolytic)	.023	.0589	SX-4 graphite
17	A	Iridium	.005	.0127	High-thermal expansion graphite
18	A	Iridium	.003	.0076	High-thermal expansion graphite

[a]Modified.

[b]0.003 in. (0.0076 cm) iridium on 0.004 in. (0.0101 cm) rhenium.

TABLE II. - Continued. INSERT TABULATION

(2) Refractory composites

Insert	Configuration	Composite material
		Graphites
19	A	SiC - ZrC plus graphite; 20 % zirconium base resin binder
20	A	SiC - ZrC plus graphite; 10 % zirconium base resin binder
21	B	ZrB_2 - SiC plus graphite (JTA)
22	B and A	ZrB_2 - SiC plus graphite (JTA)
23	A	Pyrolytic graphite; formed into washers and cones
24	B	Pyrolytic graphite; formed into washers and cones
25	B	Pyrolytic graphite; formed into wedges and cones
		Carbides
26	A	SiC; 3 axial washers
27	A	SiC; 3 axial washers; each segmented 180°
28	B	SiC; 3 axial washers; each segmented 120°
29	C	ZrC plus graphite
30	C	HfC plus graphite
31	B	ZrC(N) plus graphite; cast
32	B	ZrC(N) plus graphite; sintered
33	B	HfC(N) plus graphite; sintered
34	B	ZrC - SiC plus graphite (JT0981)
35	A	HfC - SiC plus graphite (JT0992)
36	A	HfC - SiC plus graphite; (JT0992) preoxidized
37	B	HfC - SiC plus graphite (JT0992)
		Oxides
38	A	80 wt. % SiO_2 - 20 wt. % graphite
39	A	56 wt. % ZrO_2 foam - 44 wt. % phenolic resin binder
40	B	ZrO_2; 70 % density; partially yttria statilized; coarse grain
41	B	ZrO_2; 75 % density; yttria stabilized; medium grain
42	B	ZrO_2; 90 % density; yttria stabilized; fine grain
43	B	ZrO_2; 90 % density; yttria stabilized; fine grain
44	A	ZrO_2; sintered; mixed grain size; thin wall
45	A	ZrO_2; sintered; mixed grain size
46	B	ZrO_2; sintered; mixed grain size

TABLE II. - Continued. INSERT TABULATION

(2) Concluded. Refractory composites

Insert	Configuration	Composite material
		Oxides (Concluded)
47	B	ZrO_2; mixed grain size; slip cast; CaO stabilized
48	B	ZrO_2; mixed grain size; slip cast; MgO stabilized
49	B	ZrO_2 plus graphite; mixed grain size; slip cast, MgO stabilized
50	B	ZrO_2 - 6 wt. % Cu; anion deficient
51	B	ZrO_2 - 6 wt. % Cu; anion deficient; thin wall
52	B	ZrO_2 - 11 wt. % Cu; anion deficient
53	B	ZrO_2 - 15 wt. % Cu; anion deficient; thin wall
54	B	ZrO_2 - 15 wt. % Cu; anion deficient
55	B	ZrO_2; Inconel honeycomb cell walls
56	B	ZrO_2; platinum-rhodium honeycomb cell walls
57	B	ZrO_2; tungsten honeycomb cell walls
58	B	ZrO_2; platinum-coated molybdenum honeycomb cell walls
59	A	MgO; steel honeycomb cell walls
60	A	MgO; Inconel honeycomb cell walls
61	B	MgO; platinum-coated steel honeycomb cell walls
62	B	MgO; platinum honeycomb cell walls
63	B	MgO; 5 vol. % 0.0003 in. (0.00076 cm) Inconel wires
64	B	MgO; 5 vol. % 0.005 in. (0.0127 cm) Inconel wires
65	B	MgO; 5 vol. % 0.0003 in. (0.00076 cm) tungsten wires
66	C	BeO; prestressed
67	B	BeO; 3 axial washers, each segmented 120°; tantalum sleeve
68	B	BeO; 3 axial washers, each segmented 120°; BeO sleeve
69	B	BeO microspheres; tungsten coating (68 wt. % W); pressed; sintered
70	B	BeO microspheres; tungsten coating (25 wt. % W); pressed; sintered
71	B	HfO_2 - ZrO_2 - TiO_2; 100-mesh powder
72	B	HfO_2 - ZrO_2 - TiO_2; 100-mesh powder
73	B	HfO_2 - ZrO_2 - TiO_2; 325-mesh powder
74	B	HfO_2 - ZrO_2 - TiO_2; 325-mesh powder; graded
75	B	Macrolaminate, Mo(HfO_2 - $5CeO_2$)

TABLE II. - Concluded. INSERT TABULATION

(3) Nozzle designs

Design	Configuration	Composite material
76	D	0.020 in. (0.0508 cm) SiC on graphite; cooling reservoir
77	E	0.040 in. (0.1015 cm) SiC on graphite; cooling reservoir
78	F	0.003 in. (0.0076 cm) tungsten disilicide ($W\text{-}Si_2$) on molybdenum
79	G	TaC; prestressed
80	H	HfC - TaC plus graphite
81	I	ZrO_2 and pyrolytic graphite; alternating washers
82	I	ZrO_2 washers
83	J	ZrO_2 - 5 % W-Re
84	J	ZrO_2 - 7 % W-Re

TABLE III. - CALCULATIONS

Oxidant flow:	
Venturi meter	$w_{o,v} = 0.00951 \sqrt{\Delta P_o \rho_o}$
Turbine meter	$w_{o,t} = V_{o,t} \rho_o$
Average	$w_o = (w_{o,v} + w_{o,t})/2$
Fuel flow:	
Venturi meter	$w_{f,v} = 0.00589 \sqrt{\Delta P_{f,v} \rho_f}$
Turbine meter	$w_{f,t} = V_{f,t} \rho_f$
Average	$w_f = (w_{f,t} + w_{f,v})/2$
Propellant flow	$w_{tot} = w_o + w_f$
Oxidant-to-fuel ratio	$O/F = w_o/w_f$
Vacuum thrust	$F_{vac} = F - A_B(P_B - P_{bar}) + (A_E P_{bar})$
Vacuum impulse	$I_{vac} = F_{vac}/w_{tot}$
Impulse efficiency	$\eta I_{vac} = I_{vac}/I_{vac,TE}$
Characteristic velocity	$C^* = (100 - \varphi) P_c A_t g/w_{tot}$
Characteristic velocity efficiency from -	
Chamber pressure	$\eta C^* P_c = C^*/C^*_{TE}$
Thrust	$\eta C^* I_{sp} = \eta I_{vac}/\eta C_F$
Calculated effective radius change	$\Delta R_\epsilon = \sqrt{w_{tot} C^*_K/\pi P_c g} - R_{t,0}$

TABLE IV. - COMBUSTION PERFORMANCE

Injector	Included impingement angle, deg	Characteristic velocity efficiency from thrust, $\eta C^* I_{sp}$, %	Number of calibration firings	Number of insert firings
1	30	93.7	48	1
1A	60	93.3	16	28
2	30	95.3	39	86
3	30	95.8	11	20

TABLE V. - RELATIVE ORDER OF MERIT

(1) Refractory coating systems

Relative order	Insert	Material	Time cracking first detected, sec	Time area change exceeds ±5 percent, sec	Total cycles	Total firing time, sec	Primary failure mechanism
1	16	0.023 in. (0.0589 cm) SiC on SX-4 graphite; O/F = 1.6	--	142	1	146	Oxidation of coating
2	6	0.003 in. (0.0076 cm) iridium on 0.004 in. (0.01015 cm) rhenium on tungsten	--	128	1	136	Diffusion oxidation of substrate
3	15	0.037 in. (0.094 cm) SiC on SX-4 graphite	--	110	1	121	Oxidation of coating
4	14	0.030 in. (0.076 cm) SiC on UT-6 graphite	--	94	1	94	Oxidation of coating
5	18	0.003 in. (0.0076 cm) iridium on graphite (high expansion)	--	---	1	71	Diffusion oxidation of substrate
6	13	0.005 in. (0.0127 cm) SiC on RVC graphite	--	60	1	62	Oxidation of coating
7	8	0.010 in. (0.254 cm) pyrolytic graphite plus boron on low modulus graphite	54	53	1	54	Cracking of coating and substrate followed by oxidation
8	2	0.006 in. (0.0152 cm) 50 Al_2O_3 - 50 Cr_2O_3 on TZM	--	51	1	61	Melting of coating
9	1	0.006 in. (0.0152 cm) 50 Al_2O_3 - 50 Cr_2O_3 on TZM	--	42	1	48	Melting of coating
10	4	0.006 in. (0.0152 cm) 50 HfO_2 - 50 ZrO_2 on TZM	--	41	1	54	Spallation of coating due to low temperature melting intermediate layer
11	17	0.005 in. (0.0127 cm) iridium on graphite (high expansion)	--	---	1	40	Diffusion oxidation of substrate
12	5	0.020 in. (0.0508 cm) 78 Hf - 20 Ta - 2 Mo on TZM	41	40	1	41	Thermal stress failure of coating
13	9	0.040 in. (0.1015 cm) pyrolytic graphite on low modulus graphite	--	38	1	82	Oxidation of coating
14	3	0.006 in. (0.0152 cm) 50 HfO_2 - 50 ZrO_2 on TZM	--	38	1	44	Spallation of coating due to low temperature melting intermediate layer
15	10	0.040 in. (0.1015 cm) pyrolytic graphite on low modulus graphite	56	35	1	56	Cracking of substrate and coating
16	7	0.060 in. (0.152 cm) pyrolytic graphite on low modulus graphite	--	32	1	100	Loss of coating adhesion at leading edge due to erosion of upstream ablative
17	11	0.020 in. (0.0508 cm) ZrC on ATJ graphite	--	24	2	98	Coating oxidized and removed due to stream shear forces
18	12	0.050 in. (0.127 cm) SiC on UT-6 graphite	12	---	1	12	Thermal stress cracking of coating

(2) Refractory composites

1	75	Macrolaminate, $Mo(HfO_2 - 5CeO_2)$	---	707	8	1003	Gradual erosion of surface reaction zone; total throat erosion, 0.029 in. (0.0737 cm)
2	74	$HfO_2 - ZrO_2 - TiO_2$; 325-mesh powder, graded	695	690	7	695	One minor circumferential crack on o.d.; total throat radius decrease, 0.017 in. (0.0432 cm)
3	72	$HfO_2 - ZrO_2 - TiO_2$; 100-mesh powder	723	800	7	828	Moderate cracking due to material phase change; total throat radius decrease, 0.020 in. (0.0508 cm)
4	71	$HfO_2 - ZrO_2 - TiO_2$; 100-mesh powder	---	---	1	230	No failure of any kind
5	73	$HfO_2 - ZrO_2 - TiO_2$; 325-mesh powder	703	580	7	703	Surface spallation and one minor o.d. crack; total throat radius decrease, 0.018 in. (0.0457 cm)
6	48	ZrO_2; mixed grain, slip cast, MgO stabilized	300	---	7	706	Moderate axial and circumferential cracks
7	49	ZrO_2 plus graphite; mixed grain, slip cast, MgO stabilized	300	400	8	1006	Two moderate axial cracks; total throat radius decrease, 0.028 in. (0.0712 cm)
8	68	Segmented BeO; with BeO sleeve	300	450	8	691	Several cracked segments and loss of small pieces
9	30	HfC plus graphite	---	53	6	655	No cracking of primary material; formation of adherent oxide resulted in throat radius decrease, 0.041 in. (0.104 cm); total throat erosion, 0.014 in. (0.0356 cm)
10	33	HfC(N) plus graphite; sintered	---	160	6	402	Nonadherent oxide layer, 0.100 in. (0.254 cm) thick; no cracking of primary material; total throat radius decrease, 0.014 in. (0.0559 cm)
11	35	HfC - SiC plus graphite (JT0992)	---	---	1	259	Complete ablative char through and burn through precluded further testing; no cracking
12	36	HfC - SiC plus graphite (JT0992); surface preoxidized	---	25	1	306	Complete ablative char through precluded further testing, preoxidized layer lost; total throat erosion, 0.030 in. (0.0762 cm)

TABLE V. - Continued. RELATIVE ORDER OF MERIT

(2) Continued. Refractory composites

Relative order	Insert	Material	Time cracking first detected, sec	Time area change exceeds ±5 percent, sec	Total cycles	Total firing time, sec	Primary failure mechanism
13	27	SiC washers; segmented 180°	321	215	2	321	Rapid oxidation at end of firing; minor axial cracks
14	46	ZrO_2; mixed grain, sintered, MgO stabilized	300	---	1	300	Four moderate axial cracks and some minor surface spallation
15	45	ZrO_2; mixed grain, sintered, MgO stabilized	60	---	2	360	Moderate axial and circumferential cracks; reaction with molten silica
16	52	ZrO_2 - 11 wt. % Cu	357	---	2	357	Moderate axial cracks
17	53	ZrO_2 - 15 wt. % Cu; thin wall	300	---	1	300	Moderate circumferential cracking with loss of small pieces downstream
18	54	ZrO_2 - 15 wt. % Cu	300	---	1	300	Moderate circumferential cracking
19	51	ZrO_2 - 6 wt. % Cu; thin wall	301	---	1	301	Moderate axial and circumferential cracking
20	57	ZrO_2 - W honeycomb	280	280	1	280	Moderate cracking and surface spallation; total throat radius decrease, 0.020 in. (0.0508 cm)
21	61	MgO - platinum coated steel honeycomb	300	32	1	300	Moderate cracking and spallation; total throat radius decrease, 0.040 in. (0.1015 cm)
22	59	MgO - steel honeycomb	321	50	2	321	Severe cracking with leading edge erosion and gas leak; total throat radius decrease, 0.031 in. (0.0788 cm)
23	67	Segmented BeO; Ta sleeve	221	221	1	221	BeO - Ta reaction; moderate axial cracks; total throat radius decrease, 0.019 in. (0.0483 cm)
24	32	ZrC(N) plus graphite; sintered	205	200	1	205	Rapid erosion at end of firing; moderate circumferential cracks
25	47	ZrO_2; CaO stabilized, mixed grain, slip cast	195	---	1	195	Moderate circumferential cracking and surface spallation

26	29	ZrC plus graphite	178	29	2	178	Gas leak behind insert; total throat radius decrease, 0.011 in. (0.028 cm); moderate circumferential cracks
27	70	W coated BeO powder (25 wt. % W)	---	96	1	225	Rapid erosion at end of firing due to tungsten oxidation
28	62	MgO - platinum honeycomb	---	70	1	143	Ablative failure precluded further testing; total throat radius decrease, 0.036 in. (0.0915 cm)
29	50	ZrO_2 - 6 wt. % Cu	100	---	1	100	Moderate axial and circumferential cracks
30	41	ZrO_2; 75 % density, yttria stabilized, medium grain	300	---	1	302	Severe cracking; broke into many pieces during disassembly
31	60	MgO - Inconel honeycomb	209	131	3	209	Severe cracking and surface spallation; total throat erosion, 0.014 in. (0.0356 cm)
32	69	W coated BeO powder (68 wt. % W)	---	177	1	211	Rapid erosion at end of firing due to tungsten oxidation
33	26	SiC washers	60	170	2	246	Rapid oxidation at end of firing; minor axial cracks
34	28	SiC washers (segmented 120°)	215	163	1	215	Rapid oxidation at end of firing; minor axial cracks
35	56	ZrO_2 - platinum rhodium honeycomb	240	177	1	240	Severe cracking
36	63	MgO - Inconel fibers (0.0003 in. (0.00076 cm) diam)	180	35	1	180	Severe cracking with loss of section aft of throat; total throat erosion, 0.011 in. (0.028 cm)
37	34	ZrC - SiC plus graphite (JT0981)	---	129	1	261	Rapid erosion after 125 sec
38	21	SiC - ZrB_2 plus graphite (JTA); O/F = 1.6	---	129	1	206	Rapid erosion after 100 sec
39	37	HfC - SiC plus graphite (JT0992)	---	121	1	302	Rapid erosion after 100 sec
40	22	SiC - ZrB_2 plus graphite (JTA)	---	95	2	268	Rapid erosion after 75 sec
41	65	MgO - W wires (0.0003 in. (0.00076 cm) diam)	133	80	1	133	Severe cracking and spallation; total throat radius decrease, 0.006 in. (0.0152 cm)
42	64	MgO - Inconel wires (0.005 in. (0.0127 cm) diam)	96	96	1	96	Severe cracking and spallation; total throat erosion, 0.016 in. (0.0407 cm)
43	58	ZrO_2 - platinum coated Mo honeycomb	138	60	1	138	Severe cracking and loss of insert trailing edge

TABLE V. - Concluded. RELATIVE ORDER OF MERIT

(2) Concluded. Refractory Composites

Relative order	Insert	Material	Time cracking first detected, sec	Time area change exceeds ±5 percent sec	Total cycles	Total firing time, sec	Primary failure mechanism
44	40	ZrO_2; 70 % density, yttria stabilized, coarse grain	160	70	1	160	Severe cracking with loss of pieces
45	44	ZrO_2; mixed grain, thin wall, MgO stabilized	60	147	2	156	Cracking leading to loss of throat section
46	23	Pyrolytic graphite washers and cones	---	57	2	163	Rapid oxidation after 40 sec
47	24	Pyrolytic graphite washers and cones	---	35	1	39	Rapid oxidation after 30 sec
48	66	BeO; prestressed	31	--	1	31	Severe circumferential crack due to inadequate prestress
49	25	Pyrolytic graphite wedges and cones	---	27	1	73	Rapid oxidation after 20 sec
50	19	SiC - ZrC plus graphite; Zr base resin binder	---	19	1	66	Rapid erosion after 10 sec
51	20	SiC - ZrC plus graphite; Zr base resin binder	---	18	1	97	Rapid erosion after 10 sec
52	38	80 wt. % SiO_2 - 20 wt. % C	---	12	1	120	Rapid erosion from beginning firing
53	31	ZrC(N) plus graphite, cast	---	10	1	57	Insert completely gone
54	55	ZrO_2 - Inconel honeycomb	---	5	2	31	Rapid surface spallation
55	39	ZrO_2 foam; phenolic resin binder	---	5	1	18	Rapid erosion from beginning of firing
56	43	ZrO_2; 90 % density, yttria stabilized, fine grain	8	4	1	8	Catastrophic cracking
57	42	ZrO_2; 90 % density, yttria stabilized, fine grain	7	3	1	7	Catastrophic cracking

(3) Nozzle designs

1	83	ZrO_2 - 5 vol. % W - Re wires	300	---	7	734	Moderate cracking; total throat radius decrease of 0.010 in. (0.254 cm)
2	84	ZrO_2 - 7 vol. % W - Re wires	[a]0	515	9	1258	Minor axial cracks on insert i.d.; total throat radius decrease of 0.037 in. (0.094 cm)
3	82	ZrO_2 washers	300	470	7	706	Moderate cracking and surface spallation; total throat radius decrease of 0.031 in. (0.0788 cm)
4	81	ZrO_2 washers - pyrolytic graphite washers	---	215	1	215	Moderate cracking and surface spallation of ZrO_2; oxidation of pyrolytic graphite
5	79	TaC; prestressed	228	183	2	228	Oxidation of TaC
6	76	0.020 in. (0.0508 cm) SiC on graphite with coolant reservoir	50	---	1	50	Liner cracked
7	78	0.003 in. (0.0076 cm) WSi_2 on molybdenum	---	45	1	45	Coating melted and oxidized; total throat erosion, 0.025 in. (0.0635 cm)
8	80	HfC - TaC plus graphite; graded	39	12	1	39	Cracking and oxidation
9	77	0.040 in. (0.1015 cm) SiC on graphite with coolant reservoir	16	11	1	16	Liner cracked

[a]This nozzle design was assembled using an insert with minor cracks on the outside diameter which occurred during insert fabrication.

TABLE VI. - THROAT INSERT DATA SHEET

[Characteristic length, 67 in. (170.18 cm).]

(1) Insert 1; injector 2

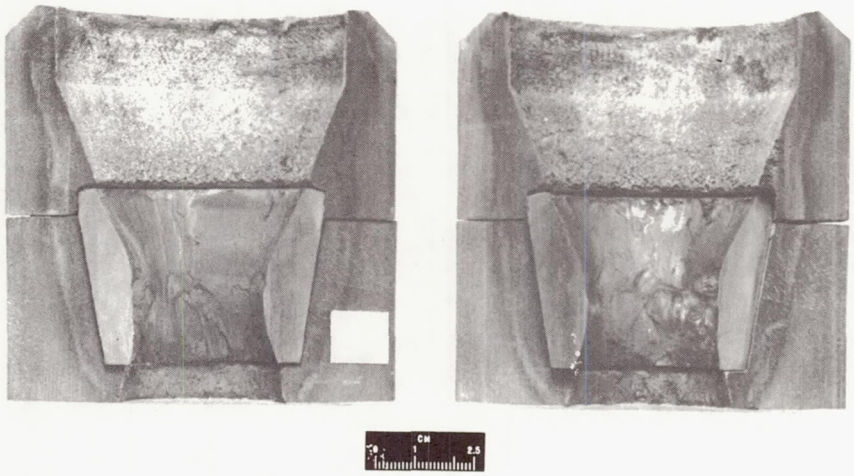

C-66-4150

	Material	Form	Manufacturer	Configuration (a)	Additional layers
Coating	0.006-in. (0.0152-cm) 50 Al_2O_2 - 50 Cr_2O_3	Flame sprayed; gas-pressure bonded	Battelle Memorial Institute	A	0.002-in. (0.005-cm) thick 50 Al_2O_3 - 50 Cr intermediate layer between TZM and i.d. coating
Insert	TZM alloy 99 (Mo - 0.5 Ti - 0.5 Zr)	----------			
Envelope	Silica phenolic (MX 2641)	Cloth 90° centerline	Fiberite	4-in. (10.15-cm) o.d.	None

Run	Chamber pressure, P_c		Oxidant-fuel ratio, O/F	Run time, sec	Total change in effective throat radius, ΔR		Remarks
	psia	kN/m^2			in.	cm	
284	102.1	703	1.99	48.2	0.017	0.043	Melting of coating; shutdown at first sign of coating failure

[a]See fig. 5.

TABLE VI. - Continued

(2) Insert 2;[b] injector 2

	Material	Form	Manufacturer	Configuration (a)	Additional layers
Coating	0.006-in. (0.0152-cm) 50 Al_2O_3 - 50 Cr_2O_3	Flame sprayed; gas-pressure bonded	Battelle Memorial Institute	A	Intermediate layer of 50 Al_2O_3 - 50 Cr between TZM and i.d. coating
Insert	TZM alloy (99 Mo - 0.5 Ti - 0.5 Zr)	----------			
Envelope	Silica phenolic (MX 2641)	Cloth 90° centerline	Fiberite	4-in. (10.15-cm) o.d.	None

Run	Chamber pressure, P_c		Oxidant-fuel ratio, O/F	Run time, sec	Total change in effective throat radius, ΔR		Remarks
	psia	kN/m^2			in.	cm	
299	98.2	676	2.01	60.7	0.133	0.338	Shutdown due to high erosion, melting of coating

[a]See fig. 5.

[b]Photograph not available. Insert 2 looked similar to insert 1.

TABLE VI. - Continued

(3) Insert 3; injector 2

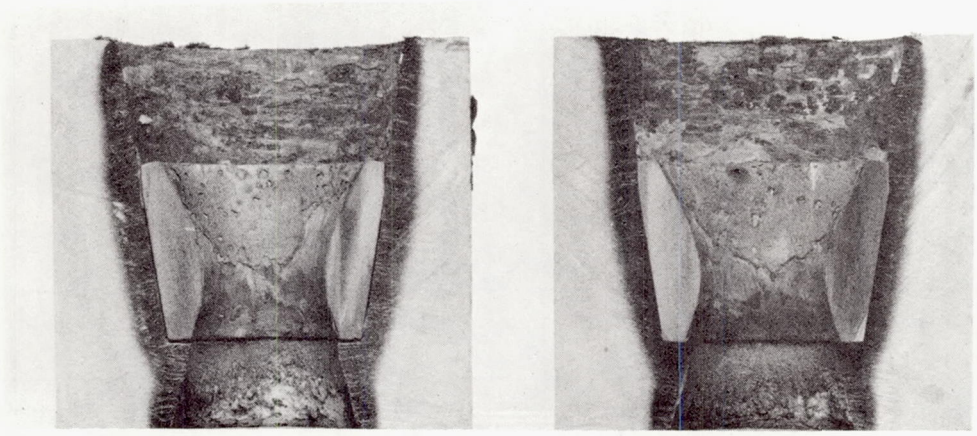

C-66-4149

	Material	Form	Manufacturer	Configuration (a)	Additional layers
Coating	0.006-in. (0.0152-cm) 50 ZrO_2 - 50 HfO_2	Flame sprayed and sintered	Battelle Memorial Institute	B	0.002-in. (0.005-cm) thick 50 ZrO_2 - 50 Cr intermediate layer between TZM and i.d. coating; JTA liner upstream of throat insert
Insert	TZM alloy (99 Mo - 0.5 Ti - 0.5 Zr)	----------			
Envelope	Silica phenolic (MX 2641)	Molded squares	---------	5-in. (12.7-cm) o.d.	None

Run	Chamber pressure, P_c		Oxidant-fuel ratio, O/F	Run time, sec	Total change in effective throat radius, ΔR		Remarks
	psia	kN/m^2			in.	cm	
634	99 to 102	682 to 703	2.00	44.2	0.033	0.084	Coating blistered and removed at throat; shutdown due to erosion

[a]See fig. 5.

TABLE VI. - Continued

(4) Insert 4; injector 2

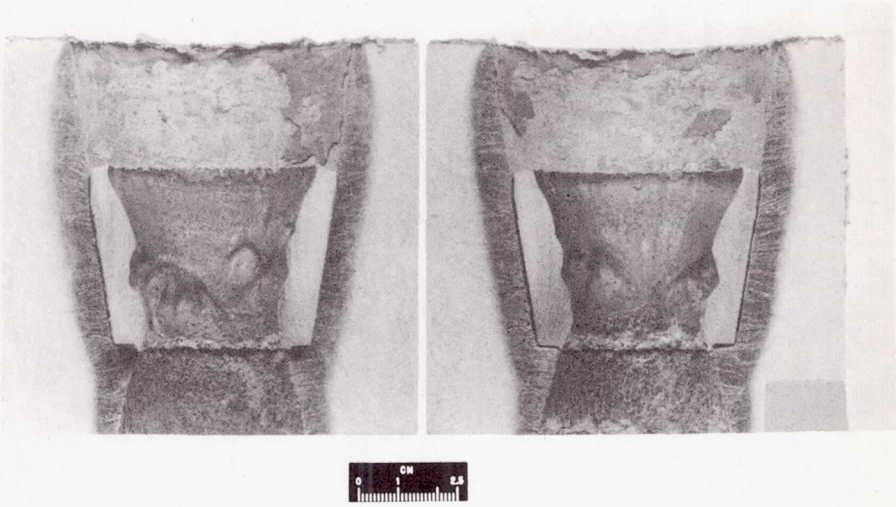

C-66-4350

	Material	Form	Manufacturer	Configuration (a)	Additional layers
Coating	0.006-in. (0.0152-cm) 50 ZrO_2 - 50 HfO_2	Flame sprayed; gas-pressure bonded	Battelle Memorial Institute	B	0.002-in. (0.005-cm) thick 50 ZrO_2 - 50 Cr intermediate layer between TZM and i.d. coating; JTA liner upstream of throat insert
Insert	TZM alloy (99 Mo - 0.5 Ti - 0.5 Zr)	----------			
Envelope	Silica phenolic (MX 2641)	Molded squares	Fiberite	5-in. (12.7-cm) o.d.	None

Run	Chamber pressure, P_c		Oxidant-fuel ratio, O/F	Run time, sec	Total change in effective throat radius, ΔR		Remarks
	psia	kN/m^2			in.	cm	
657	100 to 102	689 to 703	1.98	53.7	0.053	0.134	Shutdown because of rapid erosion

[a]See fig. 5.

TABLE VI. - Continued

(5) Insert 5; injector 2

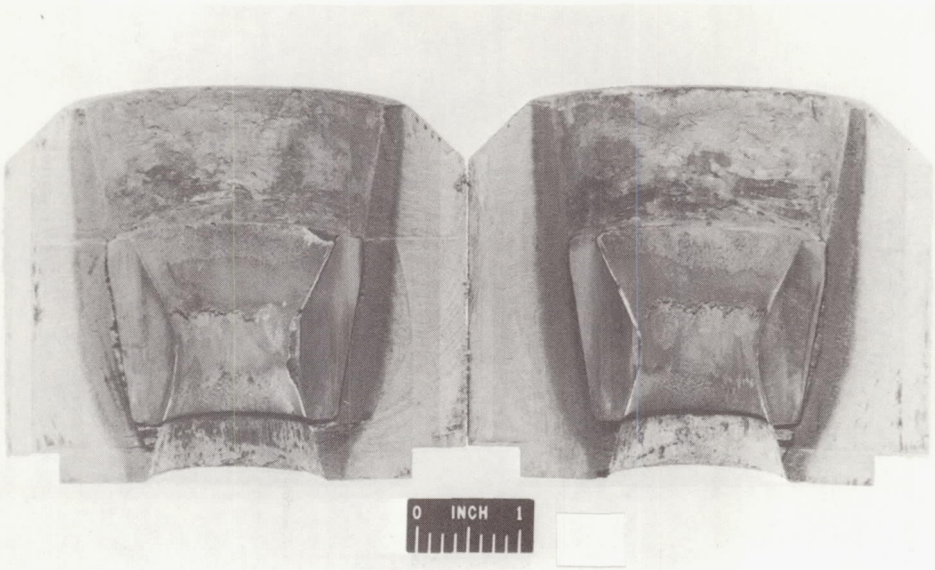

	Material	Form	Manufacturer	Configuration (a)	Additional layers
Coating	0.020-in. (0.0508-cm) 78 Hf - 20 Ta - 2 Mo	Plasma sprayed and sintered	Marquardt	B	JTA liner upstream of throat insert
Insert	TZM alloy (99 Mo - 0.5 Ti - 0.5 Zr)	----------			
Envelope	Silica phenolic (MX 2641)	Molded squares	Fiberite	4-in. (10.15-cm) o.d.	1/4-in. (0.635-cm) thick asbestos phenolic

Run	Chamber pressure, P_c		Oxidant-fuel ratio, O/F	Run time, sec	Total change in effective throat radius, ΔR		Remarks
	psia	kN/m^2			in.	cm	
324	128.6	882	2.07	41.5	0.017	0.0432	Shutdown at first sign of throat erosion; thermal stress failure of coating

[a]See fig. 5.

TABLE VI. - Continued

(6) Insert 6; injector 2

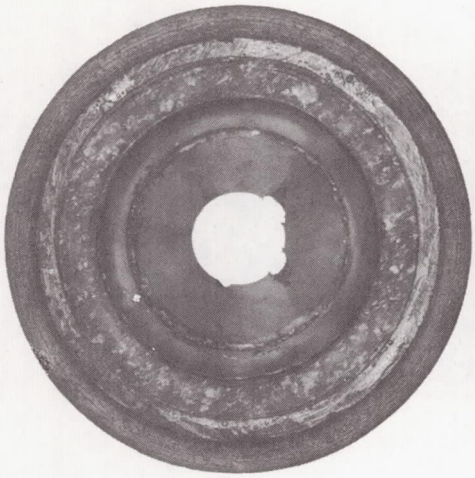

C-67-2613

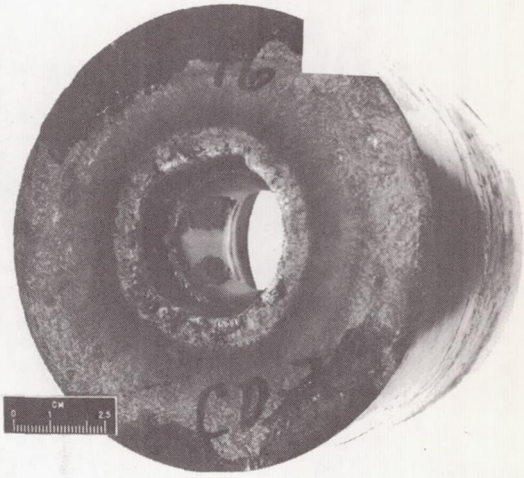

C-67-2616

	Material	Form	Manufacturer	Configuration (a)	Additional layers
Coating	0.003-in. (0.0076-cm) iridium	Slurry coated	IITRI	B (modified, 2.50-in. (6.35-cm) diam at insert leading edge)	0.004-in. (0.01015-cm) thick rhenium between tungsten and i.d. coating; JTA liner upstream of throat insert
Insert	Tungsten	Sintered			
Envelope	Silica phenolic (MX 2641)	Molded squares	-----	5-in. (12.7-cm) o.d.	None

Run	Chamber pressure, P_c		Oxidant-fuel ratio, O/F	Run time, sec	Total change in effective throat radius, ΔR		Remarks
	psia	kN/m^2			in.	cm	
783	100.1	690	2.04	136	0.009	0.0229	Shutdown at first sign of throat erosion: diffusion oxidation of substrate

[a]See fig. 5.

TABLE VI. - Continued

(7) Insert 7; injector 1A

	Material	Form	Manufacturer	Configuration (a)	Additional layers
Coating	0.060-in. (0.1522-cm) pyrolytic graphite	a-b plane axial	American Metal Products	A	None
Insert	Pyrolyzed graphite cloth-phenolic	90° centerline			
Envelope	Silica phenolic (MX 2641)	90° centerline	Fiberite	4-in. (10.15-cm) o.d.	None

Run	Chamber pressure, P_c		Oxidant-fuel ratio, O/F	Run time, sec	Total change in effective throat radius, ΔR		Remarks
	psia	kN/m^2			in.	cm	
117	101.8	701	2.16	99.6	0.069	0.175	Leading edge failure; shutdown at first sign of coating failure at throat

[a]See fig. 5.

TABLE VI. - Continued

(8) Insert 8; injector 2

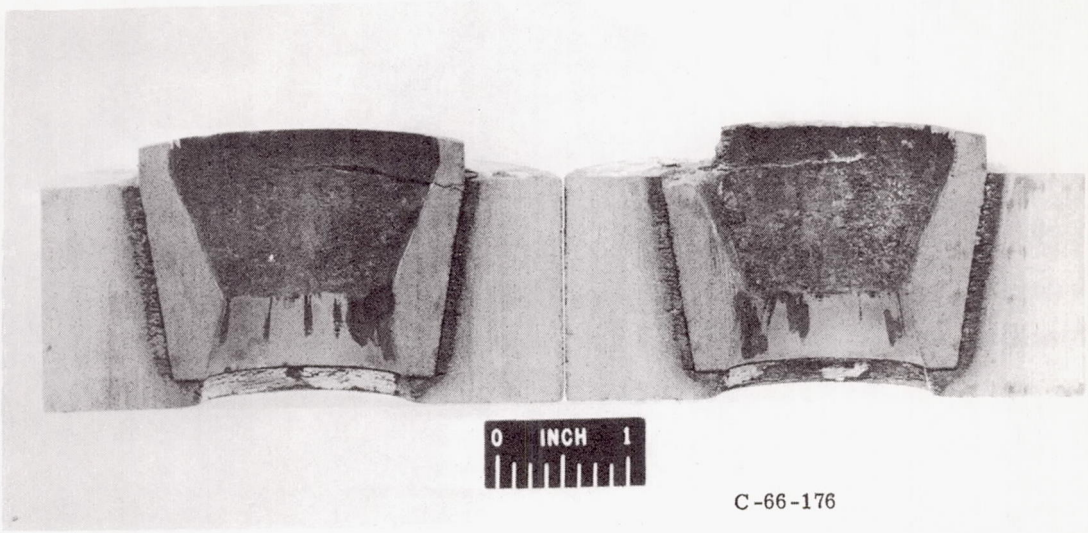

C-66-176

	Material	Form	Manufacturer	Configuration (a)	Additional layers
Coating	0.010-in. (0.0254-cm) pyrolytic graphite and boron (0.5 wt. %)	a-b plane axial	National Carbon	B	JTA liner upstream of insert
Insert	PT 0114	90° centerline			
Envelope	Silica phenolic (MX 2641)	90° centerline	--------	4.0-in. (10.15-cm) o.d.	None

Run	Chamber pressure, P_c		Oxidant-fuel ratio, O/F	Run time, sec	Total change in effective throat radius, ΔR		Remarks
	psia	kN/m^2			in.	cm	
313	100.8	693	1.99	54.0	0.033	0.084	Shutdown after significant throat erosion; substrate and coating cracking

[a]See fig. 5.

TABLE VI. - Continued

(9) Insert 9; injector 2

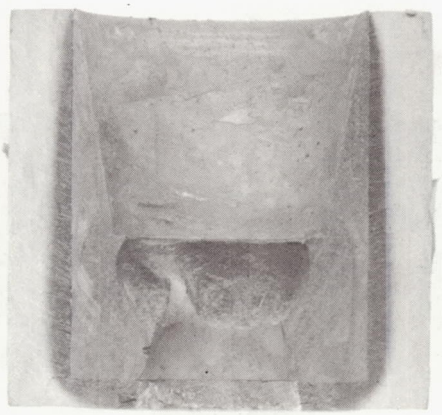

C-66-4354

	Material	Form	Manufacturer	Configuration (a)	Additional layers
Coating	0.040-in. (0.1015-cm) pyrolytic graphite	a-b plane axial	Atlantic Research	B (modified, 1.70-in. (4.32-cm) diam at insert leading edge)	ZrO_2 liner upstream of throat insert
Insert	Low-modulus pyrolyzed graphite cloth substrate	----------			
Envelope	Silica phenolic (MX 2641)	Molded squares	--------	5-in. (12.7-cm) o.d.	None

Run	Chamber pressure, P_c		Oxidant-fuel ratio, O/F	Run time, sec	Total change in effective throat radius, ΔR		Remarks
	psia	kN/m^2			in.	cm	
664	99 to 101	682 to 696	1.99	82.1	0.052	0.132	Shutdown at first sign of throat erosion; oxidation of coating starting at leading edge

[a]See fig. 5.

TABLE VI. - Continued

(10) Insert 10; injector 2

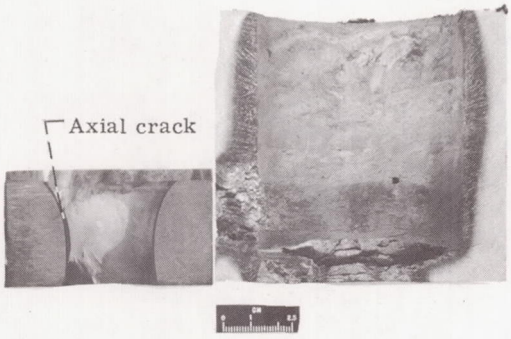

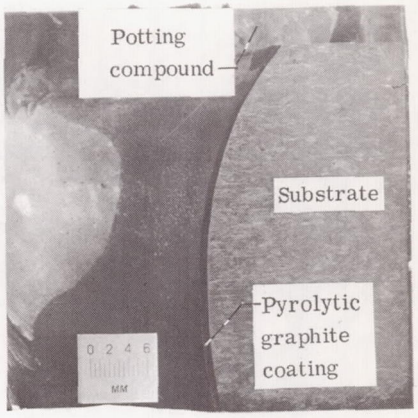

	Material	Form	Manufacturer	Configuration (a)	Additional layers
Coating	0.040-in. (0.1015-cm) pyrolytic graphite	a-b plane axial	Atlantic Research	B (modified, 1.81-in. (4.60-cm) diam at insert leading edge)	JTA graphite upstream of throat
Insert	Low-modulus pyrolyzed graphite cloth substrate	----------			
Envelope	Silica phenolic (MX 2641)	Molded squares	---------	5-in. (12.7-cm) o.d.	None

Run	Chamber pressure, P_c		Oxidant-fuel ratio, O/F	Run time, sec	Total change in effective throat radius, ΔR		Remarks
	psia	kN/m^2			in.	cm	
744	101 to 103	696 to 710	2.04	56.2	0.027	0.0686	Shutdown when throat erosion rate increased rapidly; cracking of substrate (axial)

[a]See fig. 5.

TABLE VI. - Continued

(11) Insert 11; injector 1A

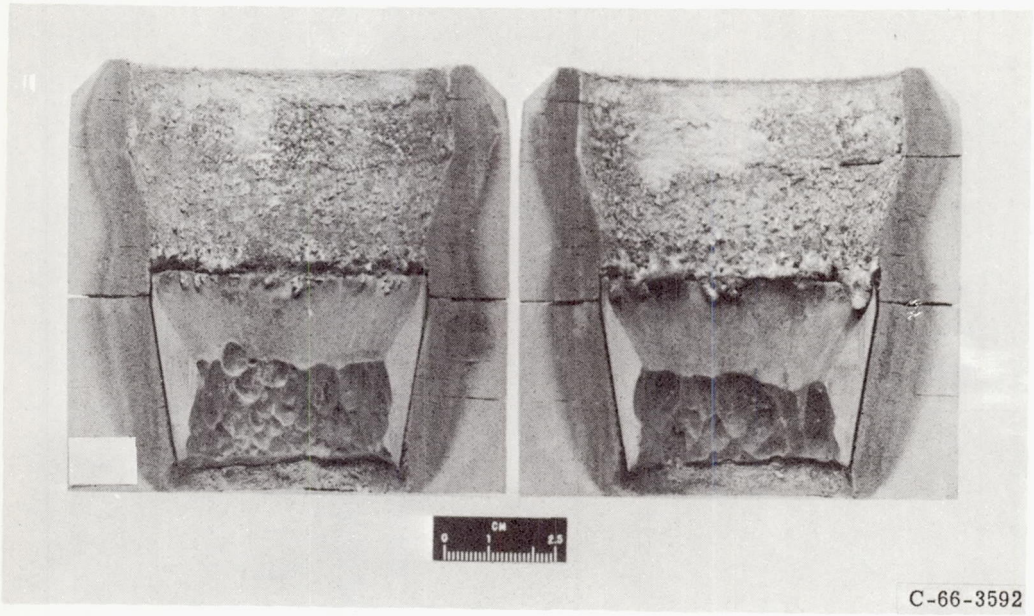

	Material	Form	Manufacturer	Configuration (a)	Additional layers
Coating	0.020-in. (0.0508-cm) ZrC	Pyrolytic deposition	High-Temperature Materials	A	None
Insert	ATJ graphite	----------			
Envelope	Silica phenolic (MX 2641)	90° centerline	Fiberite	4-in. (10.15-cm) o.d.	None

Run	Chamber pressure, P_c		Oxidant-fuel ratio, O/F	Run time, sec	Total change in effective throat radius, ΔR		Remarks
	psia	kN/m^2			in.	cm	
120	103.8	715	2.08	26.1	0.025	0.0635	Coating oxidized and completely removed due to stream shear forces
144	96.0	660	2.00	72.1	.353	.897	Erosion of ATJ alone
				98.2			

[a]See fig. 5.

TABLE VI. - Continued

(12) Insert 12; injector 1A

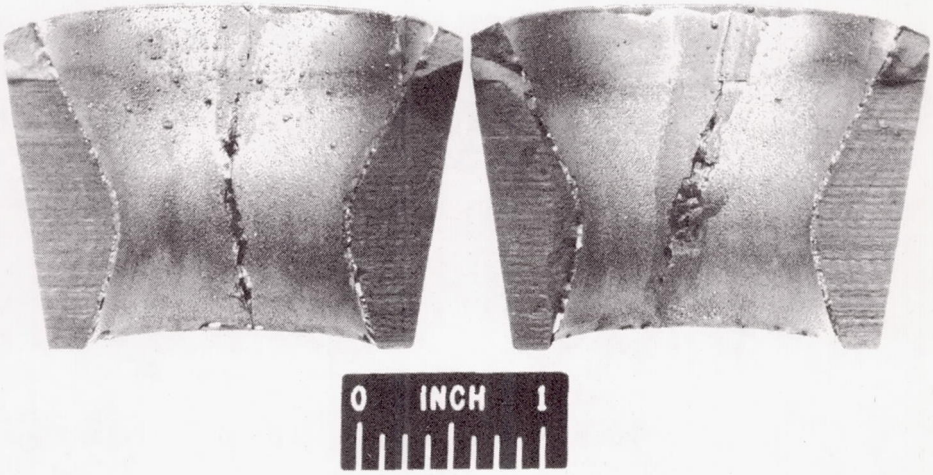

	Material	Form	Manufacturer	Configuration (a)	Additional layers
Coating	0.050-in. (0.127-cm) SiC	Pyrolytic	Dow Corning	A	None
Insert	UT-6 graphite	----------			
Envelope	Silica phenolic (MX 2641)	90° centerline	Fiberite	4.0-in. (10.15-cm) o.d.	None

Run	Chamber pressure, P_c		Oxidant-fuel ratio, O/F	Run time, sec	Total change in effective throat radius, ΔR		Remarks
	psia	kN/m^2			in.	cm	
267	96.1	661	2.01	12.2	0.010	0.0254	Coating cracked, slight substrate erosion: shutdown at first sign of coating failure

[a]See fig. 5.

TABLE VI. - Continued

(13) Insert 13; injector 1

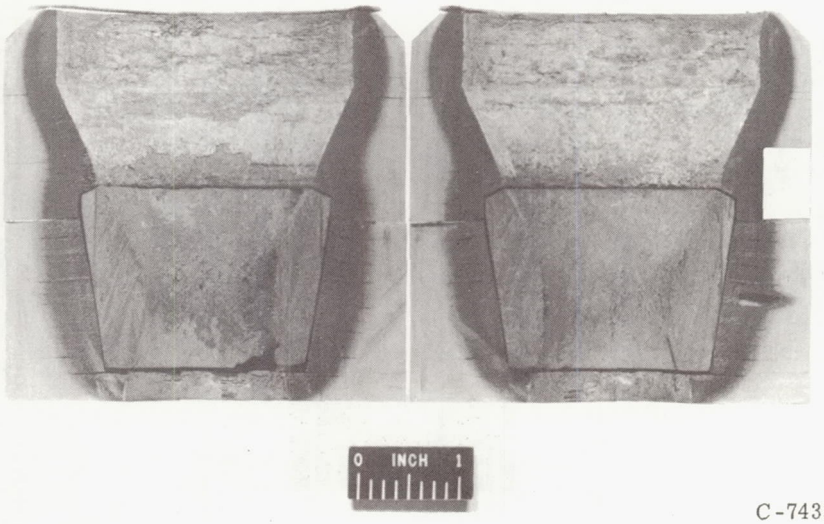

C-74334

	Material	Form	Manufacturer	Configuration (a)	Additional layers
Coating	0.005-in. (0.0127-cm) SiC plus 0.025-in. (0.0635-cm) diffusion	Pack cementation	National Carbon	A	None
Insert	RVC graphite	----------			
Envelope	Silica pehnolic (MX 2641)	90° centerline	Fiberite	4.0-in. (10.15-cm) o.d.	None

Run	Chamber pressure, P_c		Oxidant-fuel ratio, O/F	Run time, sec	Total change in effective throat radius, ΔR		Remarks
	psia	kN/m^2			in.	cm	
34	97.6	672	2.3	62.4	0.010	0.0254	Coating oxidized, substrate erosion beginning; shutdown at first sign of coating failure

[a]See fig. 5.

TABLE VI. - Continued

(14) Insert 14; injector 2

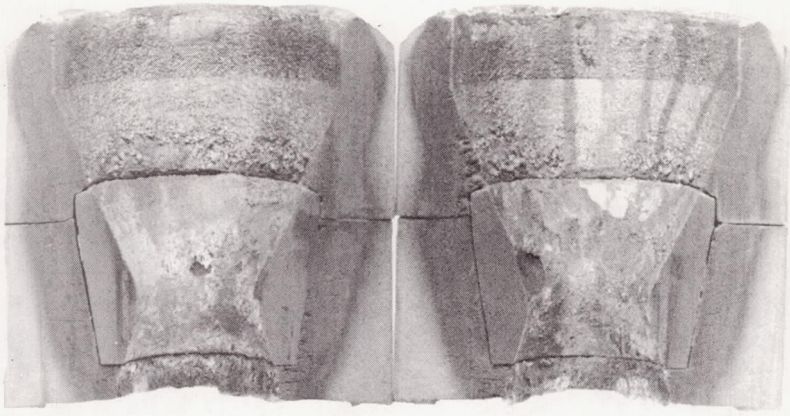

C-66-181

	Material	Form	Manufacturer	Configuration (a)	Additional layers
Coating	0.030-in. (0.0762-cm) SiC	Pyrolytic	Dow Corning	A	None
Insert	UT-6	----------			
Envelope	Silica phenolic (MX 2641)	90° centerline	Fiberite	4.0-in. (10.15-cm) o.d.	None

Run	Chamber pressure, P_c		Oxidant-fuel ratio, O/F	Run time, sec	Total change in effective throat radius, ΔR		Remarks
	psia	kN/m^2			in.	cm	
283	94.2	648	1.95	93.8	0.005	0.0127	Coating oxidized, substrate erosion beginning; shutdown at first sign of coating failure

[a]See fig. 5.

TABLE VI. - Continued

(15) Insert 15; injector 2

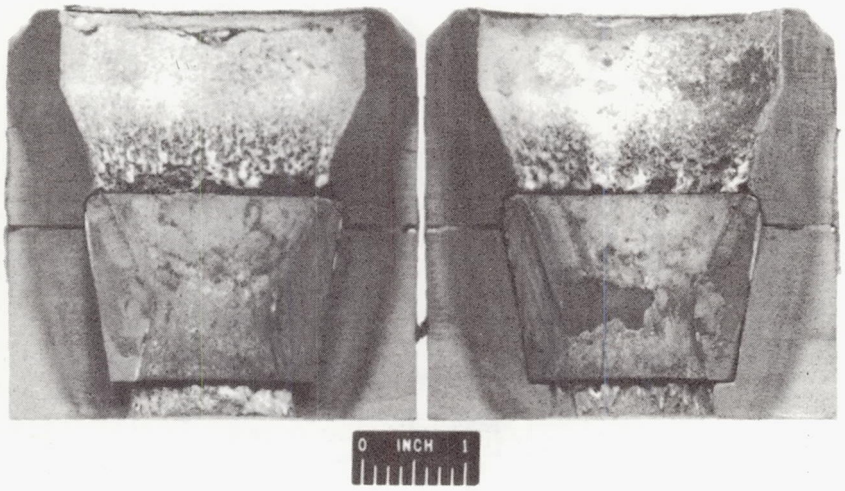

C-66-3000

	Material	Form	Manufacturer	Configuration (a)	Additional layers
Coating	0.037-in. (0.094-cm) Sic	Pyrolytic	Dow Corning	A	None
Insert	Speer SX-4 graphite	----------			
Envelope	Silica phenolic (MX 2641)	90° centerline	Fiberite	4-in. (10.15-cm) o.d.	None

Run	Chamber pressure, P_c		Oxidant-fuel ratio, O/F	Run time, sec	Total change in effective throat radius, ΔR		Remarks
	psia	kN/m^2			in.	cm	
424	101.6	698	2.04	121.4	0.034	0.0862	Shutdown at first sign of coating failure

[a]See fig. 5.

TABLE VI. - Continued

(16) *Insert 16; injector 2*

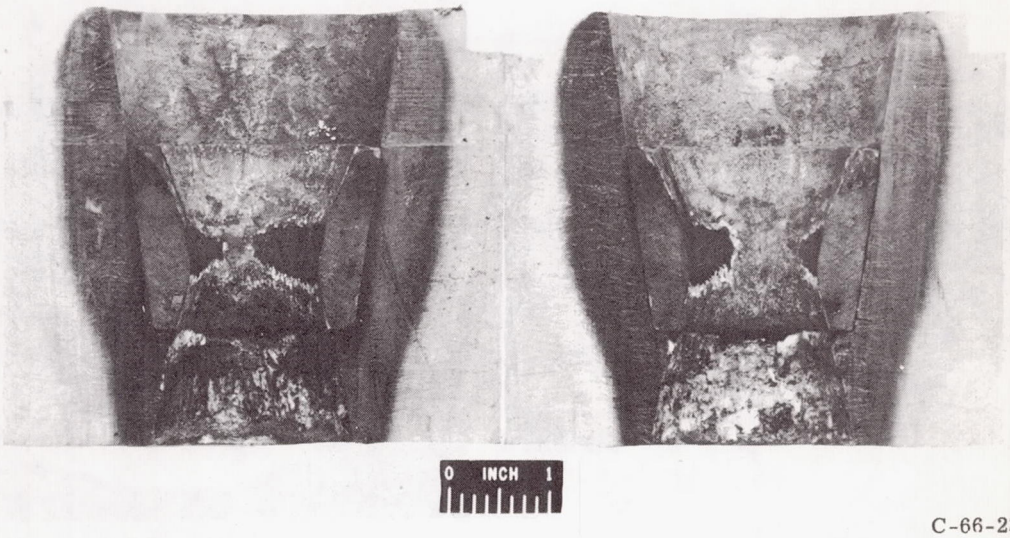

C-66-2302

	Material	Form	Manufacturer	Configuration (a)	Additional layers
Coating	0.023-in. (0.0584-cm) SiC	Pyrolytic	Dow Corning	B	JTA liner upstream of throat insert
Insert	Speer SX-4 graphite	----------			
Envelope	Silica phenolic (MX 2641)	90° centerline	Fiberite	4-in. (10.15-cm) o.d.	None

Run	Chamber pressure, P_c		Oxidant-fuel ratio, O/F	Run time, sec	Total change in effective throat radius, ΔR		Remarks
	psia	kN/m^2			in.	cm	
486	99.3	685	1.56	146.1	0.024	0.061	Shutdown at first sign of coating failure

[a]See fig. 5.

TABLE VI. - Continued

(17) Insert 17; injector 1A

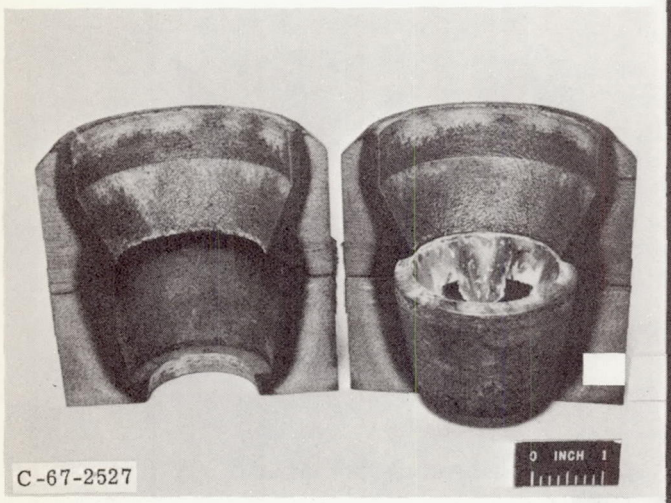

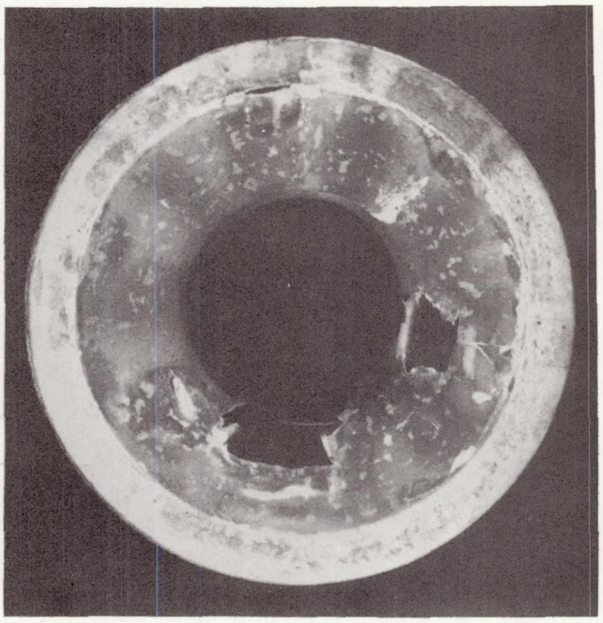

	Material	Form	Manufacturer	Configuration (a)	Additional layers
Coating	0.005-in. (0.0127-cm) iridium	Slurry dip	Union Carbide	A	None
Insert	Graphite	High-thermal expansion coefficient			
Envelope	Silica phenolic (MX 2641)	90° centerline	Fiberite	4-in. (10.15-cm) o.d.	None

Run	Chamber pressure, P_c		Oxidant-fuel ratio, O/F	Run time, sec	Total change in effective throat radius, ΔR		Remarks
	psia	kN/m^2			in.	cm	
203	99.6	684	2.04	40.0	0.002	0.00508	Coating buckled; shutdown at first sign of coating failure

[a]See fig. 5.

TABLE VI. - Continued

(18) Insert 18, injector 1A

C-66-3598

	Material	Form	Manufacturer	Configuration (a)	Additional layers
Coating	0.003-in. (0.0076-cm) iridium	Slurry dip	Union Carbide	A	None
Insert	Graphite	High-thermal expansion coefficient			
Envelope	Silica phenolic (MX 2641)	90° centerline	Fiberite	4-in. (10.15-cm) o.d.	None

Run	Chamber pressure, P_c		Oxidant-fuel ratio, O/F	Run time, sec	Total change in effective throat radius, ΔR		Remarks
	psia	kN/m^2			in.	cm	
268	102.1	704	2.01	71.0	0.005	0.0127	Partial coating loss; shutdown at first sign of coating failure

[a]See fig. 5.

TABLE VI. - Continued

(19) Insert 19; injector 1A

C-65-2526

	Material	Form	Manufacturer	Configuration (a)	Additional layers
Insert	SiC-ZrC coated graphite powder with 20 % Zr base resin binder	Sintered	Magnesium Aerospace	A	None
Envelope	Silica phenolic (MX 2641)	90° Centerline	Fiberite	4-in. (10.15-cm) o.d.	None

Run	Chamber pressure, P_c		Oxidant-fuel ratio, O/F	Run time, sec	Total change in effective throat radius, ΔR		Remarks
	psia	kN/m^2			in.	cm	
204	99.5	686	2.07	65.5	0.224	0.569	High erosion; shutdown

[a]See fig. 5.

TABLE VI. - Continued

(20) Insert 20; injector 1A

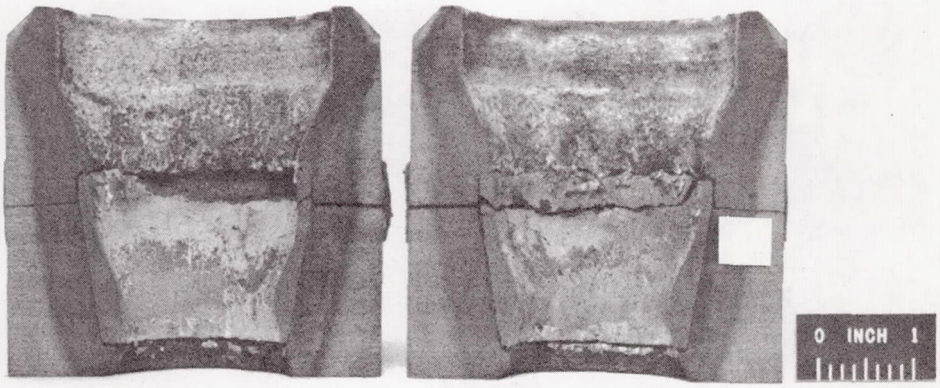

C-65-2529

	Material	Form	Manufacturer	Configuration (a)	Additional layers
Insert	SiC-ZrC coated graphite powder with 20 % Zr base resin binder	Sintered	Magnesium Aerospace	A	None
Envelope	Silica phenolic (MX 2641)	90° centerline	Fiberite	4-in. (10.15-cm) o.d.	None

Run	Chamber pressure, P_c		Oxidant-fuel ratio, O/F	Run time, sec	Total change in effective throat radius, ΔR		Remarks
	psia	kN/m^2			in.	cm	
205	99.5	686	2.07	96.6	0.212	0.538	High erosion; shutdown

[a]See fig. 5.

TABLE VI. - Continued

(21) Insert 21; injector 2

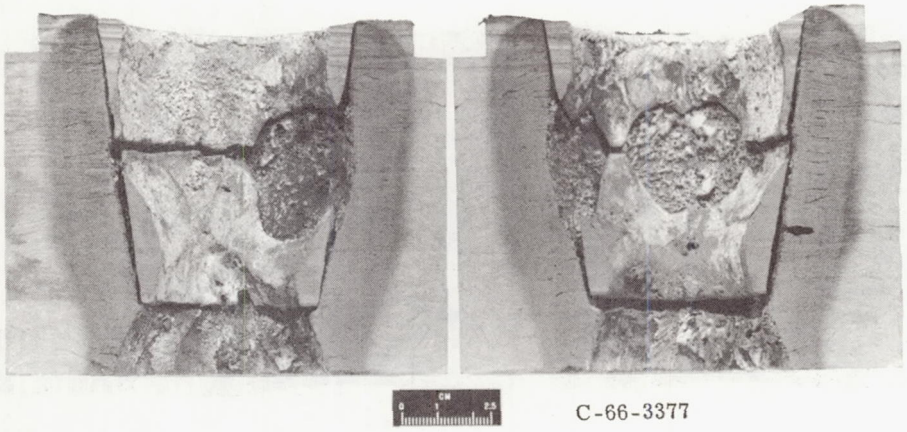

C-66-3377

	Material	Form	Manufacturer	Configuration (a)	Additional layers
Insert	48 C - 35 Zr - 8 B - 9 Si (JTA graphite)	Sintered	National Carbon	B	None
Envelope	Silica phenolic (MX 2641)	Molded squares	----------	5-in. (12.7-cm) o.d.	JTA liner upstream of throat area

Run	Chamber pressure, P_c		Oxidant-fuel ratio, O/F	Run time, sec	Total change in effective throat radius, ΔR		Remarks
	psia	kN/m^2			in.	cm	
532	101.5	700	1.6	206.2	0.156	0.396	Upstream erosion severe; shutdown due to rapid erosion

[a]See fig. 5.

TABLE VI. - Continued

(22) Insert 22; injector 3

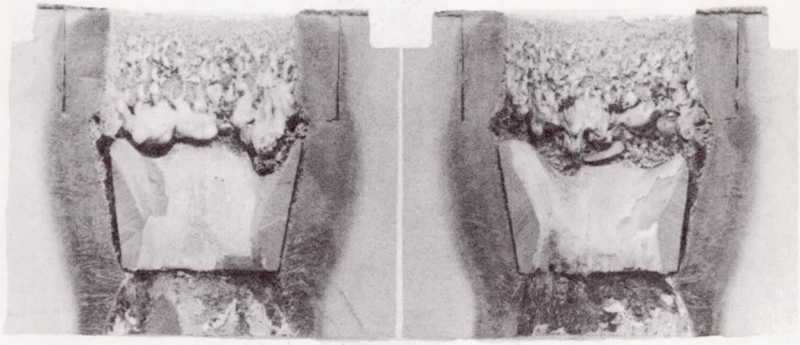

C-66-3596

	Material	Form	Manufacturer	Configuration (a)	Additional layers
Insert	48 C - 35 Zr - 8 B - 9 Si (JTA graphite)	Sintered	National Carbon	B - run 560 A - run 562	None
Envelope	Silica phenolic (MX 2641)	Molded squares	--------	5-in. (12.7-cm) o.d.	JTA liner upstream of throat insert

Run	Chamber pressure, P_c		Oxidant-fuel ratio, O/F	Run time, sec	Total change in effective throat radius, ΔR		Remarks
	psia	kN/m^2			in.	cm	
560	102	703	2.02	98.7	0.016	0.0407	JTA liner upstream; shutdown after erosion established
562	102	703	2.02	169.0 267.7	.143	.363	Ablative upstream; rapid erosion

[a]See fig. 5.

TABLE VI. - Continued

(23) Insert 23; injector 1A

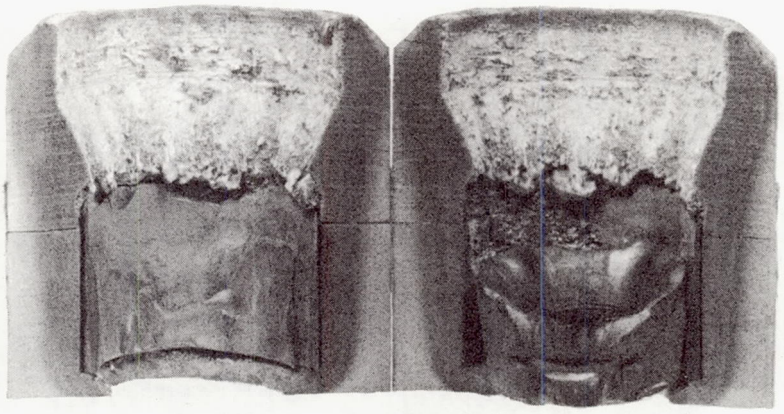

0 INCH 1

C-66-188

	Material	Form	Manufacturer	Configuration (a)	Additional layers
Insert	Pyrolytic graphite: inside diameter, washers outside diameter, cones	a-b plane radial and circumferential a-b plane axial and circumferential	Pyrogenics	A	None
Envelope	Silica phenolic (MX 2641)	90° centerline	----------	4-in. (10.15-cm) o.d.	None

Run	Chamber pressure, P_c		Oxidant-fuel ratio, O/F	Run time, sec	Total change in effective throat radius, ΔR		Remarks
	psia	kN/m^2			in.	cm	
187	101.3	697	1.93	60.3	0.013	0.033	Slight oxidation; timed shutdown
202	100.0	689	2.03	102.7	.096	.243	Erosion and oxidation; shutdown for excessive erosion rate
				163.0			

[a]See fig. 5.

TABLE VI. - Continued

(24) Insert 24; injector 2

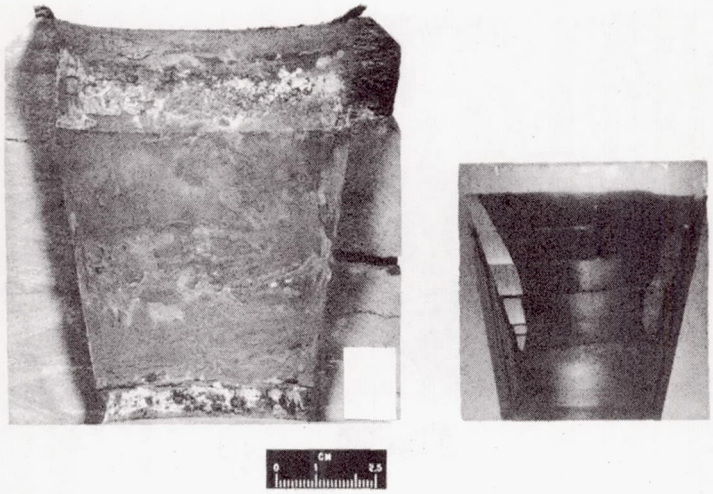

C-66-4143

	Material	Form	Manufacturer	Configuration (a)	Additional layers
Insert	Pyrolytic graphite: inside diameter, washers outside diameter, cone	a-b plane radial and circumferential a-b plane axial and circumferential	General Electric Super Temp	B	1/8-in. (0.32-cm) thick Ta ring
Envelope	Silica phenolic (MX 2641)	90° centerline	Fiberite	5-in. (12.7-cm) o.d.	None

Run	Chamber pressure, P_c		Oxidant-fuel ratio O/F	Run time, sec	Total change in effective throat radius, ΔR		Remarks
	psia	kN/m^2			in.	cm	
428	101.6	699	1.62	38.9	0.008	0.0203	Shutdown due to rapid erosion

[a]See fig. 5.

TABLE VI. - Continued

(25) Insert 25; injector 2

C-66-4142

	Material	Form	Manufacturer	Configuration (a)	Additional layers
Insert	Pyrolytic graphite: inside diameter, wedges outside diameter, cone	a-b plane radial and axial a-b plane axial and circumferential	Super Temp	B	1/8-in. (0.32-cm) thick Ta ring
Envelope	Silica phenolic (MX 2641)	90° centerline	Fiberite	5-in. (12.7-cm) o.d.	None

Run	Chamber pressure, P_c		Oxidant-fuel ratio, O/F	Run time, sec	Total change in effective throat radius, ΔR		Remarks
	psia	kN/m^2			in.	cm	
426	100.8	694	1.45	73.4	0.036	0.0865	Shutdown due to rapid erosion

[a]See fig. 5.

TABLE VI. - Continued

(26) Insert 26; injector 1A

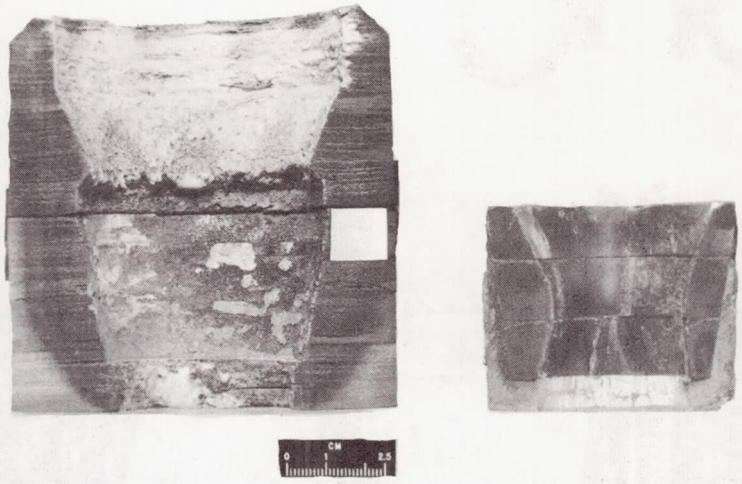

C-66-4141

	Material	Form	Manufacturer	Configuration (a)	Additional layers
Insert	SiC	Three axial washers	Avco Corp.	B	None
Envelope	Silica phenolic (MX 2641)	90° centerline	Fiberite	4-in. (10.15-cm) o.d.	None

Run	Chamber pressure, P_c		Oxidant-fuel ratio, O/F	Run time, sec	Total change in effective throat radius, ΔR		Remarks
	psia	kN/m^2			in.	cm	
185	87.9	603	1.91	60.6	0	0	Axial cracks; timed shutdown
191	99.8	687	1.93	185.3	.105	.267	Erosion and oxidation; shutdown due to rapid erosion
				245.9			

[a]See fig. 5.

TABLE VI. - Continued

(27) Insert 27; injector 1A

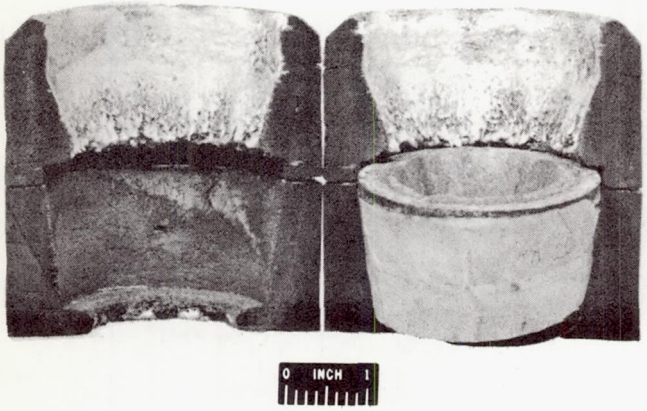

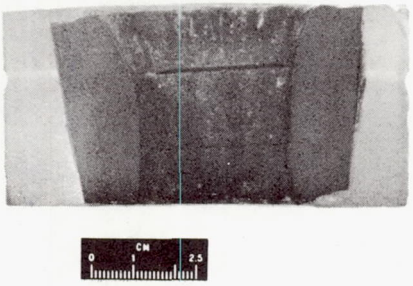

C-66-189

	Material	Form	Manufacturer	Configuration (a)	Additional layers
Insert	SiC	Three axial washers each segmented 180°	--------	A	1/4-in. (0.635-cm) thick SiC
Envelope	Silica phenolic (MX 2641)	90° centerline	Fiberite	4-in. (10.15-cm) o.d.	None

Run	Chamber pressure, P_c		Oxidant-fuel ratio, O/F	Run time, sec	Total change in effective throat radius, ΔR		Remarks
	psia	kN/m^2			in.	cm	
189	100.4	693	1.93	60.2	0	0	Axial cracks; timed shutdown
190	99.8	687	1.93	260.7 / 320.9	.161	.409	Erosion and oxidation

[a]See fig. 5.

TABLE VI. - Continued

(28) Insert 28; injector 2

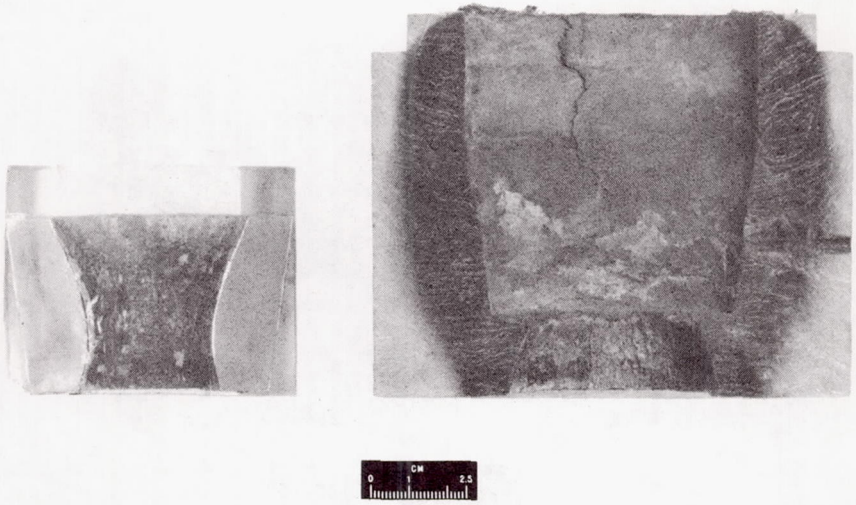

C-67-3840

	Material	Form	Manufacturer	Configuration (a)	Additional layers
Insert	SiC	Three axial washers each segmented 120°	--------	B	1/4-in. (0.635-cm) thick SiC; JTA liner upstream of throat insert
Envelope	Silica phenolic (MX 2641)	90° centerline	--------	5-in. (12.7-cm) o.d.	None

Run	Chamber pressure, P_c		Oxidant-fuel ratio, O/F	Run time, sec	Total change in effective throat radius, ΔR		Remarks
	psia	kN/m^2			in.	cm	
781	102 to 105	702 to 722	2.04	215	0.046	0.107	Preferential oxidation at segment interfaces; axial cracking; erosion and oxidation

[a]See fig. 5.

TABLE VI. - Continued

(29) Insert 29; injector 2

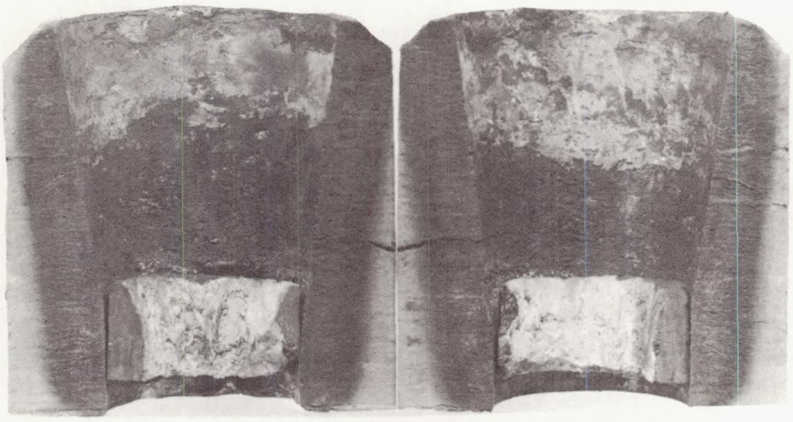

C-66-182

	Material	Form	Manufacturer	Configuration (a)	Additional layers
Insert	ZrC plus graphite	Hypereutectic cast	Aerospace Corporation	C	JTA liner upstream of throat insert
Envelope	Silica phenolic (MX 2641)	90° centerline	Fiberite	4-in. (10.15-cm) o.d.	None

Run	Chamber pressure, P_c		Oxidant-fuel ratio, O/F	Run time, sec	Total change in effective throat radius, ΔR		Remarks
	psia	kN/m^2			in.	cm	
314	101.8	701	2.03	24.9	-0.025	-0.066	Seal leak at chamber
326	104.8	721	2.00	153.1 178.0	-.011	-.029	Gas flow behind insert, oxidation

[a]See fig. 5.

TABLE VI. - Continued

(30) Insert 30; injector 2

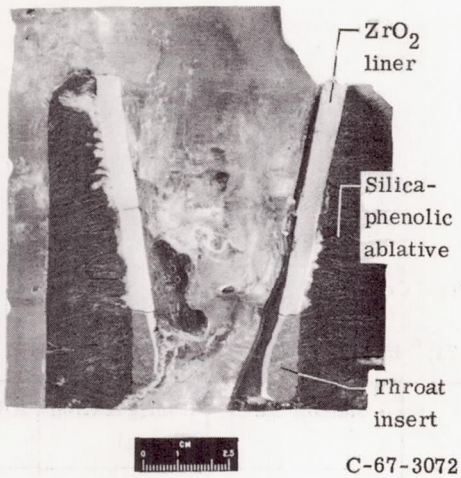

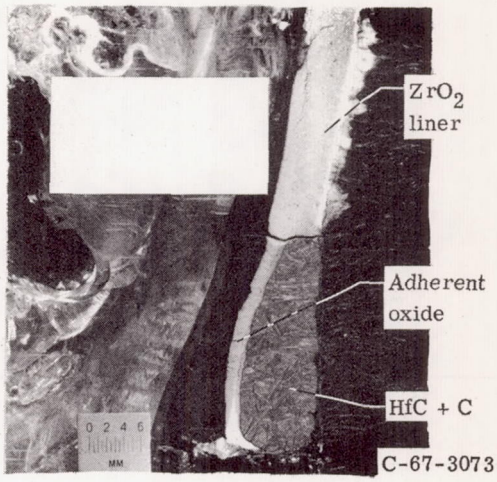

	Material	Form	Manufacturer	Configuration (a)	Additional layers
Insert	HfC plus graphite	Hypereutectic cast	Aerospace Corporation	C	ZrO_2 liner upstream of throat insert
Envelope	Silica phenolic (MX 2641)	Molded squares	Fiberite	4-in. (10.15-cm) o.d.	None

Run	Chamber pressure, P_c		Oxidant-fuel ratio, O/F	Run time, sec	Total change in effective throat radius, ΔR		Remarks
	psia	kN/m^2			in.	cm	
659	101	696	1.97	159.8	-0.041	-0.104	Shutdown due to gas leakage
663	101	696	2.00	36.3	-.037	-.094	Shutdown for water leakage
665	100	689	2.00	4.6	------	------	Accidental abort
666	101.5	698	2.04	51.2	0	0	Manual abort for erosion
753	94.5	652	2.04	212.0	-.003	-.0076	Out of propellant
766	101	696	2.03	190.8	.014	.0356	Manual abort due to gas leakage through ablative envelope
				654.7			

[a]See fig. 5.

TABLE VI. - Continued

(31) Insert 31;[c] injector 2

	Material	Form	Manufacturer	Configuration (a)	Additional layers
Insert	ZrC(N) plus graphite	Cast	Battelle Memorial Institute	B	JTA liner upstream of throat insert
Envelope	Silica phenolic (MX 2641)	90° centerline	Fiberite	4-in. (10.15-cm) o.d.	None

Run	Chamber pressure, P_c		Oxidant-fuel ratio, O/F	Run time, sec	Total change in effective throat radius, ΔR		Remarks
	psia	kN/m^2			in.	cm	
354	100.5	692	2.12	56.8	[b]0.121	0.307	Insert completely gone

[a]See fig. 5.
[b]Calculated.
[c]Photograph not available because of loss of insert.

TABLE VI. - Continued

(32) Insert 32; injector 2

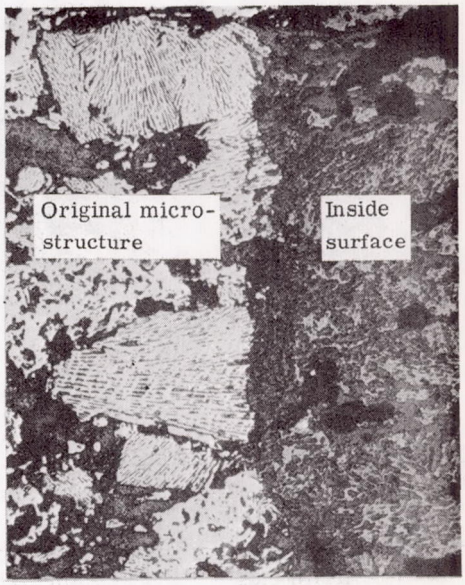

	Material	Form	Manufacturer	Configuration (a)	Additional layers
Insert	ZrC(N) plus graphite	Sintered	Battelle Memorial Institute	B	JTA liner upstream of throat insert
Envelope	Silica phenolic (MX 2641)	90° centerline	Fiberite	4-in. (10.15-cm) o.d.	None

Run	Chamber pressure, P_c		Oxidant-fuel ratio, O/F	Run time, sec	Total change in effective throat radius, ΔR		Remarks
	psia	kN/m^2			in.	cm	
355	100.8	693	2.13	204.5	0.011	0.0254	Erosion and oxidation; circumferential cracks; shutdown at first sign of erosion

[a]See fig. 5.

TABLE VI. - Continued

(33) Insert 33; injector 2

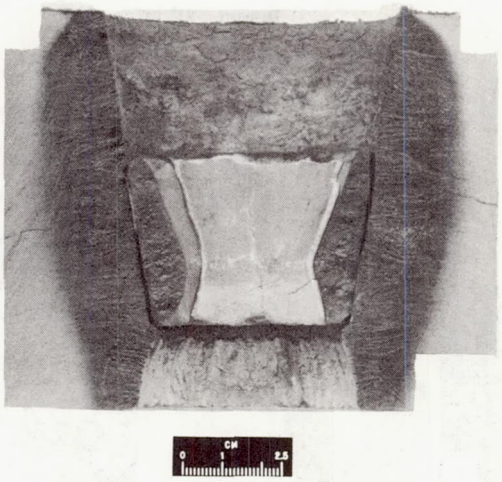

C-66-4353

	Material	Form	Manufacturer	Configuration (a)	Additional layers
Insert	HfC(N) plus graphite	Sintered	Battelle Memorial Institute	B	JTA liner upstream of throat insert
Envelope	Silica phenolic (MX 2641)	Molded squares	----------	5-in. (12.7-cm) o.d.	None

Run	Chamber pressure, P_c		Oxidant-fuel ratio, O/F	Run time, sec	Total change in effective throat radius, ΔR		Remarks
	psia	kN/m^2			in.	cm	
648	100	689	1.99	301.0	-0.022	-0.558	Timed shutdown; axial cracks
652	101	696	1.98	20.8	[b]-.021	-.0533	Timed shutdown
653	101	696	1.98	20.0	[b]-.019	-.0482	Timed shutdown
654	101.5	698	1.99	20.0	[b]-.018	-.0457	Timed shutdown
655	101.5	698	1.98	20.0	[b]-.019		Timed shutdown
656	101.5	698	1.98	20.0	-.014	-.0355	Timed shutdown; delamination upstream of throat
				401.8			

[a]See fig. 5.
[b]Calculated.

TABLE VI. - Continued

(34) Insert 34; injector 2

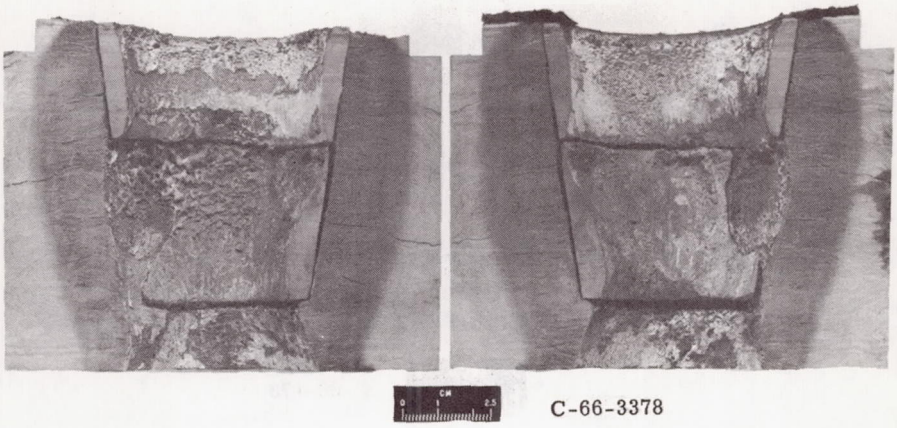

C-66-3378

	Material	Form	Manufacturer	Configuration (a)	Additional layers
Insert	ZrC - SiC plus graphite (JT0981)	Sintered	National Carbon	B	JT0981 liner upstream of throat insert
Envelope	Silica phenolic (MX 2641)	Molded squares	Fiberite	5-in. (12.7-cm) o.d.	None

Run	Chamber pressure, P_c		Oxidant-fuel ratio, O/F	Run time, sec	Total change in effective throat radius, ΔR		Remarks
	psia	kN/m^2			in.	cm	
533	101.4	698	1.56	260.7	0.182	0.462	Shutdown due to high erosion

[a]See fig. 5.

TABLE VI. - Continued

(35) Insert 35; injector 2

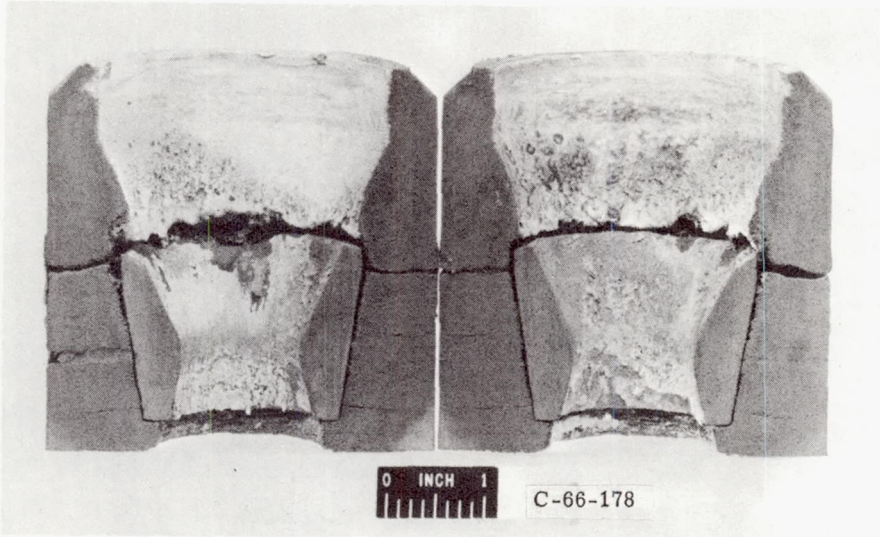

	Material	Form	Manufacturer	Configuration (a)	Additional layers
Insert	HfC - SiC plus graphite (JT0992)	Sintered	National Carbon	A	None
Envelope	Silica phenolic (MX 2641)	90° centerline	Fiberite	4-in. (10.15-cm) o.d.	None

Run	Chamber pressure, P_c		Oxidant-fuel ratio, O/F	Run time, sec	Total change in effective throat radius, ΔR		Remarks
	psia	kN/m^2			in.	cm	
300	96.7	666	2.01	258.7	0.008	0.0203	Shutdown due to burn-through of ablative envelope

[a]See fig. 5.

TABLE VI. - Continued

(36) Insert 36; injector 2

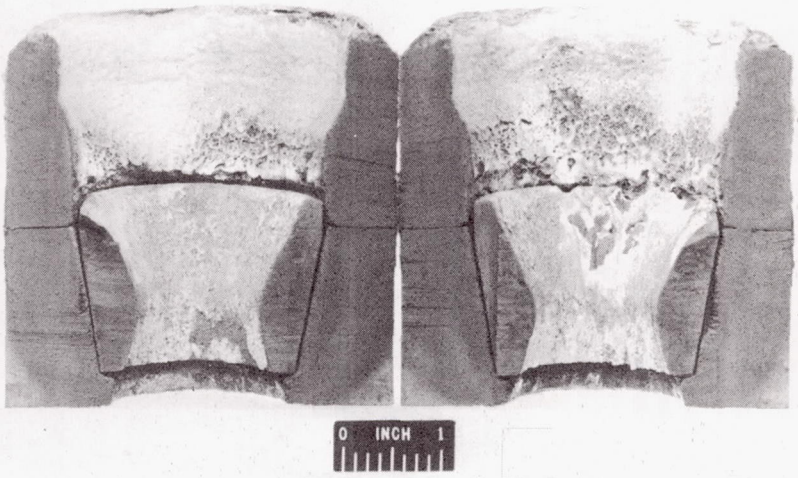

C-66-177

	Material	Form	Manufacturer	Configuration (a)	Additional layers
Coating	0.010-in. (0.0254-cm) thick preoxidized composite material		National Carbon	A	None
Insert	HfC - SiC plus graphite (JT0992)	Sintered			
Envelope	Silica phenolic (MX 2641)	90° centerline	Fiberite	4-in. (10.15-cm) o.d.	None

Run	Chamber pressure, P_c		Oxidant-fuel ratio, O/F	Run time, sec	Total change in effective throat radius, ΔR		Remarks
	psia	kN/m^2			in.	cm	
291	99.2	682	2.05	305.5	0.030	0.076	Timed shutdown; ablative completely charred

[a]See fig. 5.

TABLE VI. - Continued

(37) Insert 37; injector 2

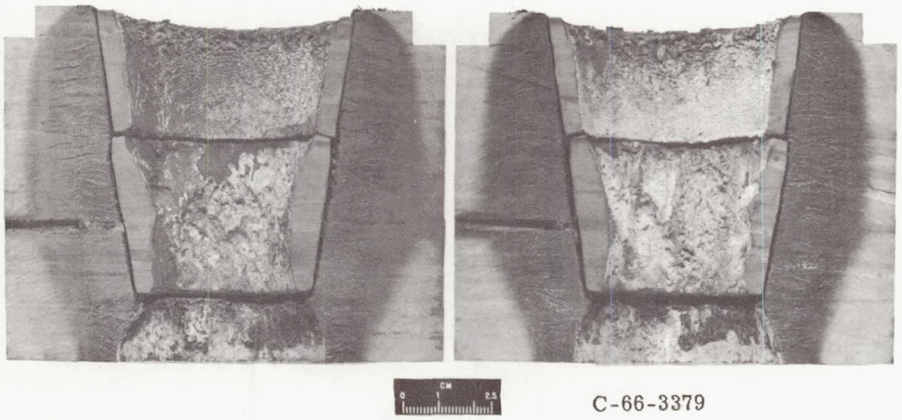

C-66-3379

	Material	Form	Manufacturer	Configuration (a)	Additional layers
Insert	HfC - SiC plus graphite (JT0992)	Sintered	National Carbon	B	JT0992 liner upstream of throat insert
Envelope	Silica phenolic (MX 2641)	Molded squares	Fiberite	5-in. (12.7-cm) o.d.	JT0992 liner upstream of throat insert

Run	Chamber pressure, P_c		Oxidant-fuel ratio, O/F	Run time, sec	Total change in effective throat radius, ΔR		Remarks
	psia	kN/m^2			in.	cm	
534	101.2	696	1.56	301.6	0.181	0.46	Timed shutdown; rapid erosion

[a]See fig. 5.

TABLE VI. - Continued

(38) Insert 38; injector 1A

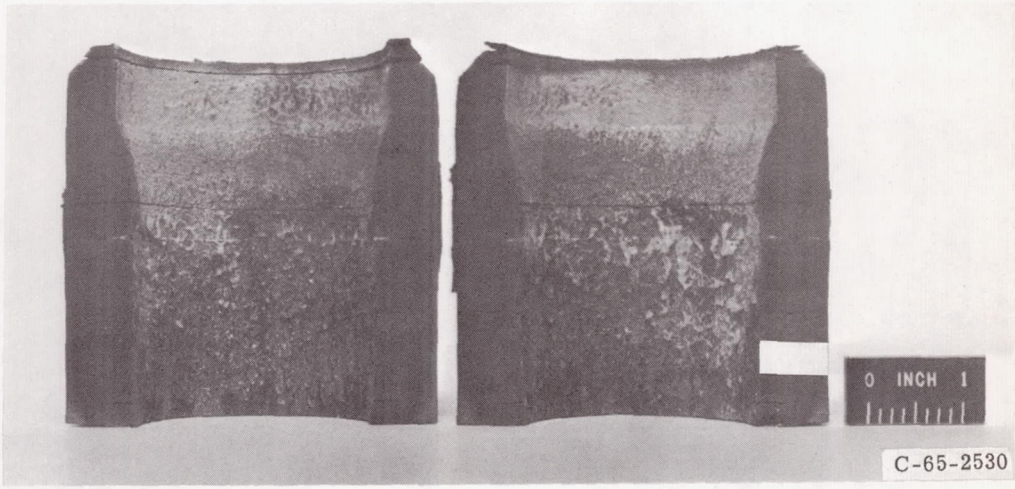

	Material	Form	Manufacturer	Configuration (a)	Additional layers
Insert	80 wt. % SiO_2 - 20 wt. % graphite	Sintered	Avco Corp.	A	None
Envelope	Silica phenolic (MX 2641)	90° centerline	Fiberite	4-in. (10.15-cm) o.d.	None

Run	Chamber pressure, P_c		Oxidant-fuel ratio, O/F	Run time, sec	Total change in effective throat radius, ΔR		Remarks
	psia	kN/m^2			in.	cm	
176	[b]60.7 [d]44.3	[b]418 [d]305	1.9	120.0	[c]0.234	[c]0.594	Insert completely eroded Low P_c due to faulty controller

[a]See fig. 5.
[b]Start.
[c]Calculated.
[d]End.

TABLE VI. - Continued

(39) Insert 39; injector 2

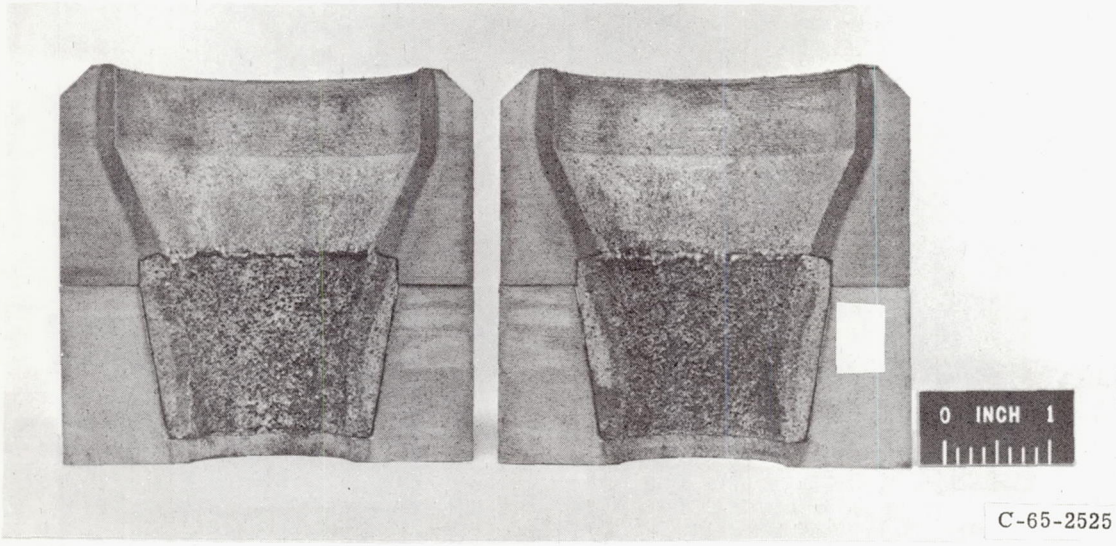

	Material	Form	Manufacturer	Configuration (a)	Additional layers
Insert	56 wt. % ZrO_2 foam, 44 wt. % phenolic	Ipsen foam	Martin Company	A	None
Envelope	Silica phenolic (MX 2641)	90° centerline	Fiberite	4-in. (10.15-cm) o.d.	None

Run	Chamber pressure, P_c		Oxidant-fuel ratio, O/F	Run time, sec	Total change in effective throat radius, ΔR		Remarks
	psia	kN/m^2			in.	cm	
186	97.9	674	1.92	17.6	0.135	0.343	Shutdown due to very high erosion rate

[a]See fig. 5.

TABLE VI. - Continued

(40) Insert 40; injector 2

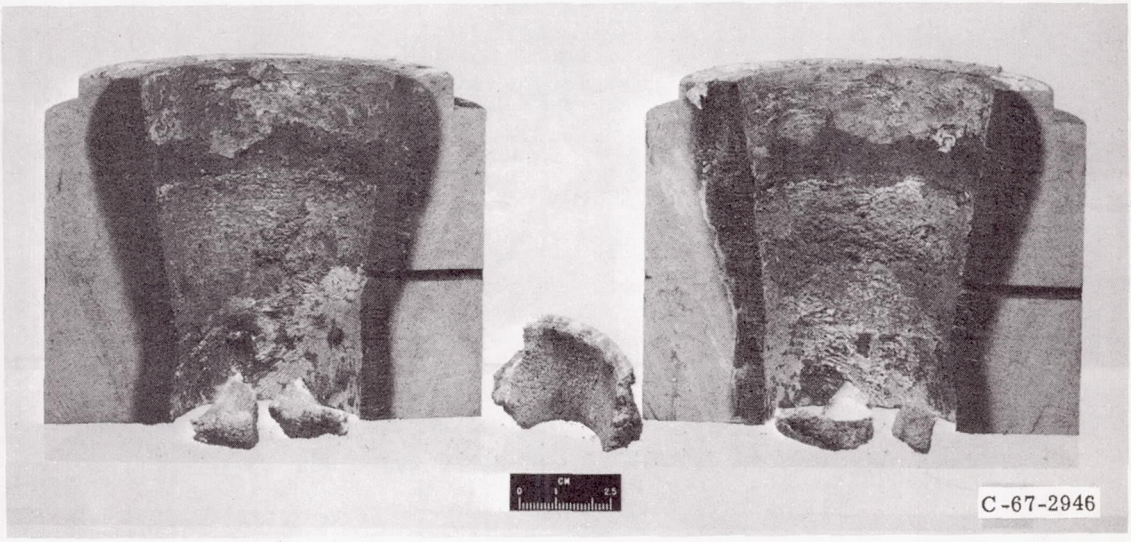

	Material	Form	Manufacturer	Configuration (a)	Additional layers
Insert	ZrO_2	70 % theoretical density; partially yttria stabilized; coarse grain; pressed and sintered	Zircoa	B	JTA liner upstream of throat
Envelope	Silica phenolic (MX 2641)	Molded squares	--------	5-in. (12.7-cm) o.d.	None

Run	Chamber pressure, P_c		Oxidant-fuel ratio, O/F	Run time, sec	Total change in effective throat radius, ΔR		Remarks
	psia	kN/m^2			in.	cm	
746	101	696	2.04	160	0.088	0.223	Shutdown at first sign of rapid erosion; severe cracking

[a]See fig. 5.

TABLE VI. - Continued

(41) Insert 41; injector 2

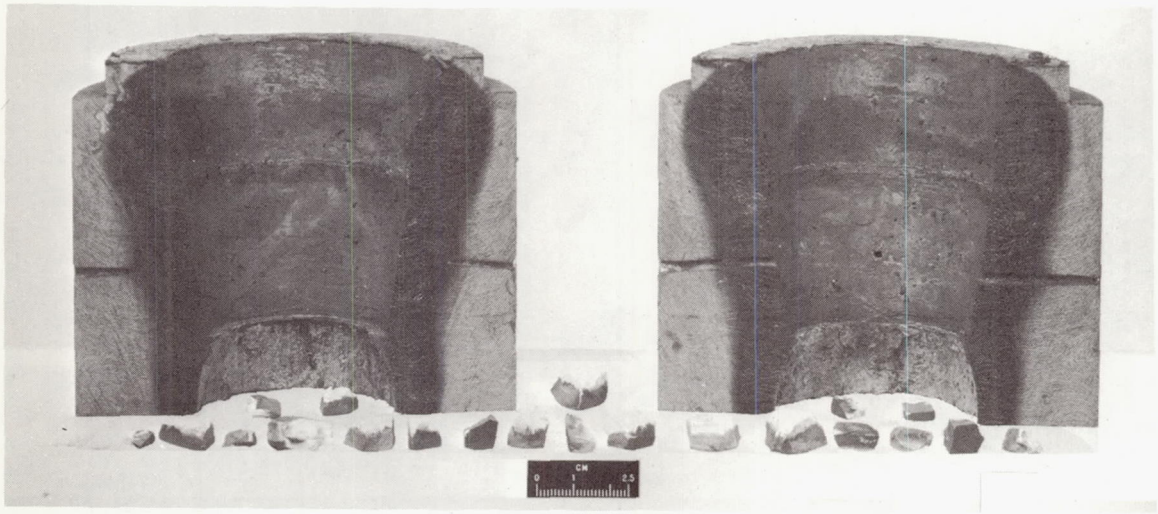

C-67-2948

	Material	Form	Manufacturer	Configuration (a)	Additional layers
Insert	ZrO_2	75 % theoretical density; fully yttria stabilized; medium grain; pressed and sintered	Coors	B	JTA liner upstream of throat
Envelope	Silica phenolic (MX 2641)	Molded squares	------	5-in. (12.7-cm) o.d.	None

Run	Chamber pressure, P_c		Oxidant-fuel ratio, O/F	Run time, sec	Total change in effective throat radius, ΔR		Remarks
	psia	kN/m^2			in.	cm	
748	101.5	698	2.03	301.9	0.009	0.0228	Timed shutdown; severe cracking

[a]See fig. 5.

TABLE VI. - Continued

(42) Insert 42; injector 2

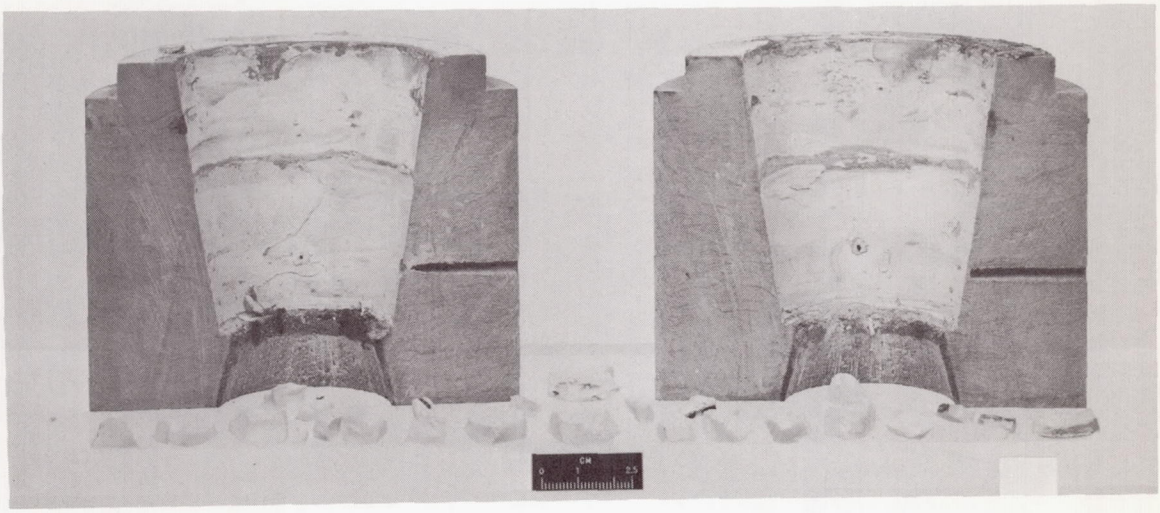

C-67-2947

	Material	Form	Manufacturer	Configuration (a)	Additional layers
Insert	ZrO_2	90 % theoretical density; fully yttria stabilized; fine grain; pressed and sintered	Zircoa	B	JTA liner upstream of throat
Envelope	Silica phenolic (MX 2641)	Molded squares	-------	5-in. (12.7-cm) o.d.	None

Run	Chamber pressure, P_c		Oxidant-fuel ratio, O/F	Run time, sec	Total change in effective throat radius, ΔR		Remarks
	psia	kN/m^2			in.	cm	
747	93.8 to 101	646 to 696	2.07	6.7	0.143	0.363	Shutdown due to rapid erosion; catastrophic cracking

[a]See fig. 5.

TABLE VI. - Continued

(43) Insert 43; injector 2

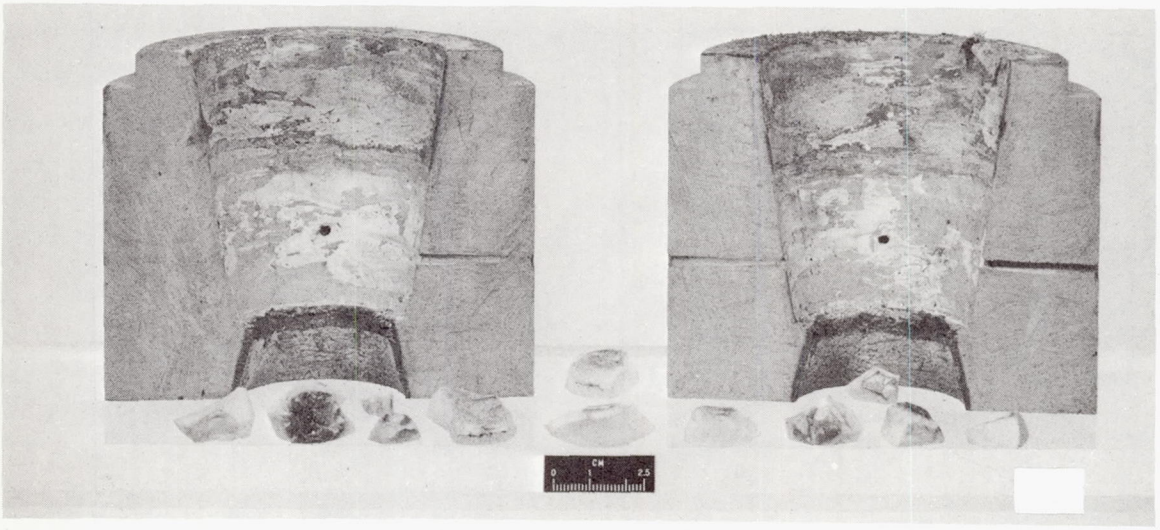

C-67-2949

	Material	Form	Manufacturer	Configuration (a)	Additional layers
Insert	ZrO_2	90 % theoretical density; fully yttria stabilized; fine grain; pressed and sintered	Coors	B	JTA liner upstream of throat
Envelope	Silica phenolic (MX 2641)	Molded squares	------	5-in. (12.7-cm) o.d.	None

Run	Chamber pressure, P_c		Oxidant-fuel ratio, O/F	Run time, sec	Total change in effective throat radius, ΔR		Remarks
	psia	kN/m^2			in.	cm	
749	100	689	2.04	8.2	0.112	0.284	Shutdown due to rapid erosion; catastrophic cracking

[a]See fig. 5.

TABLE VI. - Continued

(44) Insert 44; injector 2

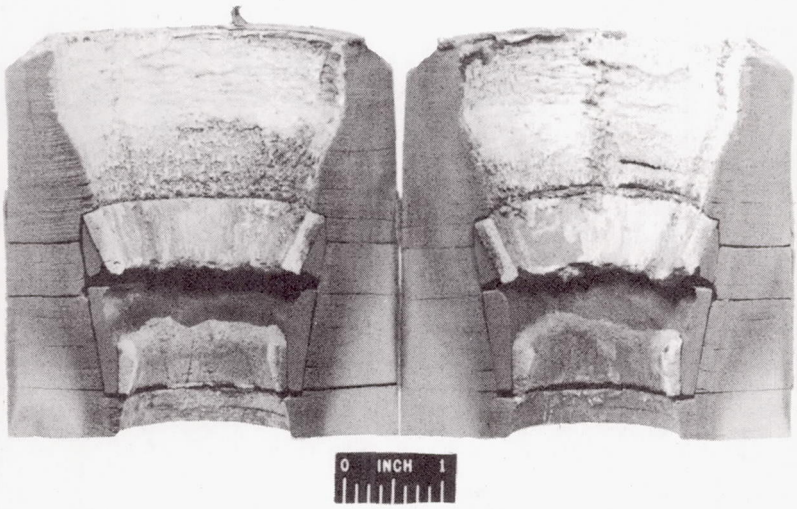

C-66-179

	Material	Form	Manufacturer	Configuration (a)	Additional layers
Insert	ZrO_2	Mixed grain; thin wall; MgO stabilized; sintered	Zircoa	A	1/4-in. (0.635-cm) thick RVC graphite behind insert
Envelope	Silica phenolic (MX 2641)	90° centerline	Fiberite	4-in. (10.15-cm) o.d.	None

Run	Chamber pressure, P_c		Oxidant-fuel ratio, O/F	Run time, sec	Total change in effective throat radius, ΔR		Remarks
	psia	kN/m^2			in.	cm	
282	99.8	688	1.94	60.0	0.003	0.0076	Timed shutdown; slight axial and circumferential cracks
285	101.7	700	1.97	96.0 156.0	[b].042	.1065	Lost throat section

[a]See fig. 5.
[b]Calculated.

TABLE VI. - Continued

(45) Insert 45; injector 1A

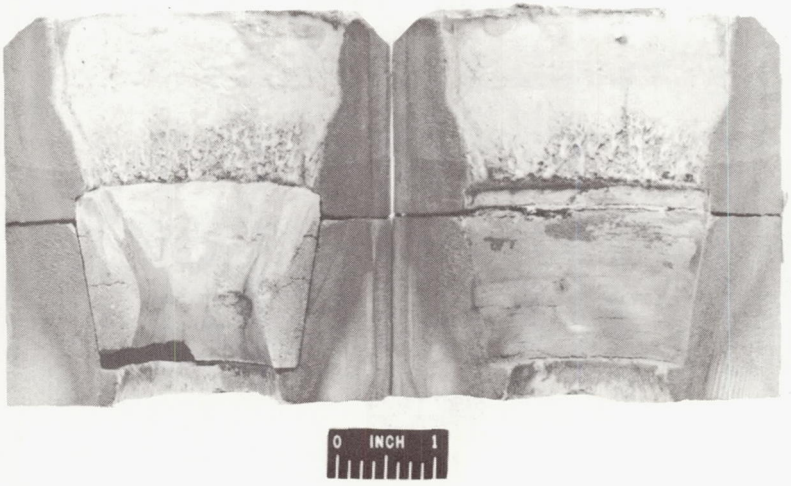

C-66-180

	Material	Form	Manufacturer	Configuration (a)	Additional layers
Insert	ZrO_2	Mixed grain; MgO stabilized; sintered; inside diameter as molded	Zircoa	A	None
Envelope	Silica phenolic (MX 2641)	90° centerline	Fiberite	4-in. (10.15-cm) o.d.	None

Run	Chamber pressure, P_c		Oxidant-fuel ratio, O/F	Run time, sec	Total change in effective throat radius, ΔR		Remarks
	psia	kN/m^2			in.	cm	
269	102.3	704	2.01	60	0	0	Timed shutdown; slight axial cracks at throat
281	96.7	665	1.89	300	-.013	.033	Timed shutdown; moderate axial and circumferential cracks; silica reaction
				360			

[a]See fig. 5.

TABLE VI. - Continued

(46) Insert 46; injector 2

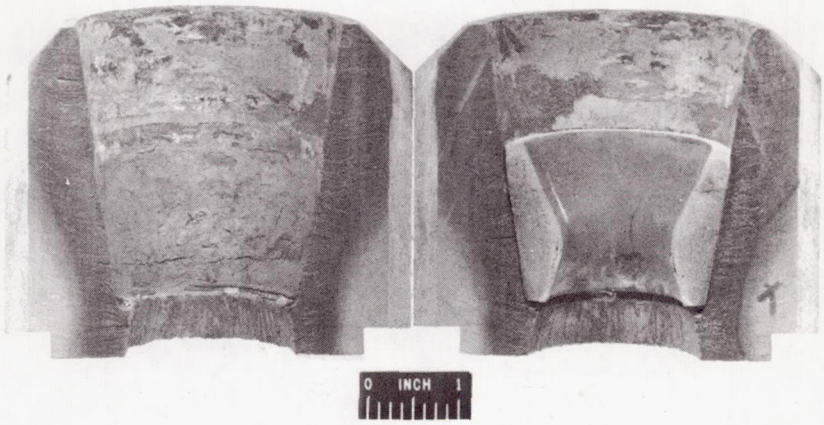

C-66-186

	Material	Form	Manufacturer	Configuration (a)	Additional layers
Insert	ZrO_2	Mixed grain; MgO stabilized; sintered; machined inside diameter	Zircoa	B	JTA liner upstream of throat insert
Envelope	Silica phenolic (MX 2641)	Molded squares	Fiberite	4-in. (10.15-cm) o.d.	1/4-in. (0.635-cm) thick asbestos phenolic

Run	Chamber pressure, P_c		Oxidant-fuel ratio, O/F	Run time, sec	Total change in effective throat radius, ΔR		Remarks
	psia	kN/m^2			in.	cm	
303	96.7	666	2.06	300.0	0	0	Timed shutdown; four axial cracks; minor spalling

[a]See fig. 5.

TABLE VI. - Continued

(47) Insert 47; injector 3

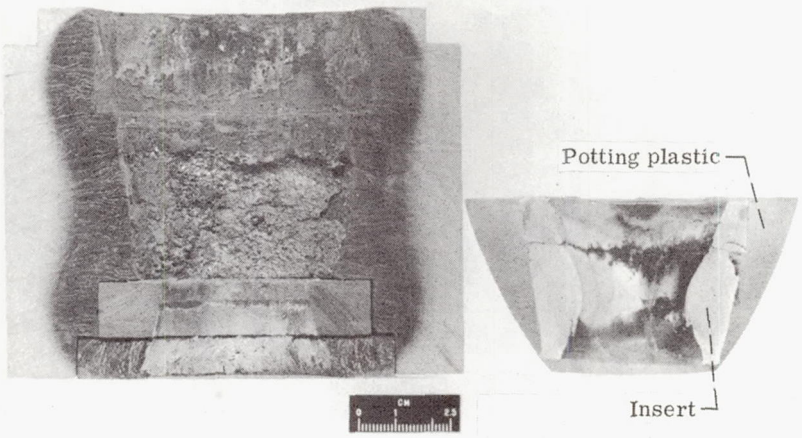

C-66-3597

	Material	Form	Manufacturer	Configuration (a)	Additional layers
Insert	ZrO_2	Cast; CaO stabilized; mixed grain size	Zircoa	B	JTA liner upstream of throat insert
Envelope	Silica phenolic (MX 2641)	Molded squares	------	5-in. (12.7-cm) o.d.	None

Run	Chamber pressure, P_c		Oxidant-fuel ratio, O/F	Run time, sec	Total change in effective throat radius, ΔR		Remarks
	psia	kN/m^2			in.	cm	
565	101.9	702	2.03	195.0	0.011	0.0279	Shutdown at first sign of erosion: moderate circumferential cracking

[a]See fig. 5.

TABLE VI. - Continued

(48) Insert 48; injector 3

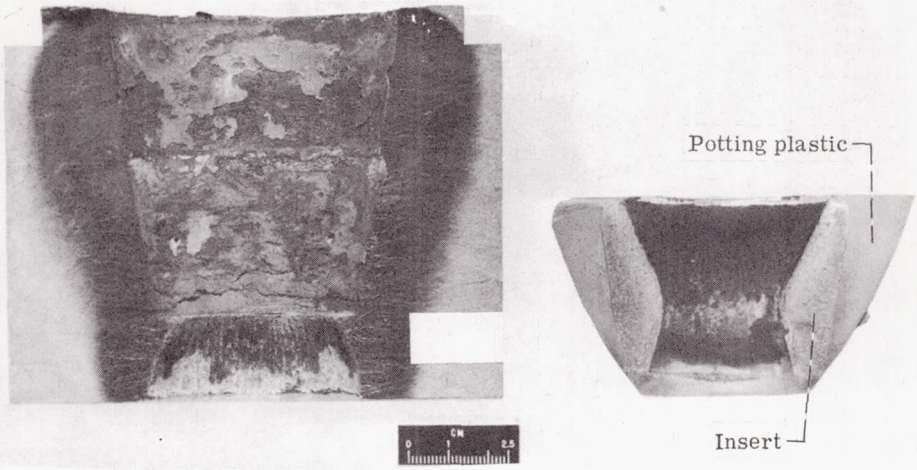

C-66-4144

	Material	Form	Manufacturer	Configuration (a)	Additional layers
Insert	ZrO_2	Cast; MgO stabilized; mixed grain size	Zircoa	B	JTA liner upstream of throat insert
Envelope	Silica phenolic (MX 2641)	Molded squares	------	5-in. (12.7-cm) o.d.	None

Run	Chamber pressure, P_c		Oxidant-fuel ratio, O/F	Run time, sec	Total change in effective throat radius, ΔR		Remarks
	psia	kN/m^2			in.	cm	
563	102.5	706	2.05	301.0	[b]-0.007	-0.0178	Timed shutdown; minor axial cracks
571	103.3	712	2.14	20.9	[b]-.007	-.0178	Timed shutdown
572	101.9	702	2.12	20.6	[b]-.008	-.0203	Timed shutdown
573	103.5	713	2.12	21.0	[b]-.008	-.0203	Timed shutdown
574	102.5	707	2.04	20.5	[b]-.011	-.0279	Timed shutdown
575	102.4	706	2.05	20.8	-.013	-.033	Timed shutdown
585	101.6	700	2.01	301.3 / 706.1	-.015	-.0381	Timed shutdown; moderate axial cracks

[a]See fig. 5.
[b]Calculated.

TABLE VI. - Continued

(49) Insert 49; injector 3

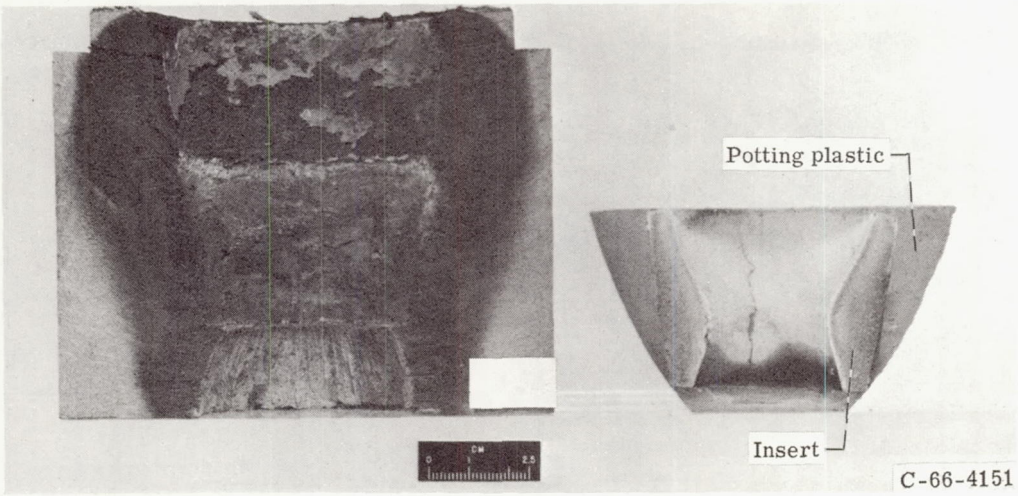

	Material	Form	Manufacturer	Configuration (a)	Additional layers
Insert	ZrO_2 plus graphite	Cast; MgO stabilized	Zircoa	B	JTA liner upstream of throat insert
Envelope	Silica phenolic (MX 2641)	Molded squares	-------	5-in. (12.7-cm) o.d.	None

Run	Chamber pressure, P_c		Oxidant-fuel ratio, O/F	Run time, sec	Total change in effective throat radius, ΔR		Remarks
	psia	kN/m^2			in.	cm	
564	102.0	702	2.04	301.1	-0.019	-0.0482	Timed shutdown; slight axial cracks
577	101.8	700	2.05	20.7	[b]-.010	-.0254	Timed shutdown
578	101.7	700	2.03	20.6	[b]-.013	-.033	Timed shutdown
579	101.0	696	2.04	20.6	[b]-.013	-.033	Timed shutdown
580	101.3	693	2.03	20.7	[b]-.014	-.0356	Timed shutdown
581	101.1	692	2.01	20.7	-.016	-.0407	Timed shutdown
586	101.3	693	2.00	301.1	-.020	-.0508	Timed shutdown
592	110.6	761	1.98	300.3	-.028	-.0712	Timed shutdown; axial cracks
				1005.8			

[a]See fig. 5.
[b]Calculated.

TABLE VI. - Continued

(50) Insert 50; injector 1A

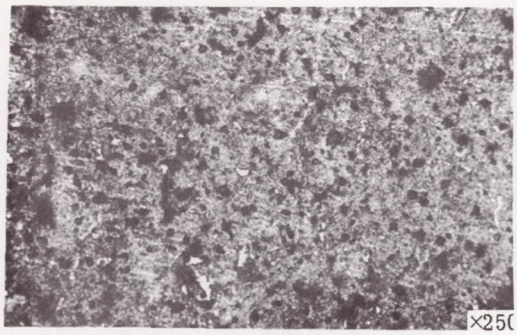

Photomicrograph of hot pressed copper-stabilized anion-deficient zirconia before firing. The darkest regions are pores, the very light regions are metallic copper inclusions.

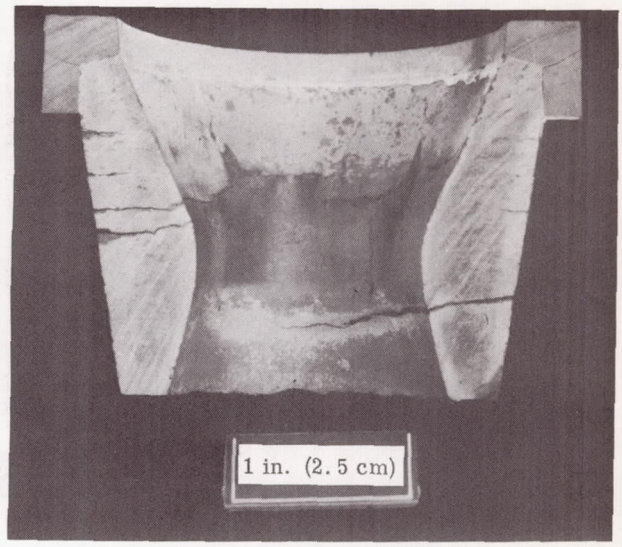

After firing

	Material	Form	Manufacturer	Configuration (a)	Additional layers
Insert	ZrO_2 - 6 wt. % Cu	Anion deficient; sintered; wall thickness, 0.53 in. (1.345 cm)	Rocketdyne	B	JTA liner upstream of throat insert
Envelope	Silica phenolic (MX 2641)	90° centerline	----------	4-in. (10.15-cm) o.d.	None

Run	Chamber pressure, P_c		Oxidant-fuel ratio, O/F	Run time, sec	Total change in effective throat radius, ΔR		Remarks
	psia	kN/m^2			in.	cm	
219	100.6	692	2.08	100.3	0.001	0.0025	Timed shutdown; axial and circumferential cracks

[a]See fig. 5.

TABLE VI. - Continued

(51) Insert 51; injector 2

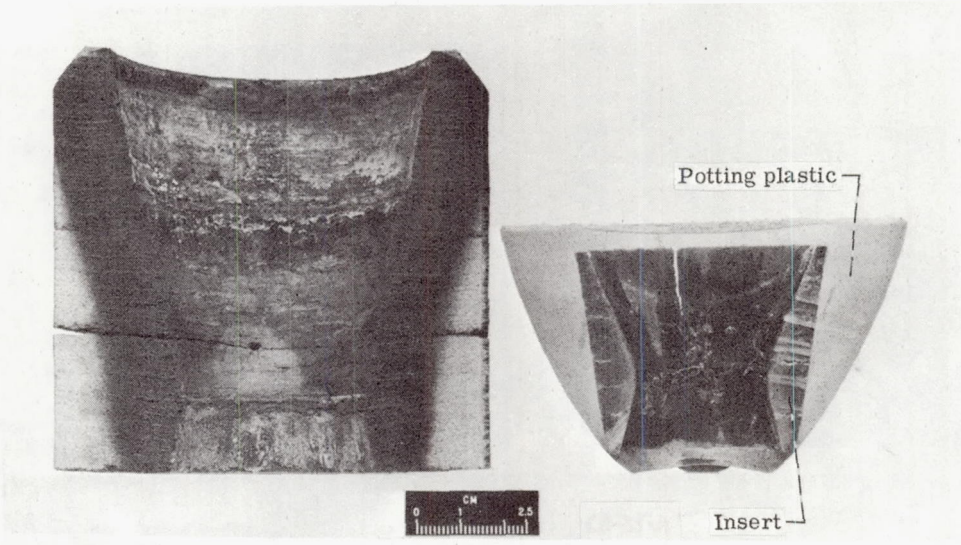

C-66-3380

	Material	Form	Manufacturer	Configuration (a)	Additional layers
Insert	ZrO_2 - 6 wt. % Cu	Anion deficient; sintered; wall thickness, 0.38 in. (0.965 cm)	Rocketdyne	B	JTA liner upstream of throat insert
Envelope	Silica phenolic (MX 2641)	90° centerline	----------	4-in. (10.15-cm) o.d.	None

Run	Chamber pressure, P_c		Oxidant-fuel ratio, O/F	Run time, sec	Total change in effective throat radius, ΔR		Remarks
	psia	kN/m^2			in.	cm	
365	100.8	693	2.09	301.2	0	0	Timed shutdown; axial and circumferential cracks

[a]See fig. 5.

TABLE VI. - Continued

(52) Insert 52; injector 2

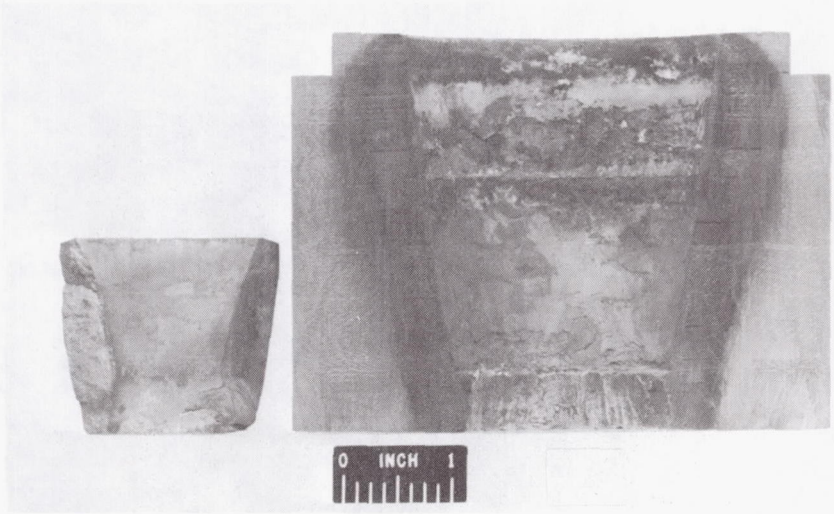

C-66-2997

	Material	Form	Manufacturer	Configuration (a)	Additional layers
Insert	ZrO_2 - 11 wt. % Cu	Anion deficient; sintered; wall thickness, 0.53 in. (1.345 cm)	Rocketdyne	B	JTA liner upstream of throat insert
Envelope	Silica phenolic (MXS 19)	90° centerline	----------	5-in. (12.7-cm) o.d.	None

Run	Chamber pressure, P_c		Oxidant-fuel ratio, O/F	Run time, sec	Total change in effective throat radius, ΔR		Remarks
	psia	kN/m^2			in.	cm	
296	95.3	656	2.08	25.5	[b]0.007	0.0178	Accidental shutdown
297	99.6	686	2.07	332.0 / 357.5	.001	.0025	Timed shutdown; axial cracks

[a]See fig. 5.
[b]Calculated.

TABLE VI. - Continued

(53) Insert 53; injector 2

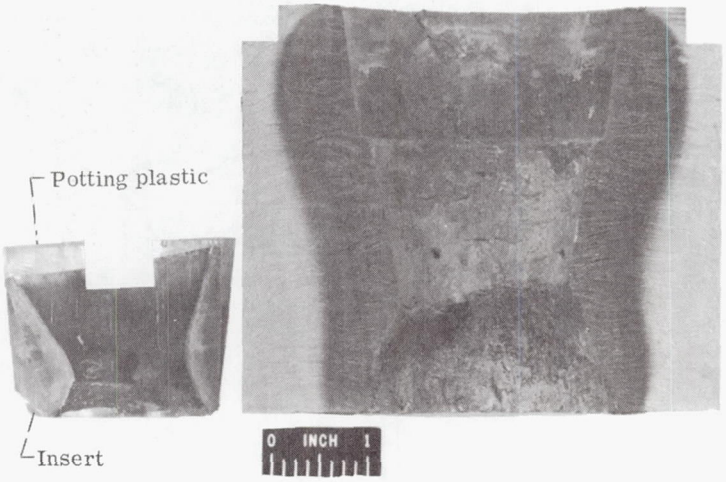

C-66-2996

	Material	Form	Manufacturer	Configuration (a)	Additional layers
Insert	ZrO_2 - 15 wt. % Cu	Anion deficient; sintered; wall thickness, 0.38 in. (0.965 cm)	Rocketdyne	B	JTA liner upstream of throat insert
Envelope	Silica phenolic (MX 2641)	Molded squares	---------	5-in. (12.7-cm) o.d.	None

Run	Chamber pressure, P_c		Oxidant-fuel ratio, O/F	Run time, sec	Total change in effective throat radius, ΔR		Remarks
	psia	kN/m^2			in.	cm	
473	100.8	694	1.97	300.2	-0.017	-0.0432	Timed shutdown; cracking, trailing-edge failure; pieces missing

[a]See fig. 5.

TABLE VI. - Continued

(54) Insert 54; injector 2

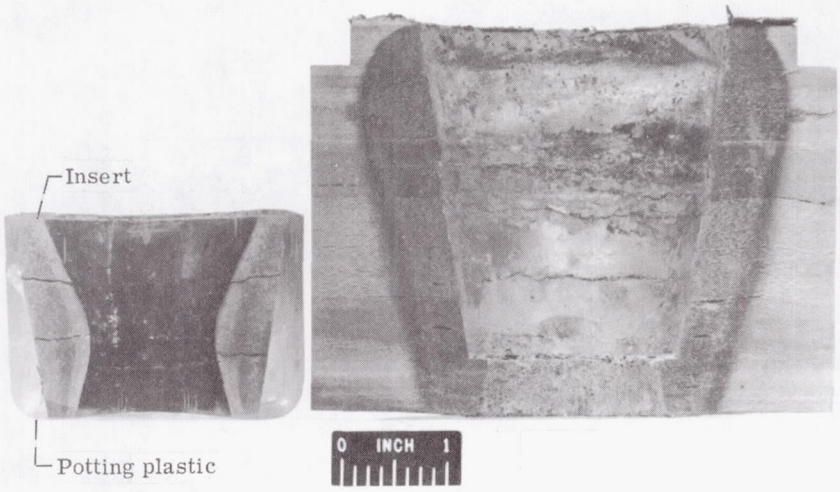

C-66-2994

	Material	Form	Manufacturer	Configuration (a)	Additional layers
Insert	ZrO_2 - 15 wt. % Cu	Anion deficient; sintered; wall thickness, 0.53 in. (1.345 cm)	Rocketdyne	B	None
Envelope	Silica phenolic (MX 2641)	90° centerline	----------	5-in. (12.7-cm) o.d.	None

Run	Chamber pressure, P_c		Oxidant-fuel ratio, O/F	Run time, sec	Total change in effective throat radius, ΔR		Remarks
	psia	kN/m^2			in.	cm	
398	101.2	697	2.02	300.2	0	0	Timed shutdown; circumferential cracks

[a]See fig. 5.

TABLE VI. - Continued

(55) Insert 55; injector 2

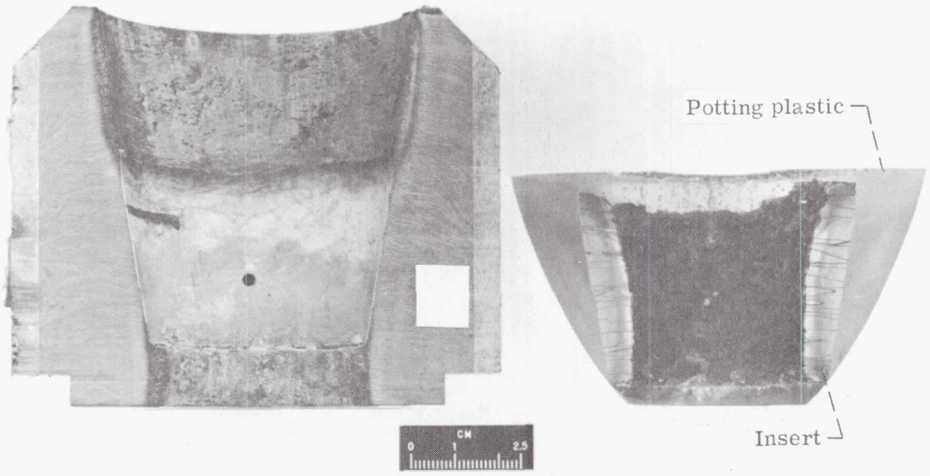

C-66-3381

	Material	Form	Manufacturer	Configuration (a)	Additional layers
Insert	ZrO_2 - Inconel honeycomb (1/4-in. (0.635-cm) cells)	Sintered	Avco Corp.	B	JTA liner upstream of throat insert
Envelope	Silica phenolic (MX 2641)	Molded squares	----------	4-in. (10.15-cm) o.d.	1/4-in. (0.635-cm) thick asbestos phenolic

Run	Chamber pressure, P_c		Oxidant-fuel ratio, O/F	Run time, sec	Total change in effective throat radius, ΔR		Remarks
	psia	kN/m^2			in.	cm	
356	100.4	693	2.05	11.4	0.055	0.140	Rapid erosion shutdown; spallation
404	99.9	689	2.06	19.4	.162	.412	Rapid erosion shutdown; spallation
				30.8			

[a]See fig. 5.

TABLE VI. - Continued

(56) Insert 56; injector 2

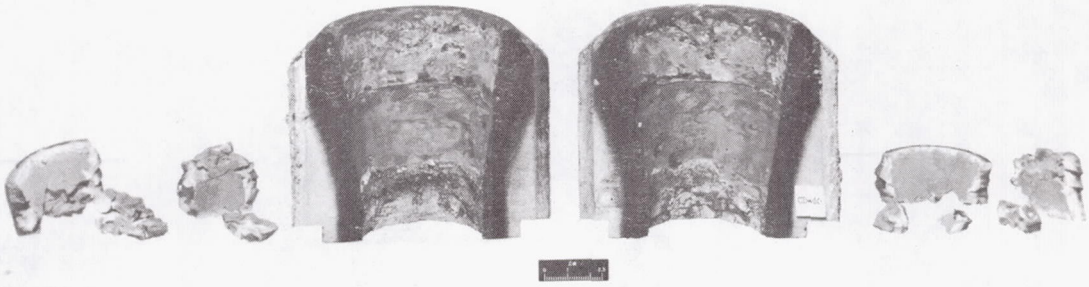

C-66-4148

	Material	Form	Manufacturer	Configuration (a)	Additional layers
Insert	ZrO_2 - platinum-rhodium honeycomb	Sintered	Avco Corp.	B	JTA liner upstream of throat insert
Envelope	Silica phenolic (MX 2641)	Molded squares	---------	4-in. (10.15-cm) o.d.	1/4-in. (0.635-cm) thick asbestos phenolic

Run	Chamber pressure, P_c		Oxidant-fuel ratio, O/F	Run time, sec	Total change in effective throat radius, ΔR		Remarks
	psia	kN/m^2			in.	cm	
357	100.4	692	2.09	239.9	0.058	0.147	Shutdown due to rapid erosion; severe cracking

[a]See fig. 5.

TABLE VI. - Continued

(57) Insert 57; injector 2

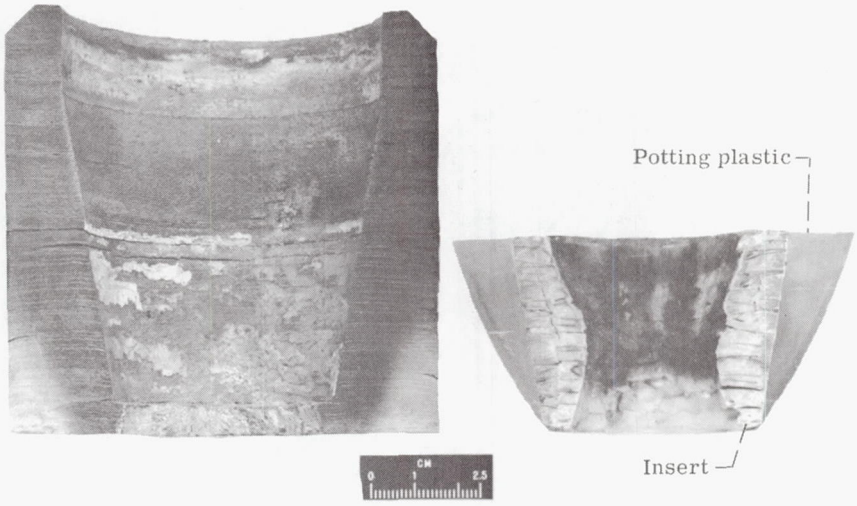

C-66-3382

	Material	Form	Manufacturer	Configuration (a)	Additional layers
Insert	ZrO_2 - tungsten honeycomb	Sintered	Avco Corp.	B	JTA liner upstream of throat insert
Envelope	Silica phenolic (MX 2641)	90° centerline	--------	4-in. (10.15-cm) o.d.	None

Run	Chamber pressure, P_c		Oxidant-fuel ratio, O/F	Run time, sec	Total change in effective throat radius, ΔR		Remarks
	psia	kN/m^2			in.	cm	
399	100.9	695	2.03	280.5	-0.020	-0.057	Shutdown; out of propellant

[a]See fig. 5.

TABLE VI. - Continued

(58) Insert 58; injector 2

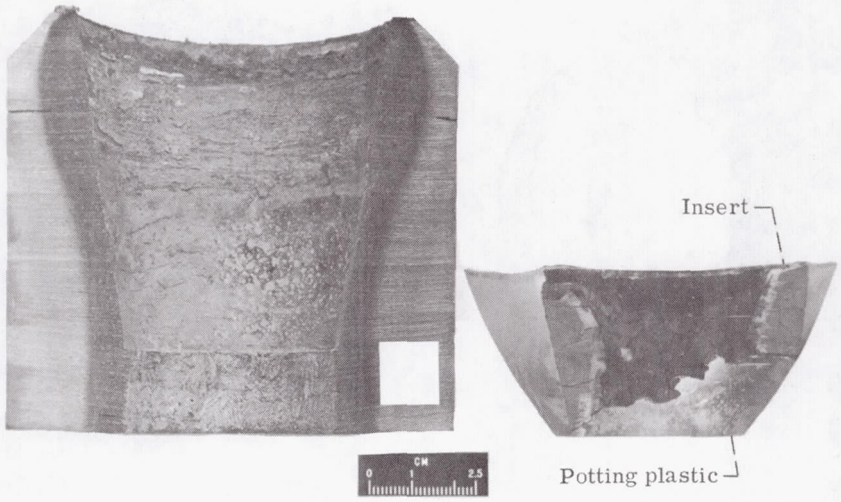

C-66-3383

	Material	Form	Manufacturer	Configuration (a)	Additional layers
Insert	ZrO_2 - platinum-coated molybdenum honeycomb	Sintered	Avco Corp.	B	JTA liner upstream of throat insert
Envelope	Silica phenolic (MX 2641)	90° centerline	Fiberite	4-in. (10.15-cm) o.d.	None

Run	Chamber pressure, P_c		Oxidant-fuel ratio, O/F	Run time, sec	Total change in effective throat radius, ΔR		Remarks
	psia	kN/m^2			in.	cm	
405	100.6	692	2.07	137.6	0.059	0.15	Shutdown for erosion; loss of insert trailing edge

[a]See fig. 5.

TABLE VI. - Continued

(59) Insert 59; injector 1A

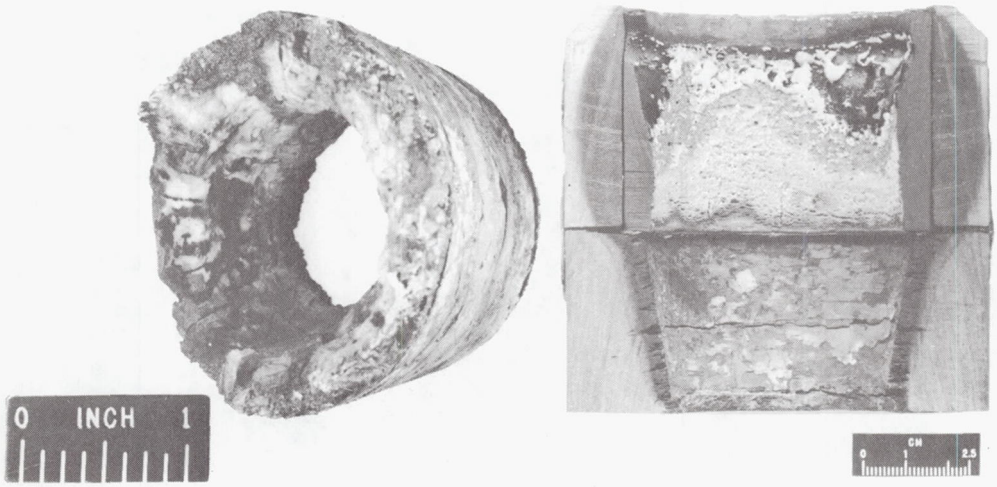

C-65-1546

C-66-3591

	Material	Form	Manufacturer	Configuration (a)	Additional layers
Insert	MgO - 1010 steel honeycomb	Sintered	Avco Corp.	A	Molded graphite-silica composite upstream of throat insert
Envelope	Silica phenolic (MX 2641)	90° centerline	Fiberite	4-in. (10.15-cm) o.d.	None

Run	Chamber pressure, P_c		Oxidant-fuel ratio, O/F	Run time, sec	Total change in effective throat radius, ΔR		Remarks
	psia	kN/m^2			in.	cm	
119	101.5	699	2.04	60.3	-0.025	-0.0635	Timed shutdown
143	95.6	658	2.01	261.0	-.031	-.0788	Shutdown for leak in nozzle; leading edge of insert badly eroded
				321.3			

[a]See fig. 5.

TABLE VI. - Continued

(60) Insert 60; injector 1A

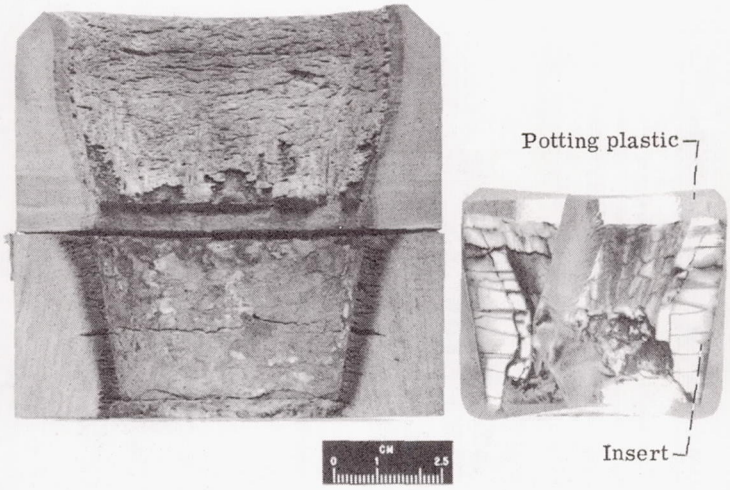

C-66-3599

	Material	Form	Manufacturer	Configuration (a)	Additional layers
Insert	MgO - Inconel honeycomb	Sintered	Avco Corp.	A	None
Envelope	$Mg(OH)_2$ phenolic	90° centerline	Johns Manville	4-in. (10.15-cm) o.d.	None

Run	Chamber pressure, P_c		Oxidant-fuel ratio, O/F	Run time, sec	Total change in effective throat radius, ΔR		Remarks
	psia	kN/m^2			in.	cm	
121	100.2	690	2.03	60.3	-0.016	-0.0407	Timed shutdown; $Mg(OH)_2$ phenolic badly eroded upstream of insert
217	100.8	694	2.10	7.3	[b]-.008	-.0203	Shutdown for oxidant leak
218	99.5	686	2.08	140.9	.014	.0356	Shutdown at start of erosion; trailing edge of insert badly eroded
				208.5			

[a]See fig. 5.
[b]Calculated.

TABLE VI. - Continued

(61) Insert 61; injector 2

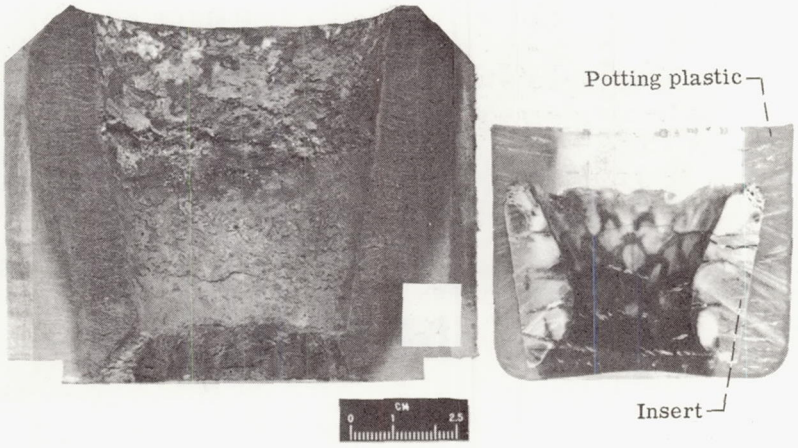

C-66-3384

	Material	Form	Manufacturer	Configuration (a)	Additional layers
Insert	MgO - platinum-coated 1010 steel honeycomb	Sintered	Avco Corp.	B	JTA liner upstream of throat insert
Envelope	Silica phenolic (MX 2641)	Molded squares	----------	4-in. (10.15-cm) o.d.	1/4-in. (0.635-cm) thick asbestos phenolic

Run	Chamber pressure, P_c		Oxidant-fuel ratio, O/F	Run time, sec	Total change in effective throat radius, ΔR		Remarks
	psia	kN/m^2			in.	cm	
406	99.6	686	2.07	300.2	-0.040	-0.101	Timed shutdown

[a]See fig. 5.

TABLE VI. - Continued

(62) Insert 62; injector 2

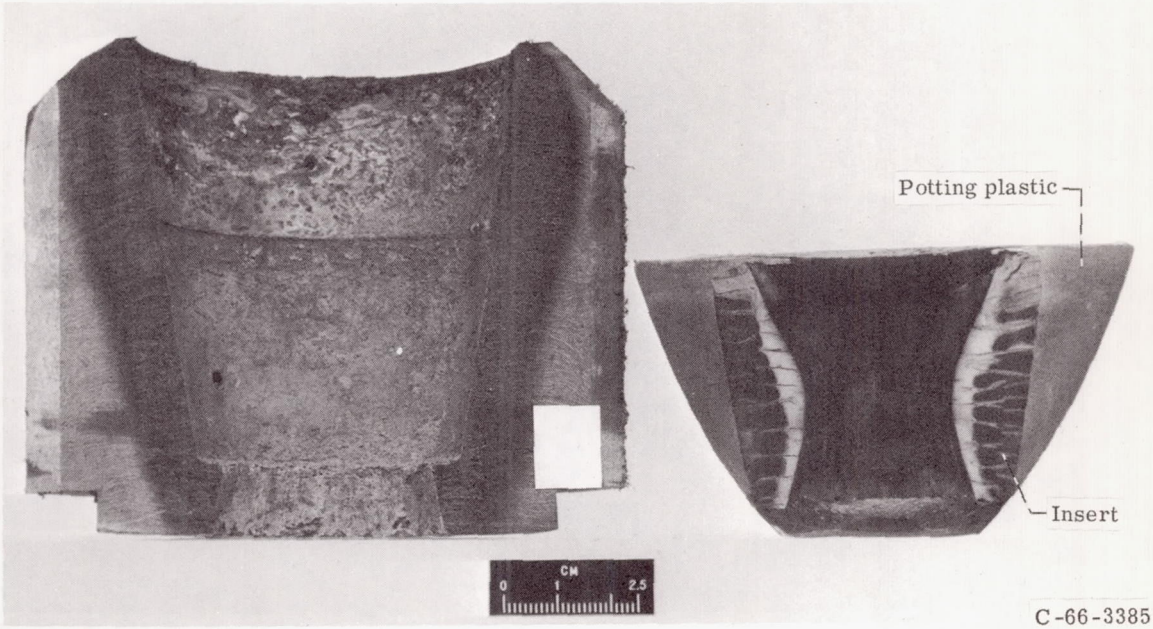

	Material	Form	Manufacturer	Configuration (a)	Additional layers
Insert	MgO - platinum honeycomb	Sintered	Avco Corp.	B	JTA liner upstream of throat insert
Envelope	Silica phenolic (MX 2641)	Molded squares	----------	4-in. (10.15-cm) o.d.	1/4-in. (0.635-cm) thick asbestos phenolic

Run	Chamber pressure, P_c		Oxidant-fuel ratio, O/F	Run time, sec	Total change in effective throat radius, ΔR		Remarks
	psia	kN/m^2			in.	cm	
407	100.8	694	2.10	143.0	-0.036	-0.0915	Ablative envelope failure; leading-edge gas leak

[a]See fig. 5.

TABLE VI. - Continued

(63) Insert 63; injector 3

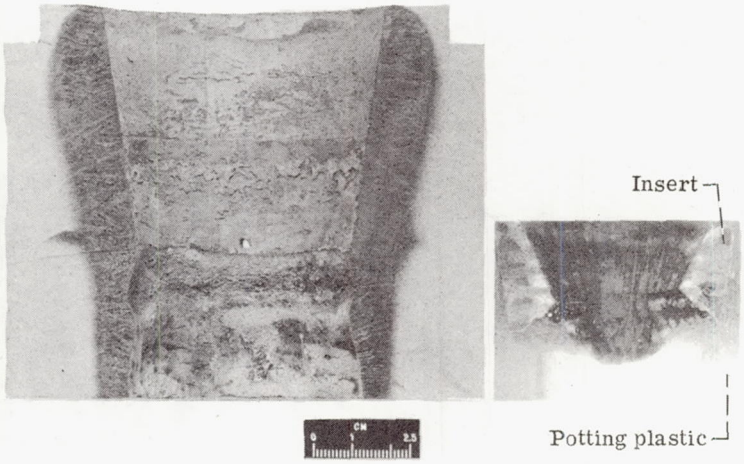

C-66-3594

	Material	Form	Manufacturer	Configuration (a)	Additional layers
Insert	MgO - 5 vol. % inconel fibers	Sintered; wire diam, 0.0003 in. (0.00076 cm)	Avco Corp.	B	None
Envelope	Silica phenolic (MX 2641)	Molded squares	----------	5-in. (12.7-cm) o.d.	None

Run	Chamber pressure, P_c		Oxidant-fuel ratio, O/F	Run time, sec	Total change in effective throat radius, ΔR		Remarks
	psia	kN/m^2			in.	cm	
582	102 to 104	702 to 716	1.97	179.7	0.011	0.0279	Shutdown at start of erosion; severe cracking; loss of trailing edge

[a]See fig. 5.

TABLE VI. - Continued

(64) Insert 64; injector 3

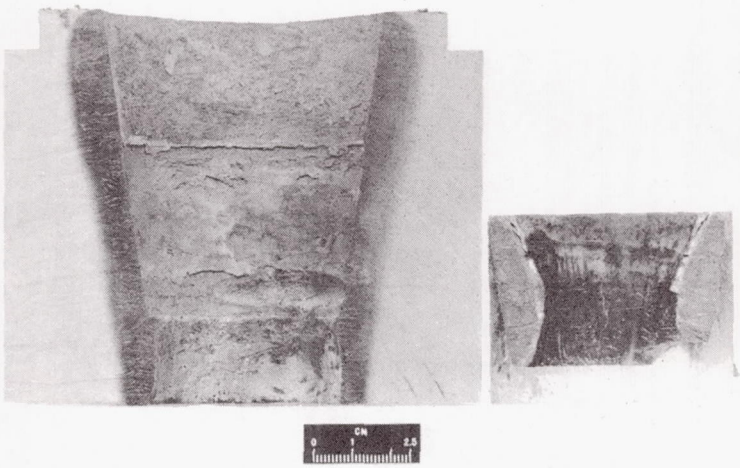

C-66-3595

	Material	Form	Manufacturer	Configuration (a)	Additional layers
Insert	MgO - 5 vol. % Inconel fibers	Sintered; wire diam, 0.005 in. (0.0127 cm)	Avco Corp.	B	None
Envelope	Silica phenolic (MX 2641)	Molded squares	Fiberite	5-in. (12.7-cm) o.d.	None

Run	Chamber pressure, P_c		Oxidant-fuel ratio, O/F	Run time, sec	Total change in effective throat radius, ΔR		Remarks
	psia	kN/m^2			in.	cm	
583	100 to 102	689 to 702	1.96	96.0	0.016	0.0407	Shutdown at start of erosion; severe cracking and spallation; loss of trailing edge

[a]See fig. 5.

TABLE VI. - Continued

(65) Insert 65; injector 3

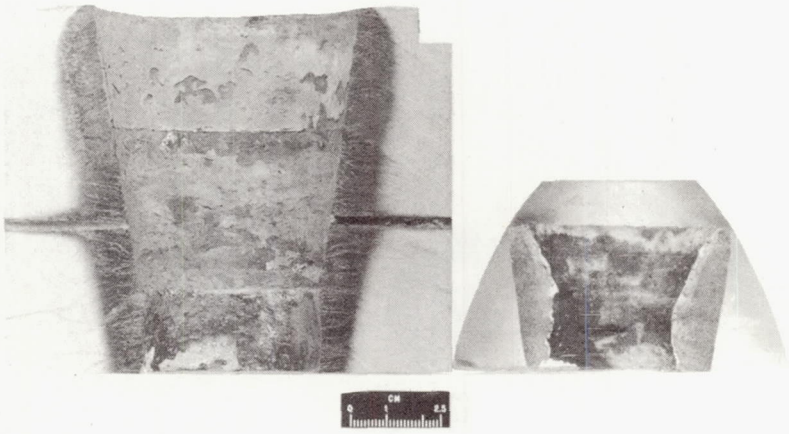

C-66-3600

	Material	Form	Manufacturer	Configuration (a)	Additional layers
Insert	MgO - 5 vol. % tungsten fibers	Sintered; wire diam, 0.0003 in. (0.00076 cm)	Avco Corp.	B	None
Envelope	Silica phenolic (MX 2641)	Molded squares	Fiberite	5-in. (12.7-cm) o.d.	None

Run	Chamber pressure, P_c		Oxidant-fuel ratio, O/F	Run time, sec	Total change in effective throat radius, ΔR		Remarks
	psia	kN/m^2			in.	cm	
584	101 to 102	695 to 702	1.97	132.9	-0.006	-0.0152	Shutdown at start of erosion

[a]See fig. 5.

TABLE VI. - Continued

(66) Insert 66; injector 3

C-65-2528

	Material	Form	Manufacturer	Configuration (a)	Additional layers
Insert	BeO	Sintered	Aerospace Corporation	C	1/8-in. (0.317-cm) thick steel
Envelope	Silica phenolic (MX 2641)	Molded squares	----------	4-in. (10.15-cm) o.d.	None

Run	Chamber pressure, P_c		Oxidant-fuel ratio, O/F	Run time, sec	Total change in effective throat radius, ΔR		Remarks
	psia	kN/m^2			in.	cm	
559	101.6	700	2.01	30.7	-0.012	-0.0305	Timed shutdown; one circumferential crack

[a]See fig. 5.

TABLE VI. - Continued

(67) Insert 67; injector 2

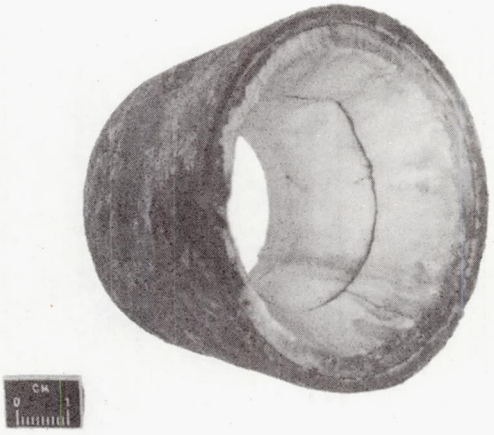

C-68-2521

	Material	Form	Manufacturer	Configuration (a)	Additional layers
Insert	BeO	3 axial washers each segmented 120°	Aerospace Corporation	B	1/8-in. (0.317-cm) thick Ta cone on outside diameter of BeO; JTA liner upstream of throat insert
Envelope	Silica phenolic (MX 2641)	Molded squares	----------	5-in. (12.7-cm) o.d.	None

Run	Chamber pressure, P_c		Oxidant-fuel ratio, O/F	Run time, sec	Total change in effective throat radius, ΔR		Remarks
	psia	kN/m^2			in.	cm	
631	100 to 101	689 to 695	1.98	220.9	-0.019	-0.0482	Tantalum sleeve partially gone at insert leading edge; shutdown due to flow increase; axial cracks

[a]See fig. 5.

TABLE VI. - Continued

(68) Insert 68; injector 2

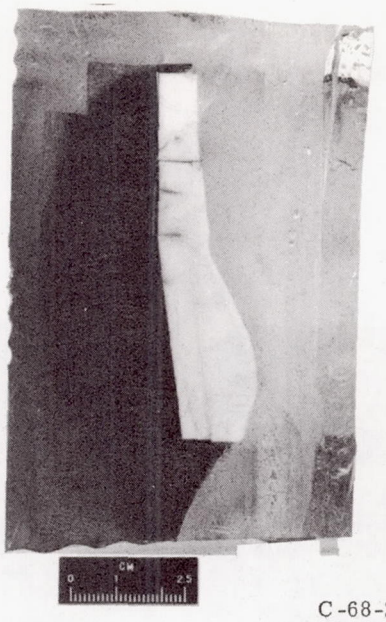

C-68-2400

	Material	Form	Manufacturer	Configuration (a)	Additional layers
Insert	BeO	3 axial washers each segmented 120°	Aerospace Corporation	B	1/4-in.(0.635-cm)thick BeO cone on outside diameter of BeO; BeO liner upstream of throat insert
Envelopes	Silica phenolic (MX 2641)	Molded squares	----------	5-in. (12.7-cm) o.d.	None

Run	Chamber pressure, P_c		Oxidant-fuel ratio, O/F	Run time, sec	Total change in effective throat radius, ΔR		Remarks
	psia	kN/m^2			in.	cm	
745	102	702	2.03	300.5	0.002	0.00508	Timed shutdown; cracking and loss of pieces
754	104.5	720	2.02	20.0	-----	-------	Timed shutdown
755	104	717	2.06	20.7	-----	-------	Timed shutdown
756	105	723	2.02	20.8	-----	-------	Timed shutdown
757	105	723	2.00	20.3	-----	-------	Timed shutdown
758	105	723	1.98	20.0	.012	.0305	Timed shutdown
810	100	689	2.08	7.9	-----	-------	Timer malfunction
811	101.5	698	2.02	280.9 / 691.1	.061	.155	Out of propellant

[a]See fig. 5.

TABLE VI. - Continued

(69) Insert 69; injector 2

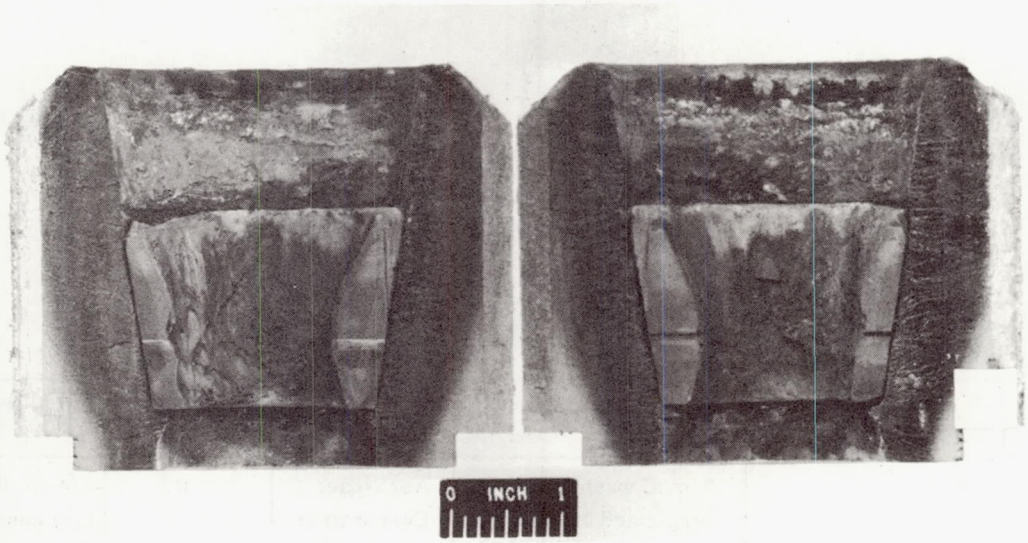

C-66-2999

	Material	Form	Manufacturer	Configuration (a)	Additional layers
Insert	Tungsten-coated BeO spheres (68 wt. % W)	Sintered	National Beryllia	B	JTA liner upstream of throat insert
Envelope	Silica phenolic (MX 2641)	Molded squares	---------	4-in. (10.15-cm) o.d.	1/4-in. (0.635-cm) thick asbestos phenolic

Run	Chamber pressure, P_c		Oxidant-fuel ratio, O/F	Run time, sec	Total change in effective throat radius, ΔR		Remarks
	psia	kN/m^2			in.	cm	
358	100.3	691	2.06	211	0.042	0.107	Shutdown at first sign of erosion: no crac

[a]See fig. 5.

TABLE VI. - Continued

(70) Insert 70; injector 2

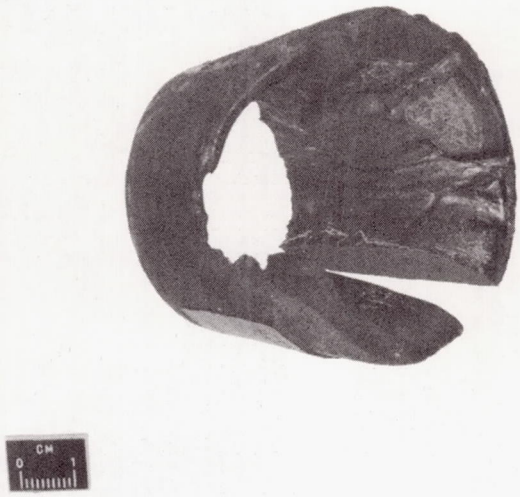

C-68-2520

	Material	Form	Manufacturer	Configuration (a)	Additional layers
Insert	Tungsten-coated BeO spheres (25 wt. % W)	Sintered	National Beryllia	B	JTA liner upstream of throat insert
Envelope	Silica phenolic (MX 2641)	Molded squares	--------	4-in. (10.15-cm) o.d.	1/4-in. (0.635-cm) thick asbestos phenolic

Run	Chamber pressure, P_c		Oxidant-fuel ratio, O/F	Run time, sec	Total change in effective throat radius, ΔR		Remarks
	psia	kN/m^2			in.	cm	
635	99 to 102	684 to 702	1.98	225.3	0.017	0.043	Erosion due to oxidation of tungsten; no cracking

[a]See fig. 5.

TABLE VI. - Continued

(71) Insert 71; injector 1A

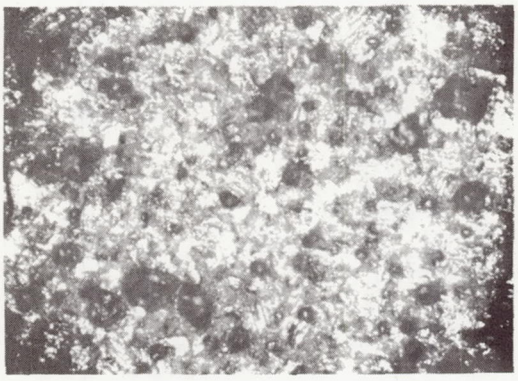

Photomicrograph of isostatically pressed and sintered hafnia-rich mixed oxide before testing. The very dark regions are pores, the lighter regions are the mixed oxide.

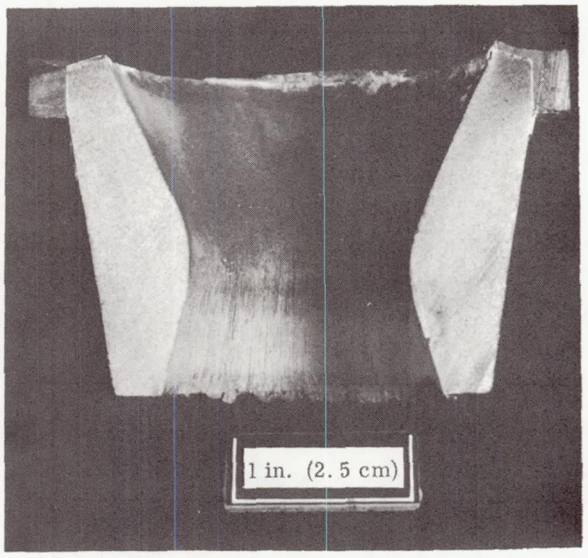

Postfiring photograph after 229.8 seconds

	Material	Form	Manufacturer	Configuration (a)	Additional layers
Insert	HfO_2 - ZrO_2 - TiO_2	Sintered; 100-mesh powder	Rocketdyne	B	JTA liner upstream of throat insert
Envelope	Silica phenolic (MX 2641)	90° centerline	----------	4-in. (10.15-cm) o.d.	None

Run	Chamber pressure, P_c		Oxidant-fuel ratio, O/F	Run time, sec	Total change in effective throat radius, ΔR		Remarks
	psia	kN/m^2			in.	cm	
220	100.6	695	2.10	229.8	-0.006	-0.0152	Accidental shutdown

[a]See fig. 5.

TABLE VI. - Continued

(72) Insert 72; injector 2

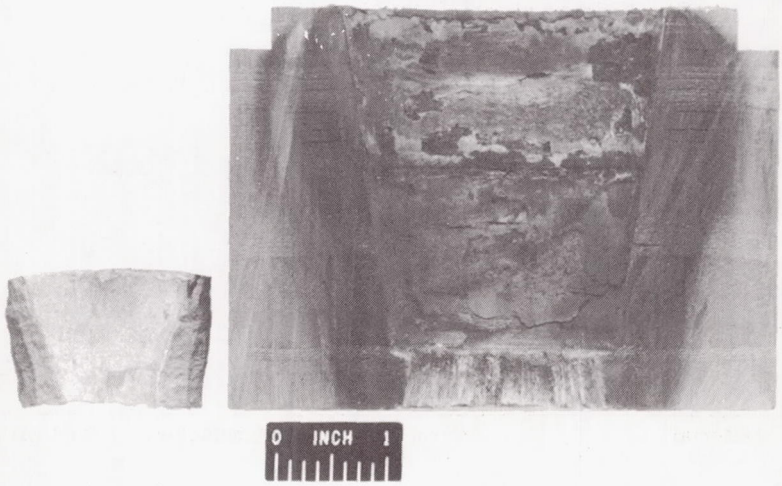

C-66-2995

	Material	Form	Manufacturer	Configuration (a)	Additional layers
Insert	HfO_2 - ZrO_2 - TiO_2	Sintered; 100-mesh powder	Rocketdyne	B	JTA liner upstream of throat insert
Envelope	Silica phenolic (MXS 19)	90° centerline	----------	5-in. (12.7-cm) o.d.	None

Run	Chamber pressure, P_c		Oxidant-fuel ratio, O/F	Run time, sec	Total change in effective throat radius, ΔR		Remarks
	psia	kN/m^2			in.	cm	
298	100.0	689	2.09	358.0	-0.005	-0.0127	Timed shutdown; no cracking
306	100.4	693	1.98	365.0	[b]-.008	-.0207	Timed shutdown; minor inside diameter fissures
308	100.0	689	1.98	21.0	[b]-.007	-.0178	Timed shutdown; no inspection
309	100.3	692	1.99	21.0	[b]-.008	-.0207	Timed shutdown; no inspection
310	100.0	389	1.99	21.0	[b]-.012	-.0305	Timed shutdown; no inspection
311	100.5	694	1.99	21.0	[b]-.015	-.0381	Timed shutdown; 6 axial cracks
312	100.4	693	1.99	21.0	-.020	-.0508	Timed shutdown; axial and circumferential cracking
				828.0			

[a]See fig. 5.
[b]Calculated

TABLE VI. - Continued

(73) Insert 73; injector 2

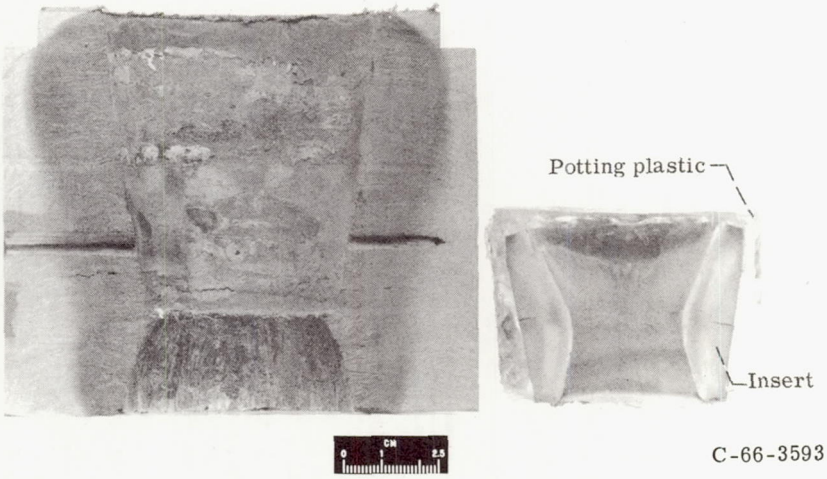

C-66-3593

	Material	Form	Manufacturer	Configuration (a)	Additional layers
Insert	HfO_2 - ZrO_2 - TiO_2	Sintered; 325-mesh powder	Rocketdyne	B	0.005-in.(0.127-cm) thick nickel on insert outside diameter; JTA liner upstream of throat insert
Envelope	Silica phenolic (MX 2641)	Molded squares	----------	5-in. (12.7-cm) o.d.	None

Run	Chamber pressure, P_c		Oxidant-fuel ratio, O/F	Run time, sec	Total change in effective throat radius, ΔR		Remarks
	psia	kN/m^2			in.	cm	
464	100.6	693	2.00	300.4	(b)	(b)	Timed shutdown; no cracking
475	101.1	695	2.18	20.2	[c]-0.024	-0.061	Timed shutdown; no cracks visible
476	101.4	699	2.16	20.2	[c]-.023	-.0584	Timed shutdown; no cracks visible
477	101.5	699	2.21	20.6	[c]-.027	-.0686	Timed shutdown; no cracks visible
478	100.9	694	2.17	20.6	[c]-.025	-.0635	Timed shutdown; no cracks visible
479	100.5	693	2.13	20.2	[c]-.010	-.0254	Timed shutdown; hairline cracks on inside diameter
480	98.8	681	2.06	300.3	-.018	-.0457	Timed shutdown; delamination upstream; outside diameter crack
				702.5			

[a]See fig. 5.
[b]Not measured.
[c]Calculated.

TABLE VI. - Continued

(74) Insert 74; injector 2

C-66-3003

	Material	Form	Manufacturer	Configuration (a)	Additional layers
Insert	HfO_2 - ZrO_2 - TiO_2; graded HfO_2 on inside diameter; TiO_2 on outside diameter	Sintered; 325-mesh powder	Rocketdyne	B	0.005-in.(0.127-cm) thick nickel on insert outside diameter; JTA liner upstream of throat insert
Envelope	Silica phenolic (MX 2641)	Molded squares	----------	5-in. (12.7-cm) o.d.	None

Run	Chamber pressure, P_c		Oxidant-fuel radio, O/F	Run time, sec	Total change in effective throat radius, ΔR		Remarks
	psia	kN/m^2			in.	cm	
474	101.2	696	1.98	300.0	-0.006	-0.0152	Timed shutdown; four hairline surface fissures
481	99.5	685	2.04	12.5	[b]-.011	-.0279	Timed shutdown
482	99.1	683	2.00	20.8	[b]-.009	-.0228	Timed shutdown
483	99.4	684	1.99	20.6	[b]-.011	-.0279	Timed shutdown
484	99.2	683	1.98	20.3	[b]-.011	-.0279	Timed shutdown
485	99.6	685	1.99	20.3	-.011	-.0279	Timed shutdown; four hairline surface fissures
487	99.3	683	1.97	300.9	-.017	-.0432	Timed shutdown; five hairline surface fissures and circumferential outside diameter cracks
				695.4			

[a]See fig. 5.
[b]Calculated.

TABLE VI. - Continued

(75) Insert 75; injector 2

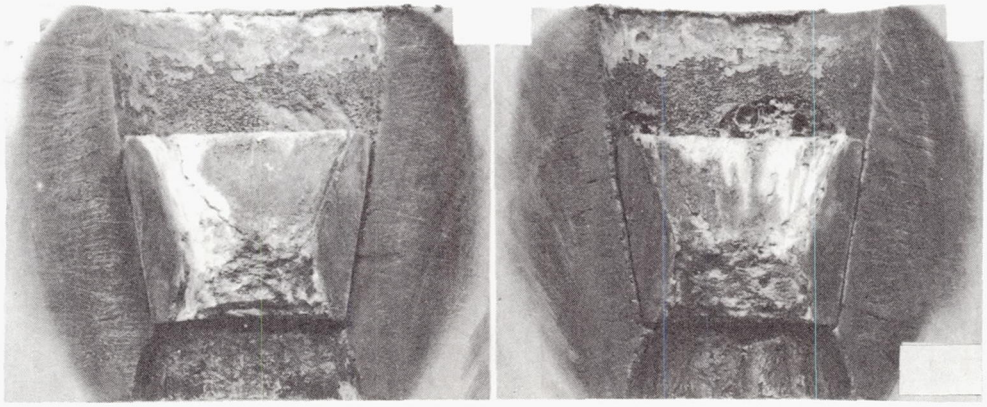

C-66-4349

	Material	Form	Manufacturer	Configuration (a)	Additional layers
Insert	$Mo(HfO_2 - 5CeO_2)$	Sintered and pressed	Boeing	B	JTA liner upstream of throat insert
Envelope	Silica phenolic (MX 2641)	Molded squares	-------	5-in. (12.7-cm) o.d.	None

Run	Chamber pressure, P_c		Oxidant-fuel ratio, O/F	Run time, sec	Total change in effective throat radius, ΔR		Remarks
	psia	kN/m^2			in.	cm	
636	100.5	692	1.98	300.0	-0.017	-0.0432	Timed shutdown
642	100.0	689	↓	20.2	------	-------	Timed shutdown
644	99.5	686	↓	20.2	------	-------	Timed shutdown
645	↓	↓	↓	20.0	------	-------	Timed shutdown
646	↓	↓	↓	20.1	------	-------	Timed shutdown
647	↓	↓	1.97	20.0	.009	.0228	Timed shutdown
649	100.0	689	1.99	301.2	.005	.0127	Timed shutdown
658	99.5	686	1.97	300.9	.029	.0737	Timed shutdown
				1002.6			

[a]See fig. 5.

TABLE VI. - Continued

(76) Design 76; injector 2

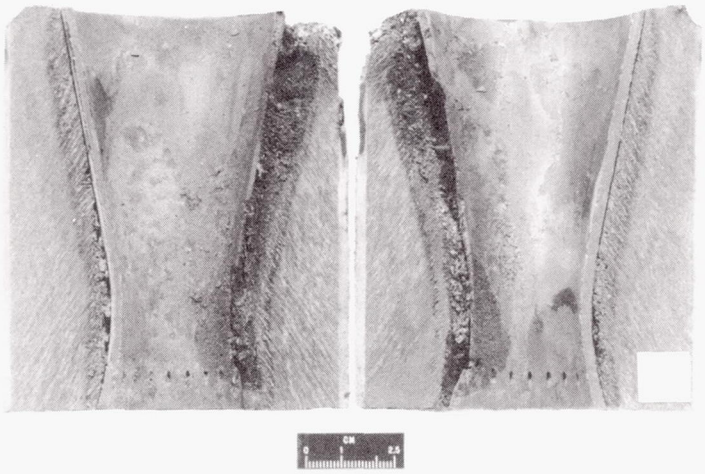

C-66-4352

	Material	Form	Manufacturer	Configuration (a)	Additional layers
Coating	0.020-in. (0.0508-cm) thick SiC	Pyrolytic	Cincinnati Testing Laboratories	I	0.020-in.(0.0508-cm) thick SiC on outside diameter of liner
Insert	RVC graphite				
Envelope	Graphite-quartz phenolic-polypropylene	Cloth, 70° centerline reversed	Cincinnati Testing Laboratories	4-in. (10.15-cm) o.d.	1/8-in. (0.317-cm) thick asbestos phenolic

Run	Chamber pressure, P_c		Oxidant-fuel ratio, O/F	Run time, sec	Total change in effective throat radius, ΔR		Remarks
	psia	kN/m^2			in.	cm	
276	101.9	702	1.91	49.7	0.009	0.0228	Leading-edge failure; coating failure (blistered); shutdown at first sign of coating failure

[a]See fig. 5.

TABLE VI. - Continued

(77) Design 77; injector 2

C-66-4349

	Material	Form	Manufacturer	Configuration (a)	Additional layers
Coating	0.040-in. (0.1015-cm) thick SiC	Pyrolytic	Cincinnati Testing Laboratories	J	0.040-in.(0.1015-cm) thick SiC on outside diameter of liner
Insert	Graphite				
Envelope	Quartz-polypropylene phenolic	Cloth, 60° centerline reversed	Cincinnati Testing Laboratories	4-in. (10.15-cm) o.d.	1/8-in. (0.317-cm) thick asbestos phenolic

Run	Chamber pressure, P_c		Oxidant-fuel ratio, O/F	Run time, sec	Total change in effective throat radius, ΔR		Remarks
	psia	kN/m^2			in.	cm	
650	100	689	2.00	15.9	-0.005	-0.0127	Shutdown due to gas leakage; axial cracks in insert

[a]See fig. 5.

TABLE VI. - Continued

(78) Design 78; injector 1A

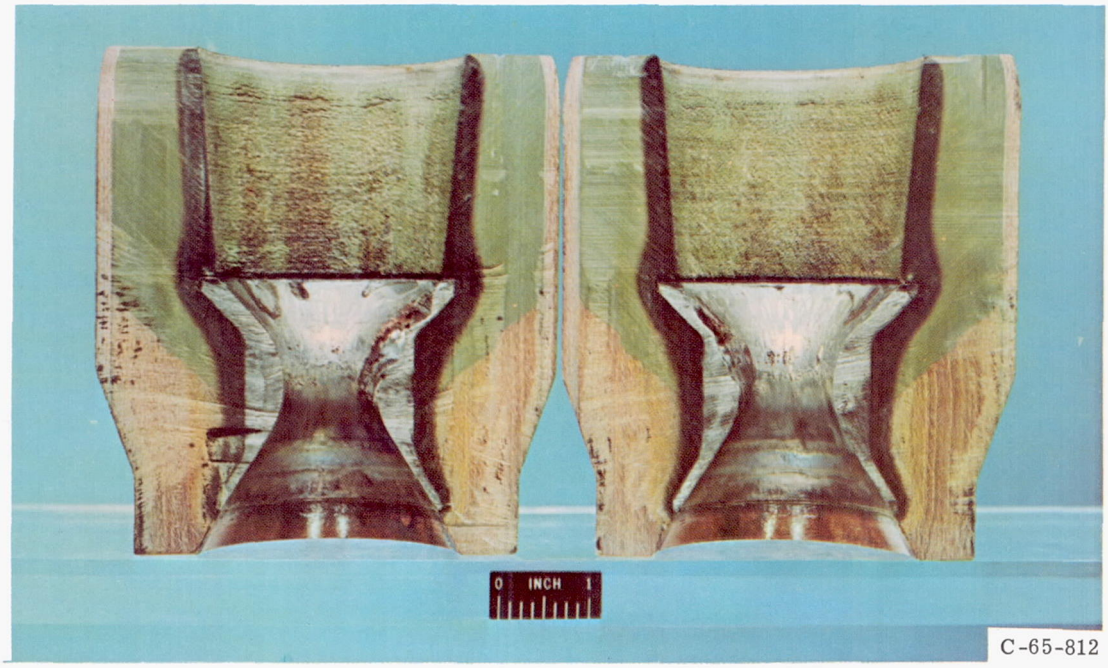

C-65-812

	Material	Form	Manufacturer	Configuration (a)	Additional layers
Coating	0.003-in. (0.0076-cm) WSi_2	----------	TRW	D	None
Insert	Molybdenum				
Envelope	Irish refrasil Silica phenolic	45° centerline 0° centerline	TRW	-----	3/8-in.(0.955-cm) thick asbestos phenolic

Run	Chamber pressure, P_c		Oxidant-fuel ratio, O/F	Run time, sec	Total change in effective throat radius, ΔR		Remarks
	psia	kN/m^2			in.	cm	
114	137.7	948	2.05	44.9	0.025	0.0635	Coating failure by oxidation; shutdown due to gas leak through ablative

[a]See fig. 5.

TABLE VI. - Continued

(79) Design 79; injector 2

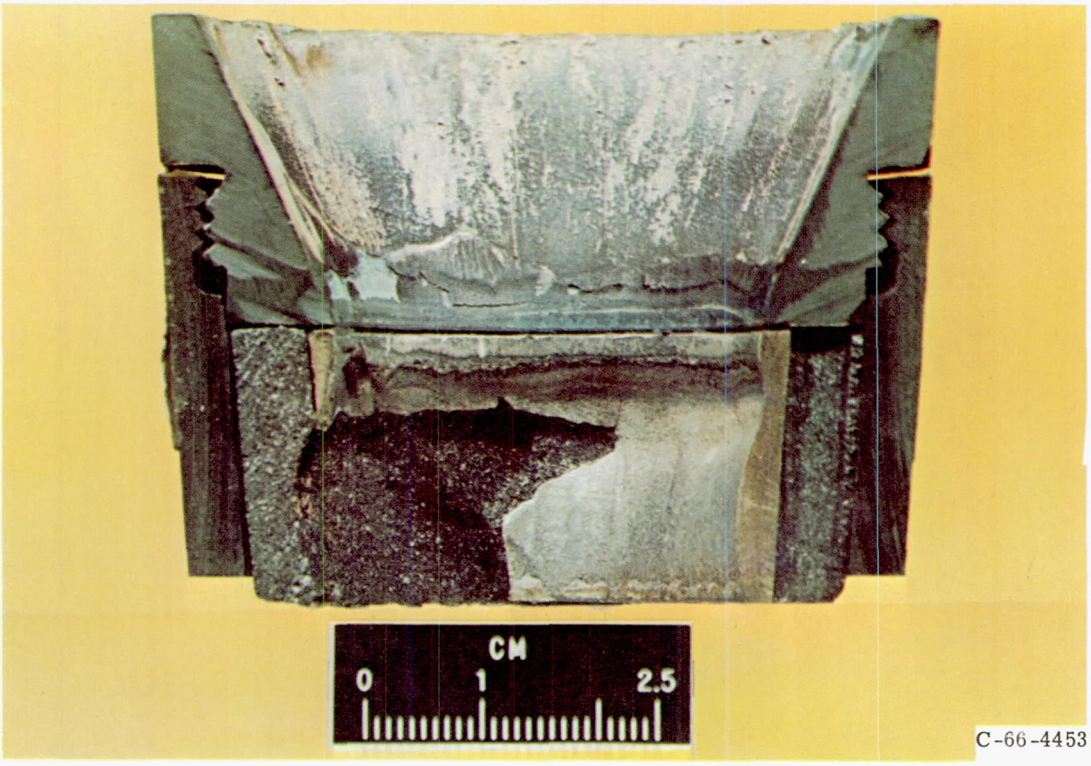

	Material	Form	Manufacturer	Configuration (a)	Additional layers
Insert	TaC; carbon brick; FS-85 ring; pyrolytic graphite	a-b plane radial	TRW	E	Carburized Ta - 10 wt. % W upstream of insert: JT0981 upstream of Ta - 10 wt. % W
Envelope	Silica phenolic	0° centerline	TRW	-----	Steel shell

Run	Chamber pressure, P_c		Oxidant-fuel ratio, O/F	Run time, sec	Total change in effective throat radius, ΔR		Remarks
	psia	kN/m^2			in.	cm	
331	100.5	693	2.02	125.1	0.005	0.127	Shutdown at first sign of erosion
350	100.1	690	2.10	102.5 227.6	.065	.175	Shutdown when erosion rate was established

[a]See fig. 5.

TABLE VI. - Continued

(80) Design 80; injector 2

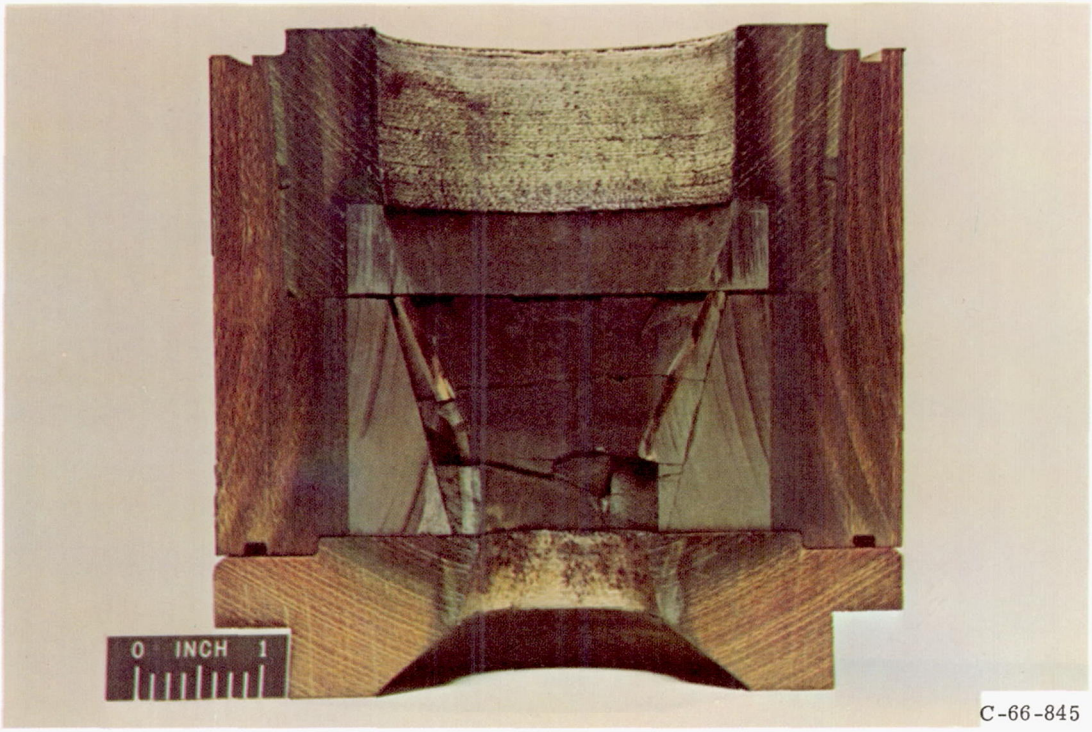

C-66-845

	Material	Form	Manufacturer	Configuration (a)	Additional layers
Insert	0.100-in. (0.254-cm) HfC; 0.100-in. (0.254-cm) TaC plus 10 % graphite; 0.100-in. (0.254-cm) TaC plus 40 % graphite; 0.100-in. (0.254-cm) TaC plus 70 % graphite; CGW graphite	----------	TRW	F	JT0981 upstream
Envelope	Carbon phenolic Silica phenolic	0° centerline 45° centerline	TRW	-----	Steel shell

Run	Chamber pressure, P_c		Oxidant-fuel ratio, O/F	Run time, sec	Total change in effective throat radius, ΔR		Remarks
	psia	kN/m^2			in.	cm	
364	101.3	696	2.04	38.6	0.031	0.0786	Shutdown after erosion rate established

[a]See fig. 5.

TABLE VI. - Continued

(81) Design 81; injector 2

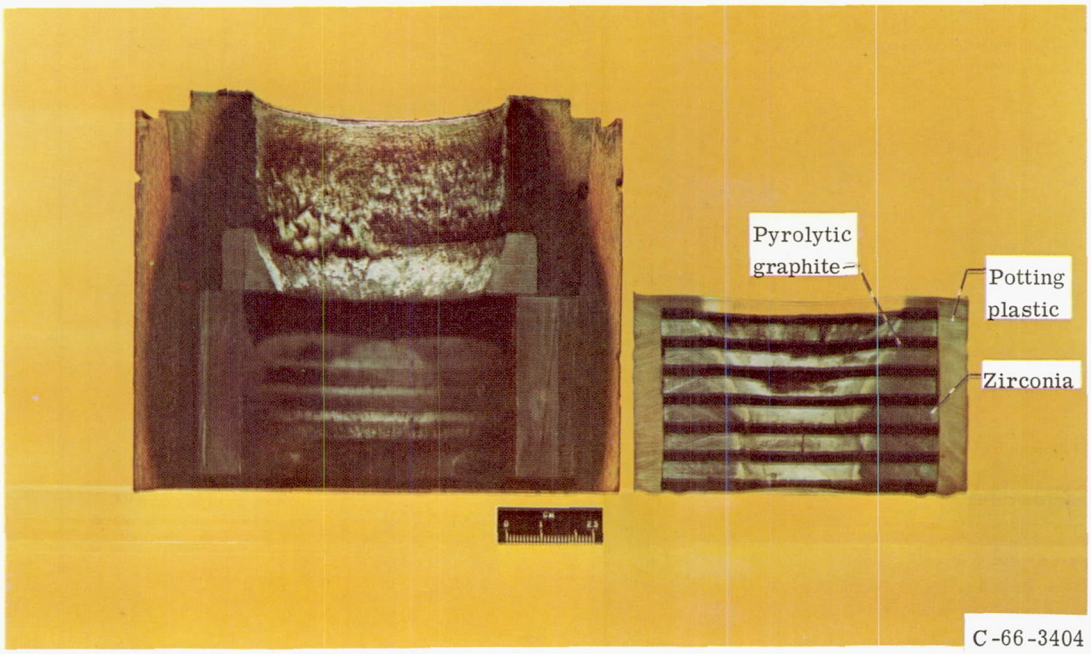

	Material	Form	Manufacturer	Configuration (a)	Additional layers
Insert	ZrO_2; pyrolytic graphite	Washers; a-b plane radial	TRW	G	JT0981 upstream of throat insert; CGW Graphite
Envelope	Carbon phenolic Silica phenolic	0° centerline 0° centerline	TRW	-----	Steel shell

Run	Chamber pressure, P_c		Oxidant-fuel ratio, O/F	Run time, sec	Total change in effective throat radius, ΔR		Remarks
	psia	kN/m^2			in.	cm	
419	101.9	702	2.08	214.7	0.005	0.0127	Shutdown at first sign of failure

[a]See fig. 5.

TABLE VI. - Continued

(82) Design 82; injector 2

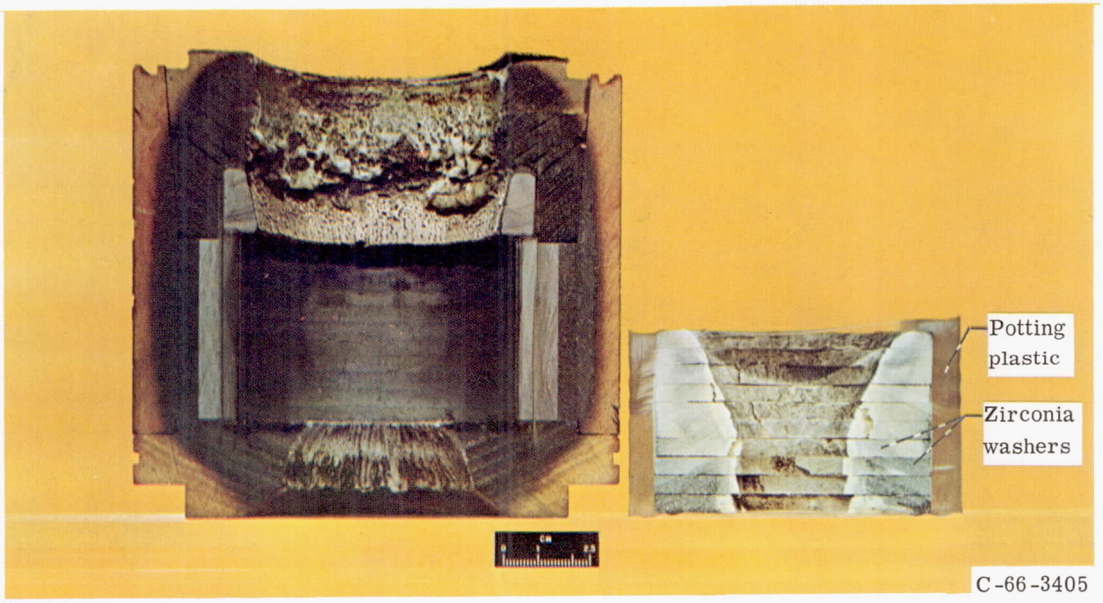

	Material	Form	Manufacturer	Configuration (a)	Additional layers
Insert	ZrO_2;	Washers; sintered	TRW	G	JT0981 upstream of throat insert; CGW Graphite
Envelope	Carbon phenolic Silica phenolic	0° centerline 0° centerline	TRW	-----	Steel shell

Run	Chamber pressure, P_c		Oxidant-fuel ratio, O/F	Run time, sec	Total change in effective throat radius, ΔR		Remarks
	psia	kN/m^2			in.	cm	
492	101.6	698	1.96	300.1	-0.021	-0.0533	Timed shutdown; axial cracks
495	101.8	701	1.97	20.6	[b]-.005	[b]-.0127	Timed shutdown
496	102.1	703	1.98	20.6	[b]-.010	[b]-.0254	Timed shutdown
497	101.7	698	1.98	20.6	[b]-.008	[b]-.0122	Timed shutdown
498	101.9	702	1.98	20.8	[b]-.008	[b]-.0122	Timed shutdown
499	100.7	692	2.00	20.6	[b]-.008	[b]-.0122	Timed shutdown; cracking and spallation
500	101.5	698	1.96	301.3 705.6	-.031	-.0788	Timed shutdown; cracking and spallation

[a]See fig. 5.
[b]Calculated.

TABLE VI. - Continued

(83) Design 83; injector 2

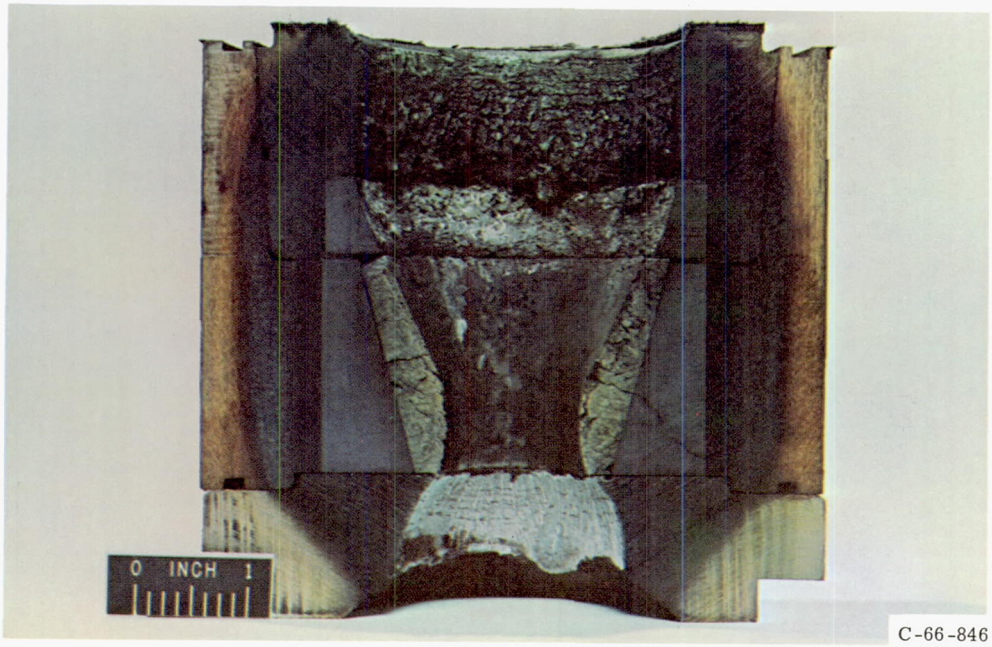

C-66-846

	Material	Form	Manufacturer	Configuration (a)	Additional layers
Insert	ZrO_2 - 5 vol. % tungsten-rhenium wires	0.0035-in. (0.009-cm) diam wire, 3/16-in. (0.476-cm) long; random orientation uniformly dispersed	TRW	H	JO0981 liner upstream of throat insert; CGW Graphite
Envelope	Carbon phenolic Silica phenolic	0° centerline 0° centerline	TRW	-----	Steel shell

Run	Chamber pressure, P_c		Oxidant-fuel ratio, O/F	Run time, sec	Total change in effective throat radius, ΔR		Remarks
	psia	kN/m^2			in.	cm	
351	100.6	693	2.15	310.4	-0.002	-0.00508	Timed shutdown; axial cracks
359	100.6	693	2.09	22.3	------	--------	Timed shutdown
360	100.5	693	2.11	22.6	------	--------	Timed shutdown
361	100.7	694	2.09	22.9	------	--------	Timed shutdown
362	100.3	691	2.11	22.8	------	--------	Timed shutdown
363	100.8	694	2.14	23.1	-.006	-.0152	Timed shutdown
366	100.9	695	2.04	309.7 733.8	-.010	-.0254	Timed shutdown; circumferential cracks

[a]See fig. 5.

TABLE VI. - Concluded

(84) Design 84; injector 2

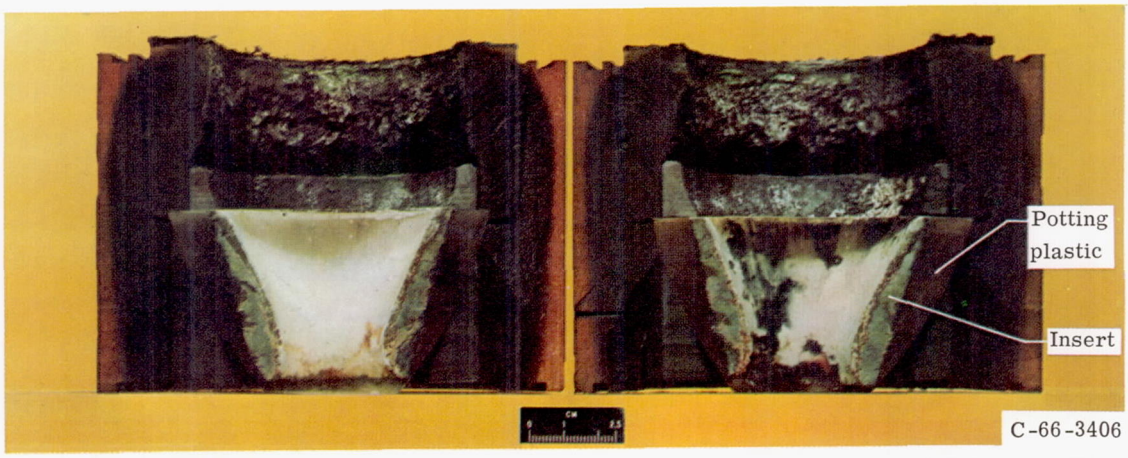

	Material	Form	Manufacturer	Configuration (a)	Additional layers
Insert	ZrO_2 - 7 vol. % tungsten-rhenium wires	0.0035-in. (0.009-cm) diam wire, 3/16-in. (0.476-cm) long; random orientation, uniformly dispersed	TRW	H	JO0981 upstream of throat insert; CGW Graphite
Envelope	Carbon phenolic Silica phenolic	0° centerline 0° centerline	TRW	-----	Steel shell

Run	Chamber pressure, P_c		Oxidant-fuel ratio, O/F	Run time, sec	Total change in effective throat radius, ΔR		Remarks
	psia	kN/m^2			in.	cm	
493	102.3	704	2.00	181.4	[b]-0.004	[b]-0.010	Accidental shutdown
494	101.4	698	1.98	300.5	[b]-.013	[b]-.033	Timed shutdown; axial cracks on inside diameter
501	101.4	698	1.98	20.5	-------	------	Timed shutdown
502	101.8	700	2.00	20.5	-------	------	Timed shutdown
503	101.7	700	1.98	20.7	-------	------	Timed shutdown
504	101.5	699	1.99	20.5	-------	------	Timed shutdown
505	101.3	698	1.96	20.6	-.024	-.061	Timed shutdown
511	101.1	696	2.03	300.8	-------	------	Timed shutdown
555	101.6	700	2.10	373.4	-.037	-.094	Manual abort; flow behind insert
				1257.9			

[a]See fig. 5.
[b]Calculated.